An Experimental Investigation of Mode-I Crack Tip Deformation

Thesis by

Peter D. Washabaugh

In Partial Fulfillment of the Requirements
for the Degree of
Doctor of Philosophy

California Institute of Technology
Pasadena California
1990

(Submitted November 28, 1989)

To my father

Acknowledgements

I am indebted to Dr. Wolfgang Knauss for his insightful guidance, support, and for providing an unusually flexible work environment. I am also grateful for having the opportunity to interact with Mr. Richard Pfaff whose boundless curiosity and attention to detail has been a source of intellectual inspiration. Interaction with my colleagues, and the comraderie and enthusiasm fostered at the Institute have been constant sources of encouragement. Specifically, I thank Dr. A.J. Rosakis for his time, advice, and equipment. Partial support for this work was provided by the National Science Foundation and the Office of Naval Research. Finally, my eternal thanks to my wife, Susan, for her gratuitous patience and advocacy.

Abstract

The out-of-plane displacement of amorphous polymethylmethacrylate plates rupturing at slow (0.1 mm/s), and fast (0.5 to 0.9 mm/μs) rates are measured using a Twymann-Green interferometer. The measured surface shapes within one plate thickness of the crack-tip do not compare well with the two-dimensional planar asymptotic approximation, but compare favorably with the published slopes for three-dimensional finite element solutions when normalized with the static material properties. Discrepancies, on the order of ten percent, between the magnitude of the three-dimensional finite element solutions suggest that the stress intensity factor does not fully characterize the near tip deformations.

A dynamically propagating crack is found to move in a non-steady, periodic, sub-microsecond fashion. This result is supported both by the surface measurements and the fracture morphology. The material toughening, as measured by the surface roughness, correlates well with the stress intensity factor and not with the crack velocity. The details of the sub-microsecond propagation and toughening was not resolvable with the microsecond temporal resolution of the experiment.

Inhibiting the material toughening at the crack tip by artificially introducing a weak material plane augments the crack motion to velocities close to the material's shear wave speed. The crack propagates more steadily along the weak plane than through a virgin solid, while maintaining the character of the out-of-plane displacement of a crack propagating in an unsullied material.

Table of Contents

List of Illustrations

1. Introduction

Fracture mechanics is the branch of the study of structural failure that deals with a material's loss of cohesive ability. The local material separation is typically studied in terms of the instantaneous surrounding conditions (e.g., strain, temperature) and external history (e.g., fatigue). The goal of such a fracture mechanics investigation is to determine the surrounding environments and local criteria under which material separation can evolve and the rate of decohesion once it occurs.

In general the entire fracture process is quite complex due to the intertwining of numerous and insufficiently understood phenomena which occur over disparate length scales. Rupture ensues as the result of the agglomeration of a number of material dependent atomistic and microstructural events. These small-scale processes are driven by the environment surrounding the fracture site and in turn give rise to such macroscopic phenomena as time dependent behavior and inelastic deformations. Such microstructural processes and their resulting average continuum behavior are normally studied independently; however, in rupture problems they are inexorably married. Consequently the general problem of material decohesion is imbedded in regions of intermediate scale where the knowledge of the material constitutive behavior is dubious. Further, the macro-material dependence on the underlying microstructural phenomena seems to limit the universal applicability of any particular investigation.

In order to make experiments and analyses more tractable, ambitious assumptions that bury the microstructural detail in continuum mechanical constructs are usually made. Typically, these assumptions are to homogenize the material response of the solid, limit the response function to energetically conservative behavior, and to limit the dimensionality of the investigation. Unfortunately, in even these simplified situations, analytical solutions to the governing equations have been stubbornly intractable except under limited circumstances. For more practical specimen geometries and more realistic specimen

material models the increased complexity of an already intractable problem has forced the extensive use of numerical solution methods. Nevertheless, even with these difficulties substantial progress has been made in tying together environmental conditions with material rupture.

Modern fracture mechanics has its roots in the simple concept that fracture will ensue when energy that escapes inelastic processes in the body, is made available to form new surfaces. The energetics of the processes that govern decohesion are almost invariably imbedded in the surface fracture energy . The difficulty with this concept in practice is to determine what energy in the surrounding material environment is made available for surface creation. Energy input from the boundaries of a solid are also absorbed by other processes in the material and may not be available at the local site of decohesion. The grail of these investigations has historically been to distill the surrounding environment down to a few parameters or a simple one that "governs the crack tip behavior."

Within the framework of two-dimensional, planar elastodynamics, single parameters such as the stress intensity factor [1], and certain path independent integrals [2], have been suggested as adequately describing the effect of an elastic environment on the local fracture process [3]. However, applications of these developments to more complicated problems has led to discrepancies with experimental observation. These differences include variability of rupture strength with specimen thickness [4], and for a constant fracture parameter both non-unique plastic zone development [5], and non-unique crack propagation velocity [6]. Explanations for some of the observed discrepancies are that three-dimensional effects and the non-singular terms in the two-dimensional solution account for thickness variations in fracture toughness and the evolution of inelastic zones [7]. Further, the apparent non-unique dynamic crack propagation velocities as a function of the fracture parameter, and observed crack speeds in amorphous materials that are at most half of the theoretical maximum [8], have been attributed to inadequate local dynamic measurement and modeling. These inadequacies include spatially limited

measurement methods [9], questionable interpretation of observations through planar theories [10], and no accounting for the fraying of the crack tip at high velocities [10].

Considerable effort has been expended in extending the planar elastic theories to more general three-dimensional, dynamic, and inelastic problems [11,12,13,14]. These studies typically address issues seen in practical applications, and are quickly complicated by the influence of numerous parameters (e.g., material inhomogeneity, viscoplasticity), especially near the crack tip [15,16,17]. Difficulties persist in establishing proposed models because along with the analytical intractability of solving the governing equations, simplifying assumptions (such as specimen geometry) are typically made that are impractical for experimental purposes. Even when assumptions (e.g., geometry) are tailored to an experiment, measurements are still troublesome. Experimental evidence is often open to differing interpretations because of parametric interaction or the measurements implicitly combine several quantities of interest. When confronted with experimental and theoretical discrepancies, it is imperative to eliminate unnecessary parameters and unambiguously measure the individual modeled quantities at the expense of general applicability. As a consequence of this simplification of limiting parameters, this work will take a humble departure from the existing two-dimensional planar elastodynamic theory and focus on examining the observed discrepancies in the dynamic fracture of brittle solids.

Dynamic experiments that reduce the influence of specimen geometry through wave reflections, and simulate an infinite planar problem are rare [6,18]. The problem discussed here is limited to a semi-infinite crack in an infinite plate, under Mode-I loading at infinity [19], that can be modeled as an elastic solid except for a small (relative to the plate thickness) region at the crack tip. The elastic body can be modeled as a plane stress problem at distances greater than one plate thickness. This plane stress configuration [6] is preferred over a plane strain investigation [18], because full surfaces can be measured and compared at the crack tip even for opaque materials. With present technology the expense

of choosing a plane stress geometry to obtain spatial measurements compared with a plane strain configuration is approximately a two order of magnitude loss in loading rate and temporal resolution. The reward of making spatial measurements is that full field behavior can be observed.

Many experiments that use the plane stress specimen geometry although not necessarily simulating an infinite flat plate, have been used to investigate the dynamic rupture process. It is often not known whether a finite specimen geometry or other implicit assumptions in using a particular measurement technique lead to inaccuracies. Experiments using photoelasticity conclude that as the spatially averaged deformation surrounding a dynamically moving crack tip is increased, its propagation velocity is augmented [20,21,22]. However, when other methods of measurements are employed that are spatially more precise, the instantaneous intensity of deformation is not uniquely related to the crack velocity [6]. Further study and more careful analysis have shown that the deformation intensity and velocity relationship is dependent on the crack's apparent instantaneous acceleration [23]. Additional complications arise as the crack velocity is increased. Surface waves are radiated from the crack tip and branching can occur. These waves have been examined and modeled as arising from small voids or micro-cracks opening in front of, and coalescing with, the main crack [24]. Such microstructural details are thought to be responsible for measurement discrepancies as well as determining a material's limiting crack propagation velocity and crack branching characteristics. The goal of this study is to further investigate these microstructural details at the crack tip.

In order to closely examine such microstructural detail, three-dimensional influences cannot be avoided. As the crack tip is approached, the original planar approximations no longer apply. Consequently, experimental techniques that are not influenced by the loss of validity in the planar assumptions, and the nature of the three-dimensional region need to be established.

The following chapters, two through five, include the reasoning behind choosing a particular method of measurement, the expected material response based on previously published results, selection of a test material and experiment configuration. The remaining sections discuss and compare the experimental results with published predictions. The difficulty in measuring near tip material response and the philosophy of isolating a test from theoretical predictions dictates some characteristics of the measurement technique. A review of published three-dimensional numerical predictions of the out-of-plane surface deformation reveal discrepancies when normalized with the stress intensity factor. This difference suggests that the stress intensity factor does not adequately scale the near tip deformation.

The outcome of this research is that while the out-of-plane surface measurements near a crack in a plate is not described by a singular field, the deformation is consistent with static three-dimensional numerical solutions. This result is true for both quasi-static and dynamic crack propagation experimental data. Further, based on the surface deformation and fracture morphology, cracks in PMMA dynamically propagate in a non-steady, periodic, sub-microsecond, fashion as the crack branching velocity is approached. This non-steady crack propagation is attributed to an apparent material toughening, perhaps by material yielding or void nucleation preceding the main crack, or non-uniform crack propagation through the specimen thickness. Weakening the material by artificially introducing a planar imperfection inhibits the material toughening as well as the non-steady behavior and augments the crack velocity. The details of the non-steady crack propagation were not resolvable with the resolution of the experiment.

2. Local Measurement Techniques

Numerous techniques have been employed to examine the validity of both numerical and analytical predictions. Preferably the method used will make simultaneous measurements that are spatially disperse to establish the field surrounding a rupture. Various multiple point, or field measurement methods have been used in fracture mechanics problems; these include photoelasticity [25,26,27], shadowgraphic techniques [28,29,30,31,32], and interferometric methods [33]. By far the most productive method in terms of quantitatively supporting two-dimensional elastodynamic fracture mechanics has been the method of photoelasticity [20,21,22,34,35,36]. Schlieren techniques [29], and their close cousin, the method of caustics [37,38,39,6,23,40], and other shadowgraphic methods [41], have also been employed in examining two-dimensional elastodynamic situations. Other techniques such as speckle [42], Mach-Zehnder [43], Moire [44], and holographic [45,46] interferometry have contributed to static measurements.

Most of these methods (e.g., transmitted Schlieren, photoelasticity, and transmitted caustic) require specimens with specific material properties such as transparency or birefringence. This specialization limits the type of materials that can be directly studied and the techniques used on such materials implicitly measure an average of a property through a specimen's thickness. This averaging procedure is suitable for examining two-dimensional theories. However, as the crack tip is approached to examine microstructural detail, three-dimensional effects become important and many of these techniques are no longer adequate. The transparent material limitation also severely restricts studies on more common opaque specimens.

In recent years measurement methods that make use of the reflective properties of a surface have been advanced to increase the type of materials that can be measured and

improve precision. The techniques that have been used in reflection can be divided into the two categories of shadowgraphy and interferometry.

Shadowgraphic methods used in reflection include Schlieren [47], caustics [31], and the Stress Intensity Factor Tracer [32]. These methods are related because they make use of a non-unique mapping from the illumination source to the detector or an aperture to mask certain reflected rays. An optical system employing the Schlieren technique is usually focused on the specimen, the surface is illuminated with parallel light, and uses an aperture to select a single slope on the specimen surface. On the resulting image the selected slope is a transition, along with diffraction from the aperture, from illumination to shadow. Thus, the Schlieren technique can be used to measure the location of a line of constant slope on the surface.

A close relative of the Schlieren technique is the method of caustics. When this method is used in reflection, the optical system is focused behind the specimen. Again the specimen is illuminated with parallel light, but this method does not make use of an aperture. The resulting shadow pattern when viewing a loaded fracture surface is due to a non-unique mapping of the light from the illumination source, to the specimen surface, through the optical system, and on to the image plane. Here the shadow spot is surrounded by a bright region that is a result of the non-unique mapping. The diameter of the resulting caustic has been found to be simply related to the stress intensity factor of two-dimensional elastostatics [31], and elastodynamics [31a].

The Stress Intensity Factor Tracer is similar to the Schlieren method, except that a Fourier plane mask is used and the light is collected at a single detector that integrates the total light intensity reflected from the specimen. The advantage of this method is that a single high-speed detector can be used and its output can be simply related to two-dimensional elastostatics [32]. This added temporal resolution is at the expense of all of the spatial information.

The chief limitation of the shadowgraphic techniques, in contrast with interferometric methods, is that they do not yield information over an entire field of view. Information is obtained only from selected regions. The restricted spatial information is not a question of limited resolution, but deformation information is lost either at an aperture (e.g., Schlieren) or rendered irretrievable through a non-uniquely invertible process (e.g., caustics and the Stress Intensity Factor Tracer). Further, in order for the method of caustics and the Stress Intensity Factor Tracer to be easily interpreted they rely on the two-dimensional elastostatic or elastodynamic asymptotic field to govern the elastic state of the material surrounding the crack tip. This asymptotic assumption somehow needs to be justified, and if the assumption is not valid the easy interpretation yields to an extensive analysis [59]. The limited spatial information and the unnecessary reliance on an existing theory is sufficient to abandon these methods in favor of the more direct and precise interferometry techniques.

The method of caustics has found widespread use. It has been applied in elastodynamic situations of brittle media [23,31,6], and in more ductile materials [40,48,49,50]. Once the assumption of the validity of the two-dimensional asymptotic field surrounding the fracture zone has been accepted the subsequent analysis of the magnitude of the elastic strains is straightforwardly determined from the caustic size. Qualitative information has also been determined about the fracture region from the caustic shape [48].

There is compelling evidence that the use of caustics in transmission on brittle materials under Mode-I loading is justified in a small region (radius from crack tip / plate thickness of > 0.5) surrounding the crack tip. When caustics are used in transmission, the optical effect is apparently primarily caused by the in-plane strains. Compensation for the three-dimensional out-of-plane deformation allows transmitted caustics to yield consistent stress intensity factors and caustic shapes, at regions much closer to the crack tip (radius

from the crack tip / plate thickness > 0.1) than the uncompensated experiments [51,52,53]. However, the justification of the use of caustics in reflection is much more tenuous.

There are several difficulties in using caustics in reflection. The ease of use and direct interpretation of caustics of brittle fracture hinges on the surface dimpling as predicted by the two-dimensional plane stress asymptotic solution [54]. This surface deformation is given in equation (1) with the coordinate system shown in Figure (1). Here υ is Poisson's ratio, h is the plate thickness, E is Young's modulus, and K is the stress intensity factor. The validity of this assumption will be addressed in later sections by direct measurement of the surface deformation.

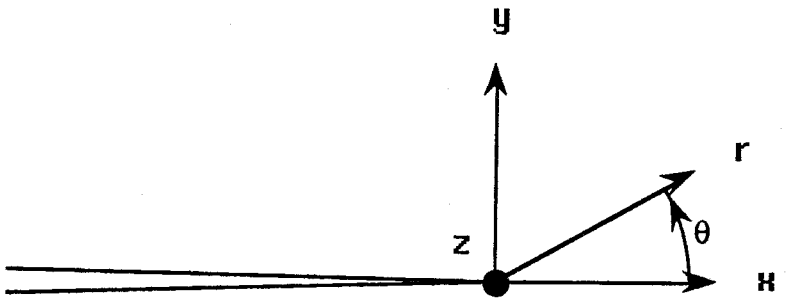

Figure (1) Coordinate system defined at the tip of a crack moving self-similarly with velocity, s. Displacements u,v,w are in the x,y,z directions, respectively.

$$w = \frac{\upsilon h}{E\sqrt{2\pi}} \frac{K}{\sqrt{r}} \cos\left(\frac{\theta}{2}\right) \qquad (1)$$

Other problems arise, depending on how the caustic measurement is taken. Figure (2) is a schematic of a simple caustics set-up. The more general problem of considering the entire asymptotic deformation has already been addressed by Rosakis [55] and Pfaff [58]. For the discussion here it is sufficient to examine the deformation along a single line.

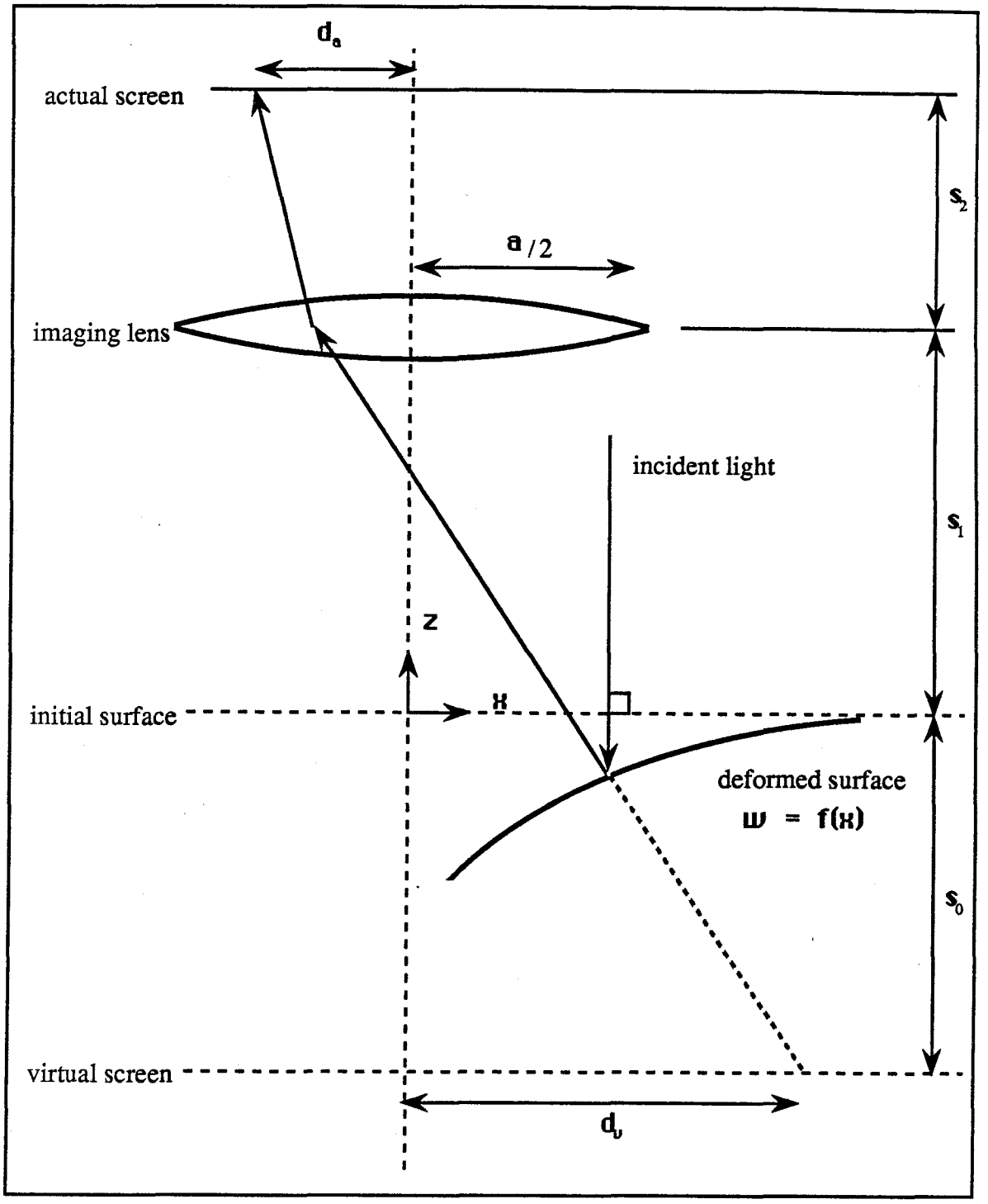

Figure (2) Schematic of a simple caustic experiment.

Setting the deformation equal to a square root singular field as in equation (1), along the x axis, and setting k equal to the remaining terms yields equation (2).

$$w = \frac{k}{\sqrt{x}} \tag{2}$$

Performing the caustic analysis [55], and assuming both small deformations and small angles, the classic formula for the caustics [55] is recovered as shown in equation (3). Here, c is a constant and m is the magnification of the optical system. The abscissa of the point on the deformed surface from which the caustic emanates, the initial curve (here a point), is also approximately one-third of the virtual screen caustic diameter [55].

$$k = \frac{1}{s_0}\left(\frac{d_a}{mc}\right)^{\frac{5}{2}} \tag{3}$$

This analysis also demonstrates how well k can be evaluated. Assuming a perfect simple lens of focal length f, the sensitivity of k to the experimental parameters is given by equation (4).

$$\frac{\Delta k}{k} = \frac{5}{2}\frac{\Delta d_a}{d_a} + \frac{\Delta s_1}{s_0} + \frac{2f - 5s_0 m}{2s_0 m}\frac{\Delta m}{m} \tag{4}$$

In experiments [51,52] that vary the virtual screen distance from far behind, to just behind the initial surface, the caustic formed on the virtual screen shrinks along with the

abscissa of the initial point. It is evident from equation (4) that as the initial point approaches the crack tip, for a given measurement accuracy, the determination of k becomes less precise (random error), or less accurate (systematic error), depending how the experiment is executed . Thus, if a measurement is to be taken close to the crack tip, precise and accurate distance measurements are required.

Furthermore, as the crack tip is approached the ability of the optical system to capture the reflected light must be evaluated. Depending on the placement of the imaging lens the optical arrangement can collect rays of certain angles. As the crack tip is approached, the angle required to capture the light forming the caustic increases, although not necessarily enough to invalidate equation (1) due to the small angle approximation. At some initial point the aperture of the lens, "a," is reached, and thereafter a caustic is no longer formed on the actual screen; instead, a shadow spot with the light defracting from the edge of the lens remains. A caustic set-up for large angle rays, if improperly implemented, is akin to a Schlieren arrangement with an unknown aperture location. To determine if a given image is a caustic (with a shadow spot) or just a shadow spot requires a much more extensive analysis of the differences in intensity distribution outside of the shadow spot [56].

In fracture experiments that approach the crack tip [51,52] or tests with known large angle difficulties, such as plastic zone experiments [48,49,57], careful application and calibration of the method of caustics is required. As the crack tip is approached, the stress intensity factor becomes sensitive to distance measurements. Measurements near a crack-tip or involving plastic specimens require large aperture optics to insure formation of a caustic. It is not obvious that a given image is a caustic or merely a shadow spot. These issues of distance sensitivities or aperture limitations are of concern and are not typically explicitly considered or addressable from published experimental information [48,49,51,52,57].

Because of the limited information returned, increased sensitivity as the crack tip is approached, and the other interpretation difficulties with reflective shadowgraphic methods, interferometric techniques are judged preferable. An overriding concern in selecting an interferometric measurement method is the ability to perform the experiment under dynamic conditions with available equipment. Because dynamic experiments typically require timing on the microsecond scale, illumination limitations require light efficiency. For reflective specimens this fact translates into selecting a method that uses specular rather than diffuse reflection. One such technique, the Twymann-Green interferometer has been found suitable for dynamic fracture mechanics measurement purposes and has been extensively developed by Pfaff [58]. This interferometer measures the difference in surface elevation between a reference surface and the test surface. When the reference surface is a flat mirror, the interferometer measures the deviation of the test surface from flatness. This interferometric technique will be further explained in section four.

3. Three-Dimensional Fracture Considerations

Measurement of surface characteristics near the tip of a fracture in elastodynamic situations requires an accounting for three-dimensional effects [59]. However, the precise nature of the three-dimensionality at the crack tip, in an infinite plate, has yet to be established. There have been numerous contributions of closed form and asymptotic analytical work with the aim of determining the effect of the plate thickness on plate fracture problems [60,61,62,14]. In addition there have been scores of fruitful numerical studies [63 - 73].

The numerical investigations have progressed with increasing computational refinement capability. To limit the size of the numerical problem, initial studies incorporated singular elements which enforced a two-dimensional asymptotic solution at the crack tip even though the plate thickness was explicitly modeled [63 - 65]. These studies qualitatively captured the tendency for a crack to curve during fracture [66]. More recent investigations do not use any special assumptions and tackle the stress "concentration" at the crack front with a fine discretization [67 - 73]. Some of these studies also include inelastic material models.

A concise review of the results of the numerical work involving linear elastic material behavior under Mode-I loading, is that outside of a radial distance of about one plate thickness, the two-dimensional elastic plane stress solution is a good model. Within one plate thickness, three-dimensional effects become apparent. As the crack tip is approached the out-of-plane strains, as well as the in-plane strains at the plate surface, are the first to deviate significantly from the planar theory. The in-plane stresses and strains at the center of the plate agree in magnitude with the two-dimensional theory, at approximately one-half of a plate thickness from the crack tip. This summary is supported by various experimental observations. Experimental techniques that are sensitive to in-

plane strains such as photoelasticity, transmission caustics, and Moire interferometry, measure behavior that can be potentially modeled as two-dimensional at distances closer to the crack tip than methods such as reflected caustics that are sensitive to out-of-plane behavior [44,45,46,51,52].

Since the fracture relevant microstructural detail occurs near the crack tip, i.e., in this three-dimensional zone, and many engineering materials are opaque, establishing a three-dimensional solution for the surface deformation is of primary interest. Figures (3) and (4) compile the numerical results for the out-of-plane displacement from several sources and compare the data with the two-dimensional asymptotic plane stress solution. The out-of-plane displacement has been normalized by the leading coefficient in the first term of the asymptotic solution. Thus the numerically calculated displacements, w_c , are normalized as shown in equation (5).

$$w = \frac{w_c E \sqrt{2\pi}}{K \upsilon \, h} \tag{5}$$

The radial distance from the crack tip was non-dimensionalized by dividing by the plate thickness. The data for these figures were supplied by the authors of various published finite element studies [59,71,72,73]. For each study the data were available only along certain radial angles. This fact accounts for the apparent haphazard selection of the angle for the out-of-plane displacement plots in the following figures.

These studies were selected because they are straightforward numerical approximations to the linear elastic, homogeneous, isotropic, governing equations with the only intended assumptions being the finite element discretization. All of the studies are carried out for different finite specimen geometries under various loading conditions and were independently formulated and implemented. Even though the elastic fields far from the crack are different, classic fracture mechanics wisdom dictates that the behavior at the

crack tip be self-similar and governed in magnitude by a single parameter such as the applied stress intensity factor.

Each figure contains a curve of the first term of the two-dimensional plane stress Mode-I asymptotic solution (the K-field), normalized and labeled "2-D K Static." Nakamura's calculation [72], applies to a plate that is loaded at five plate thicknesses from the crack tip with a K-field determining the boundary conditions, and is called "3-D K Static" in the figures. This K-field loaded geometry is notably artificial from an experimental viewpoint, but quantitatively shows the effect of three dimensions on an otherwise two-dimensional problem. Salient points are that the surface shows the effects of the added dimension at approximately one plate thickness from the crack front and the two-dimensional approximation is an adequate model along the center of the plate and close to the crack front [72]. These results are consistent with experimental observation [51,52,53]. Under the normalization of equation (5), the out-of-plane surface deformation is very weakly dependent on material property selection.

The other studies use geometries that are more directly amenable to experimentation [71,72,59]. The curves labeled "3-D SEN Static" denotes the Single Edge Notch specimen analyzed by Parsons [71]. This specimen is loaded with a uniform tensile load far from the crack front and perpendicular to the crack flanks. The curves "3-D TPB Static" and "3-D TPB Dynamic" are derived from the analysis of the Three Point Bend specimens where the static analysis was offered by Narasimhan [73] and the dynamic work, for a specimen with a stationary crack under impact loading, was performed by Krishnaswamy [59]. In the dynamic case the data were normalized by the instantaneous stress intensity factor, after several waves had reflected to the crack front from the boundaries.

Figure (3) shows the calculated out-of-plane displacement at a radial distance up to five plate thicknesses from the crack tip. At a radius of zero the numerically calculated displacements tend toward finite values in contrast to the asymptotic solution. At larger radii, the calculations differ appreciably due to the differences in the far field boundary

conditions. Surprisingly, at a distance of one plate thickness, where the K-field is ostensibly dominate [51], there are noticeable differences in the gradient of the deformation between the numerical specimens and the K-field. As expected the three-dimensional K-field simulation converges to the K-field, and the single edge notch specimen appears to remain tensile at the larger distances. The three point bend specimens have a compressive region that accounts for a positive displacement at a radius as close as two plate thicknesses from the crack tip. Along the crack flanks (180 degrees), the numerical simulations predict a non zero displacement in contrast with the two-dimensional asymptotic approximation.

Note that there is little difference in the out-of-plane displacements for the three point bend specimens between the static and dynamic loading cases. This either indicates that the out-of-plane displacements are insensitive, or that there were small dynamic effects throughout the specimen in the impact simulation.

Figure (4) is a detailed rendition of the previous figure at radial distances up to only one plate thickness. Again the numerical studies indicate a non-singular out-of-plane deformation at the crack front. The slopes predicted by the numerical investigations are consistent with each other. In front of the crack, the slopes of the deformation compare favorably with the asymptotic solution, while along the crack flank, the slopes are markedly lower.

The magnitude of the normalized displacement between the various simulations agree, surprisingly, only to ten percent within one plate thickness. The calculations for the three point bend specimen displacements have an equal yet significant offset from the other calculations and predict a smaller total deformation at the crack front. All calculations use comparable finite element discretizations while using implementations derived independently by the individual authors. Consequently, as long as the finite element discretization is appropriate, errors in the numerical simulation are deemed unlikely. The normalization (e.g, equation (5)) could be improved to include the influence of other stresses that are found at the crack tip. The effect of the non-singular two-dimensional

stress terms has been addressed for the three point bend specimen geometry [7]. These terms would only account for approximately one percent of the total out-of-plane deformation at the crack front.

The slope of the normalized displacements between the various numerical simulations are consistent. However, with the present information the discrepancies in the magnitude of the normalized deformation is unresolved. This difference in magnitude has at least two troubling implications. The choice of specimen geometry indicates a non-autonomous local deformation with respect to changes in specimen configuration. Since these specimen are tailored (in two dimensions) to isolate local fracture behavior from external loading details, this observation does not bode well for the application of fracture mechanics in more complicated scenarios. A still more troubling possibility is that in general the stress intensity factor does not scale the local deformation, and hence is not a governing fracture mechanics parameter.

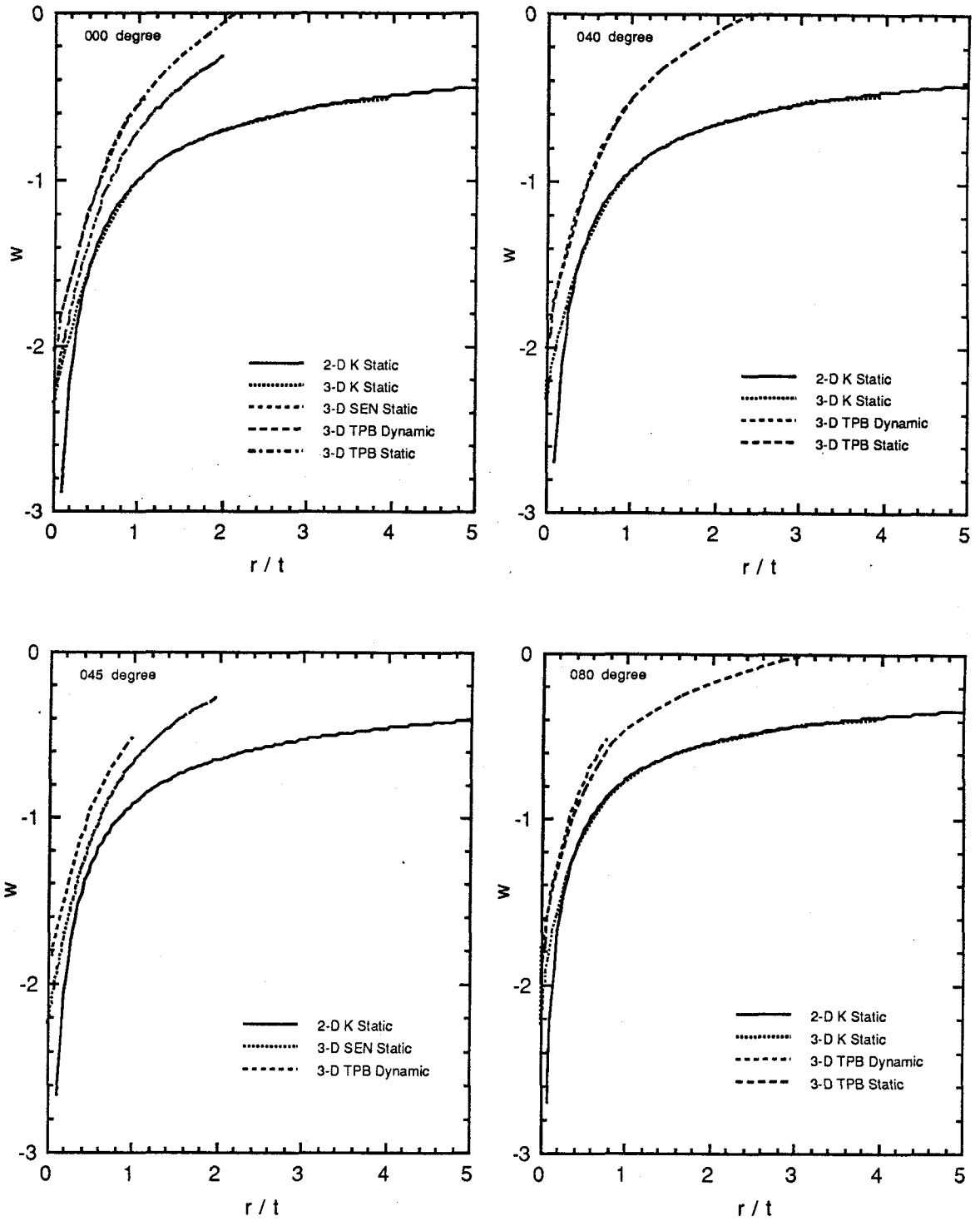

Figure (3a) Comparison of static three-dimensional numerical solutions for the out-of-plane displacements near a crack tip with the two-dimensional asymptotic plane stress solution. Displacements are shown along radial lines at angles of 0, 40, 45, and 80 degrees to ligament [59,71,72,73].

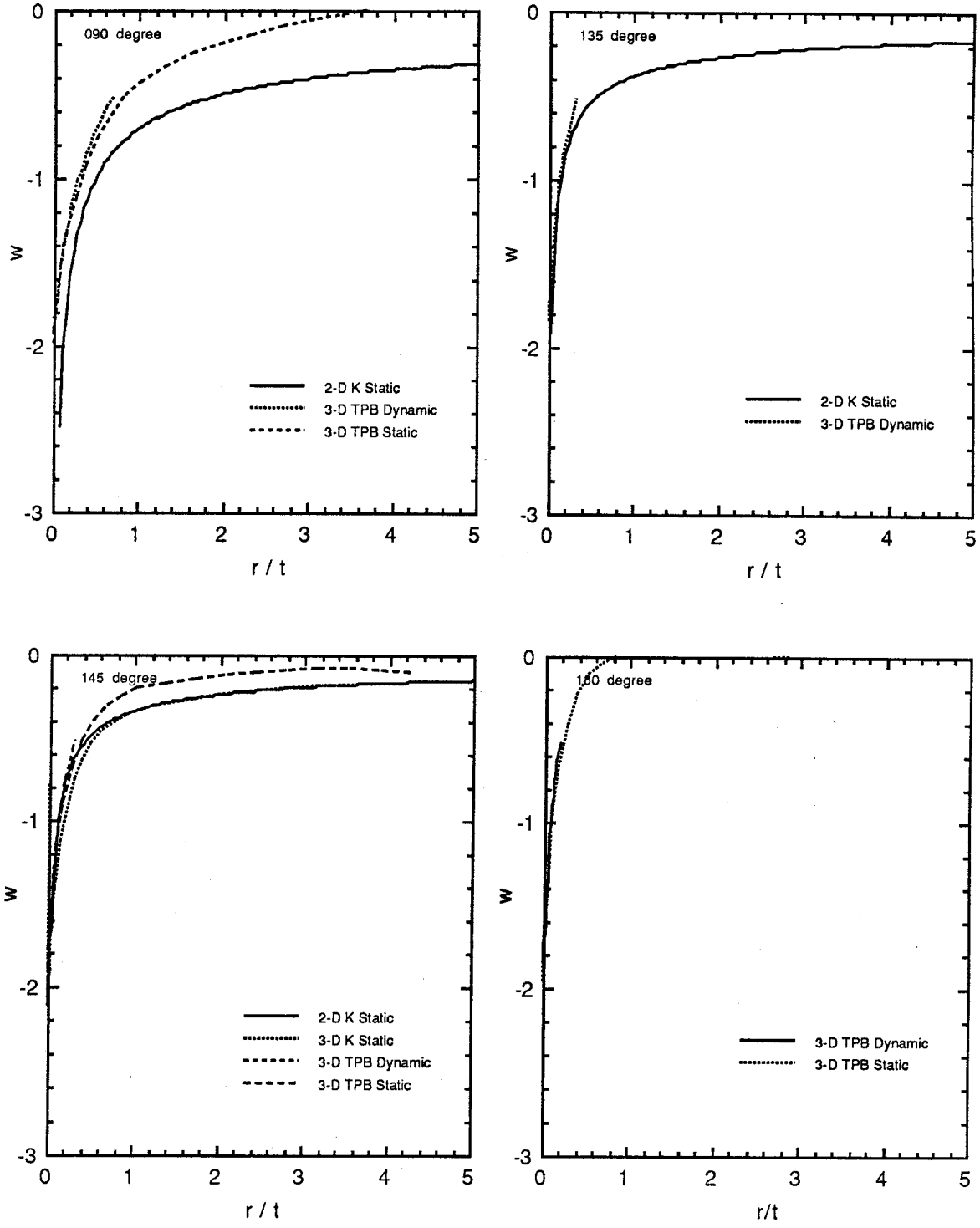

Figure (3b) Comparison of static three-dimensional numerical solutions for the out-of-plane displacements near a crack tip with the two-dimensional asymptotic plane stress solution. Displacements are shown along radial lines at angles of 90, 135, 140, and 180 degrees to ligament [59,71,72,73].

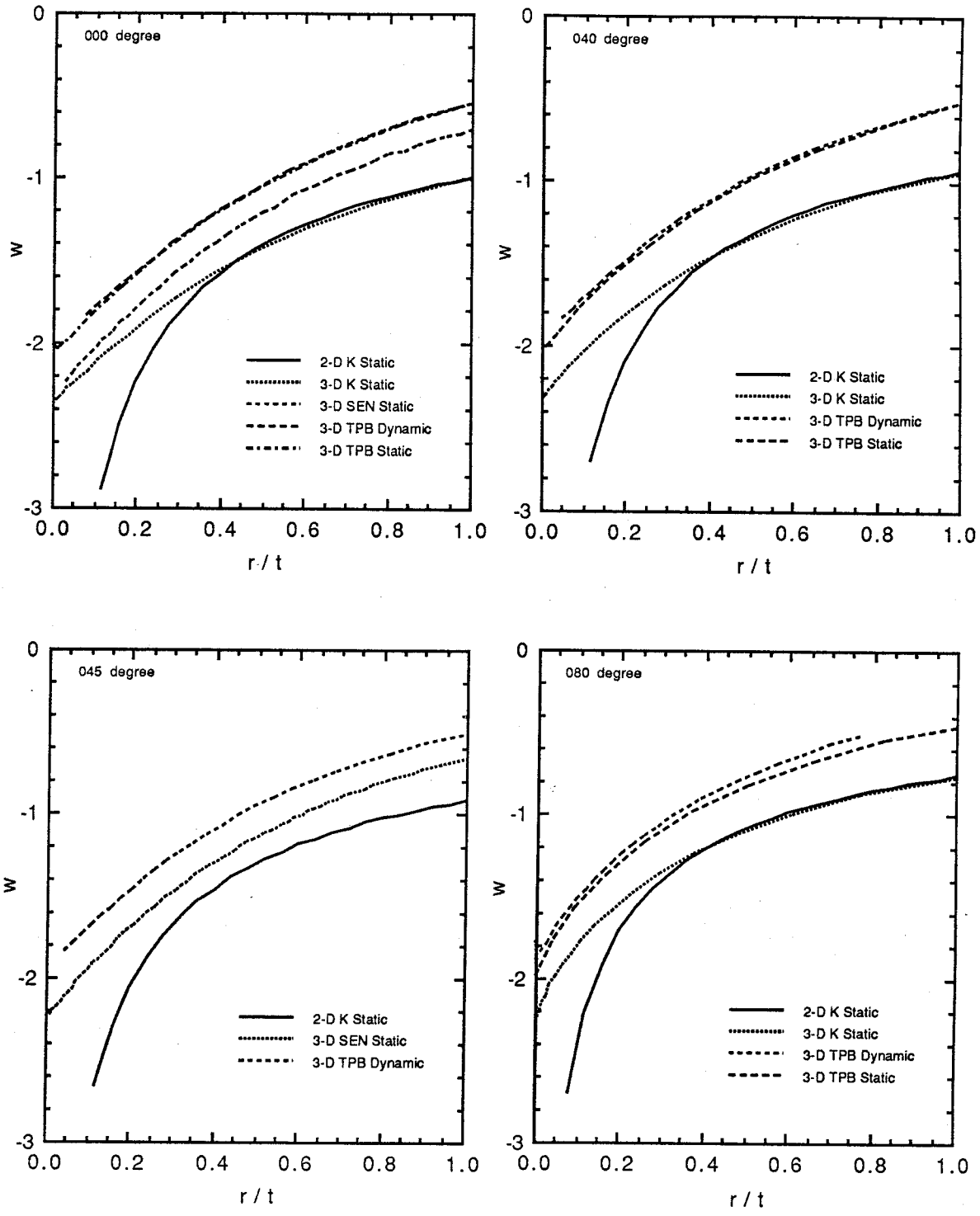

Figure (4a) Detailed comparison of static three-dimensional numerical solutions for the out-of-plane displacements near a crack tip with the two-dimensional asymptotic plane stress solution. Displacements are shown along radial lines at angles of 0, 40, 45, and 80 degrees to ligament [59,71,72,73].

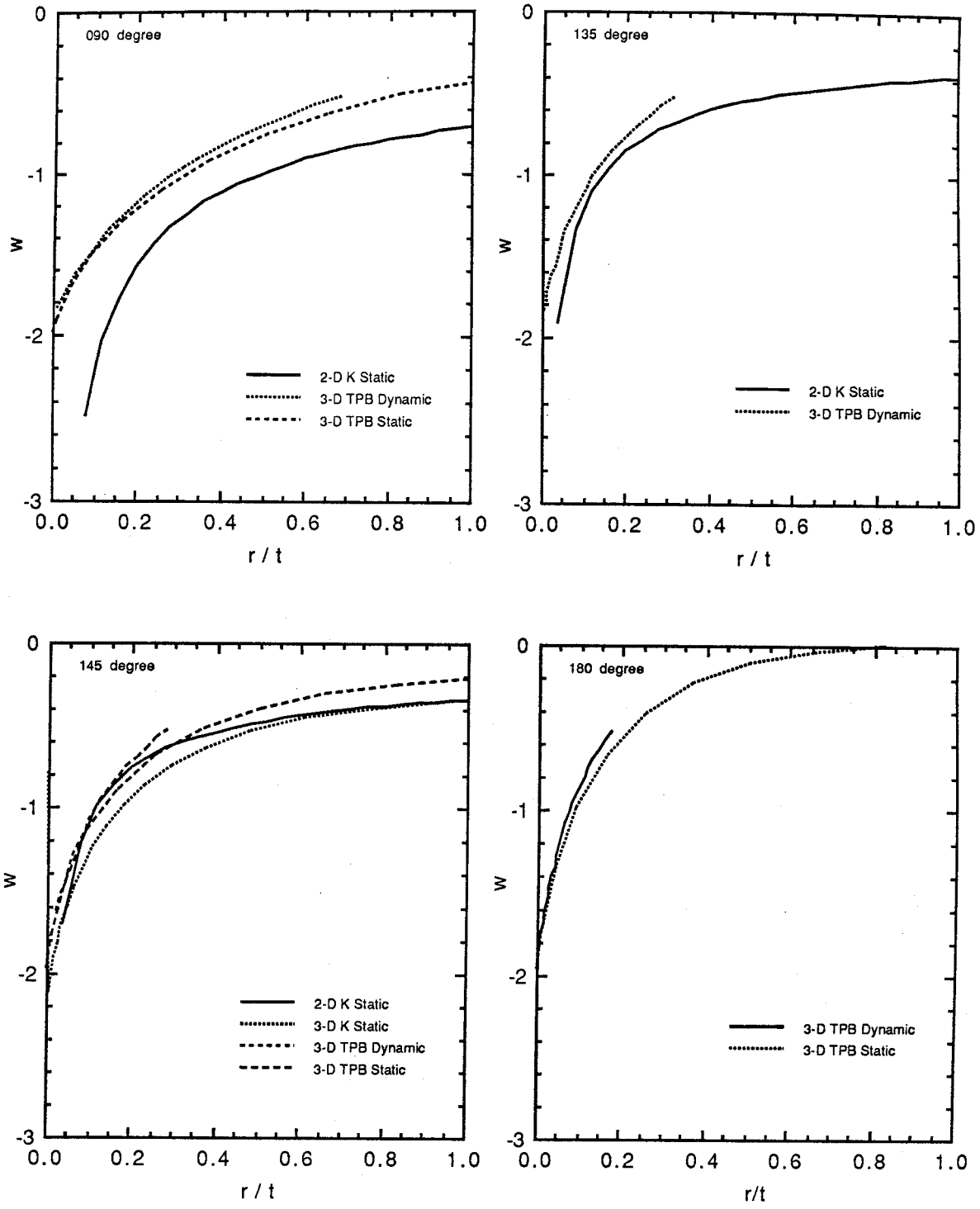

Figure (4b) Detailed comparison of static three-dimensional numerical solutions for the out-of-plane displacements near a crack tip with the two-dimensional asymptotic plane stress solution. Displacements are shown along radial lines at angles of 90, 135, 140, and 180 degrees to ligament [59,71,72,73].

4. Experiment Description

The detailed material behavior near a crack-front is deemed responsible for a crack's growth characteristics as a function of external loading [6]. In particular, possible void formation and coalescence in certain material systems is thought to govern a crack's propagation velocity [9,10]. The goal of this investigation is the direct measurement of the material behavior near a crack front under static and dynamic loading conditions.

Philosophically, the purpose of an experiment is to discover and isolate phenomena, and to establish the difference between observation and models. The discussion in this section applies this pristine experimental approach to fracture mechanics problems.

To facilitate discovery, refined experimental methods are continuously under development to make direct and definitive measurements [58]. Techniques that only rely on surface measurements will be used so that there is general applicability to common materials. Commensurate with a refinement of measurement capabilities, material and specimen topics require more detailed consideration. To isolate phenomena, it is imperative to determine or control parameters such as material properties, microstructures and spurious effects such as wave reflections in dynamic situations.

To establish discrepancies between observations and theory, measurements must tie together regions that are well-modeled, with areas that are less understood and under scrutiny. In fracture mechanics problems, this link with theory translates into making direct and simultaneous measurements of both the far and near field (with respect to the crack front) material response.

4.1. Material Considerations

As mentioned before, the material chosen for a particular fracture mechanics study restricts the generality of results, especially when non-elastic processes are involved.

Preferably, the chosen material system should be capable of both simple (well-modeled) and complex (not well-modeled) material response just by altering some parameter within the experimenter's control. For example a viscoelastic material can be altered to respond in a glassy or rubbery fashion for a fixed duration experiment, just by altering the specimen temperature. To limit the number of macroscopic length scales associated with the material, the latter should be noncrystalline. This requirement eliminates most metallics and many polymers. Noncrystalline or amorphous thermoplastics are preferred over thermosets because they are, in general, tougher and because purely temperature driven diffusion of the molecule can be used to govern interfacial bonding studies [79,80]. This diffusion characteristic will allow modification of the local microstructural fracture process by preferential introduction of weak material planes, in an otherwise amorphous material.

The particular thermoplastic chosen was polymethylmethacrylate (PMMA). This material was used because many of its properties are very well characterized and it is readily available in consistent grades and molecular weights [74]. It is mechanically stable in that it is not sensitive to pressure densification, it does not age significantly during the time of a prolonged study [75], and is also stable when heated under vacuum, thus allowing molding of the material without thermal degradation [76]. Furthermore, the material also fractures in a predominantly brittle mode, but has some small-scale toughening due to craze formation at room temperature [77]. PMMA is initially amorphous so that from a continuum aspect no other macroscopic length scales, such as grain boundaries, need to be considered at the outset of the investigation. The material is transparent which allows the use of less general techniques to investigate the internal consequences of the surface measurements.

PMMA is also sufficiently versatile to be used in studying a wide range of material response problems. Since it is only mildly viscoelastic and possesses a glass transition temperature of about $105^{\circ}C$, the viscoelastic response can be easily enhanced by heating; but at room temperature and at low stress levels the response is predominantly glassy.

Another variable which is easily altered is the molecular weight of the material. Both higher and lower molecular weights than that of the common grade used in this study are available. An increase in the molecular weight can be used to enhance craze formation in the absence of solvents [78]. For the work reported here all tests were performed using material with a mean molecular weight of 10^5 at temperatures of 22°C to 24°C.

The specific material used in this study were Plexiglas™ UVA-II manufactured by Rohm-Haas, an ultraviolet stabilized PMMA available in the form of cast sheets of four to five millimeters thickness. Also used was Aldrich EM-12 available in the form of polymerized resin pellets.

4.2 Molding

Because the Aldrich material was available as pellets it had to be molded to form plates. Even though the Plexiglas was already available in the form of plates, they were not flat enough for testing by means of interferometric techniques. A special mold was therefore constructed to cast plates from the polymerized pellets, to flatten existing plates, and to mold specimens with intentional weak planes. The mold is capable of casting plates 300 mm on a side with a thickness of up to 12 mm. The mold consists of two 25 mm thick 17-4 ph stainless steel plates, called platens, that sandwich the material to be cast and of 10 mm thick side plates that constrain the polymer from extruding out along the sides. The platens were lapped flat to less than 10 nm/mm and then polished smooth with diamond grit as fine as 1μm.

The pellets and Plexiglas were treated equally once the material was placed in the mold. The correct mass of pellets for a given thickness plate were evenly distributed in the mold, on top of the lower platen. The plexiglas sheets had paper that adhered to the surface to protect its finish. Removal of this paper was followed by an acetone rinse to remove any residual adhesive. The sheets were then placed in the mold. This operation was performed

in a room that was cleaned to prevent excessive dust contamination, and the vacuum pump was in a remote room to prevent contamination from oil vapors. The upper platen was then placed on top of the polymeric material. The entire assembly was next surrounded with woven glass breather material. This is a porous medium which allows gasses to escape during the molding process. The breather material was surrounded and sealed with a thin sheet of impermeable nylon bagging cloth. The interface between the breather and bagging material was vented to a small piston, oil vacuum pump. The assembly was then placed in a press that had independent temperature controlled platens.

To mold the material, a vacuum (29 in Hg) was established for 10^4s after which the seal on the system was verified. With the vacuum maintained, the temperature of both upper and lower surfaces of the mold was increased to the softening temperature in the time of about 10^3s and the pressure was increased to 100 psi above atmospheric conditions using a hydraulic press. The flow temperature used to cast the sheets from the original stock was 150°C. The time the material was kept at the molding temperature, the cure time, was 10^5s. At the end of the cure time the pressure from the hydraulic press was removed leaving the specimen under vacuum. Then the material was slowly cooled to back to room temperature. This slow cooling determines the specimen's flatness once it is removed from the mold. A "fast" cooling rate of about 10^{-2} °C/s produced plates that were about the same flatness as the original Plexiglas sheets. A cooling rate of at most 10^{-3} °C/s was required to obtain specimens that were and order of magnitude flatter than the original Plexiglas sheets. These slowly cooled specimens were flat to within 75 nm/mm. Once the mold and the material were at room temperature vacuum was slowly removed and the material carefully separated from the mold platens.

Specimens are constructed by machining into the test geometry. The machining is performed without lubricants to prevent the lubricants from acting as possible plastisizers. The machine tools are cooled only with compressed, filtered air. After the specimen has been shaped into its final configuration, the specimen is placed in a high vacuum chamber

and a thin layer of aluminum is deposited on the surface, in order to achieve a highly reflective surface.

4.3. Curing Calibration

To ascertain the accuracy and extent of the molding of the resin pellets and to demonstrate that weak planes could be manufactured into an otherwise homogeneous specimen the following test was performed. Two sheets were cut from the same previously molded material. The edges of the plates were finished with a high-speed end-mill and not subsequently touched. The two plates were finished to a length so that when they were place together and compressed with the sides of the mold, the material was strained in its plane to about 0.1%. The same molding procedure was followed as outlined in section 4.2, except that the curing time and molding temperature were varied. Extra care was taken

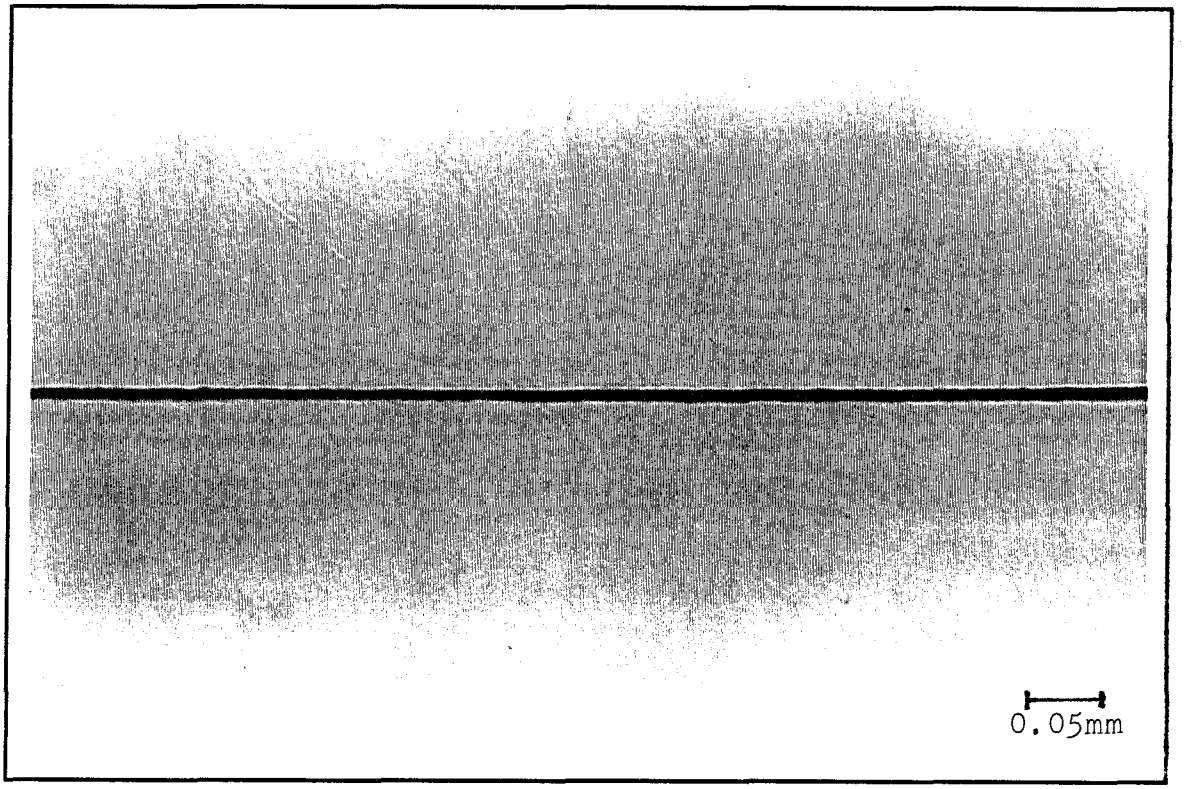

Figure (5) Magnified view of the interfacial region healed at 110°C for 3 hours and illuminated in transmission.

so as to not to load the interface once the specimen was removed from the mold. An interface from this procedure, and resulting in healed material is shown in Figure (5).

From the healed plate a compact fracture specimen was machined as shown in Figure (6). This geometry is close to a standard ASTM specified "compact fracture specimen" geometry except that the thickness is less than required. The notch was slit saw cut, filed to a radius of approximately 0.5 mm and the crack started with the impact of a razor blade.

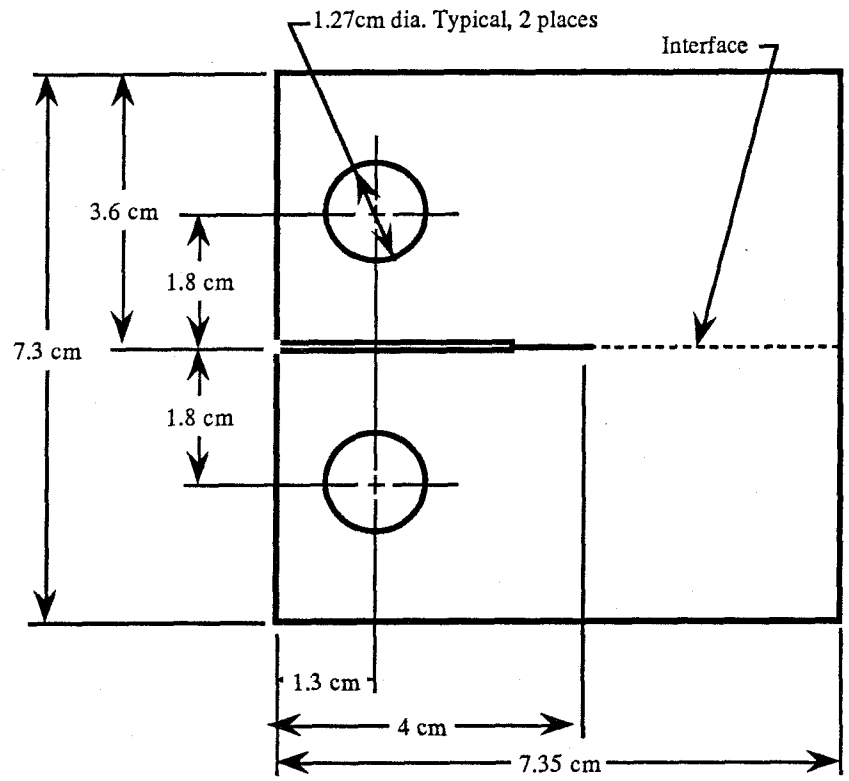

Figure (6) Compact fracture specimen geometry used to calibrate interfacial strength, 5 mm thick.

The blade-started crack was fatigue loaded with a 1.0 Hz sinusoidal waveform until the crack propagated to a length of 40.0 mm. Once at this length the end displacement was slowly increased and the load recorded until the crack started to propagate. The maximum recorded load was taken as a measure of the of the strength of the interface. The crack

always propagated straight and in a brittle fashion. The same tests were repeated on specimens manufactured out of the identical virgin material without the interface. The results of these tests are shown in Figure (7). As one would expect, as the molding temperature or cure time is increased the strength of the interface also increases. Tests at higher cure temperatures of 150°C and 140°C were performed, however, the interface was either not distinguishable from the parent material, or achieving crack propagation along the interface was not accomplished.

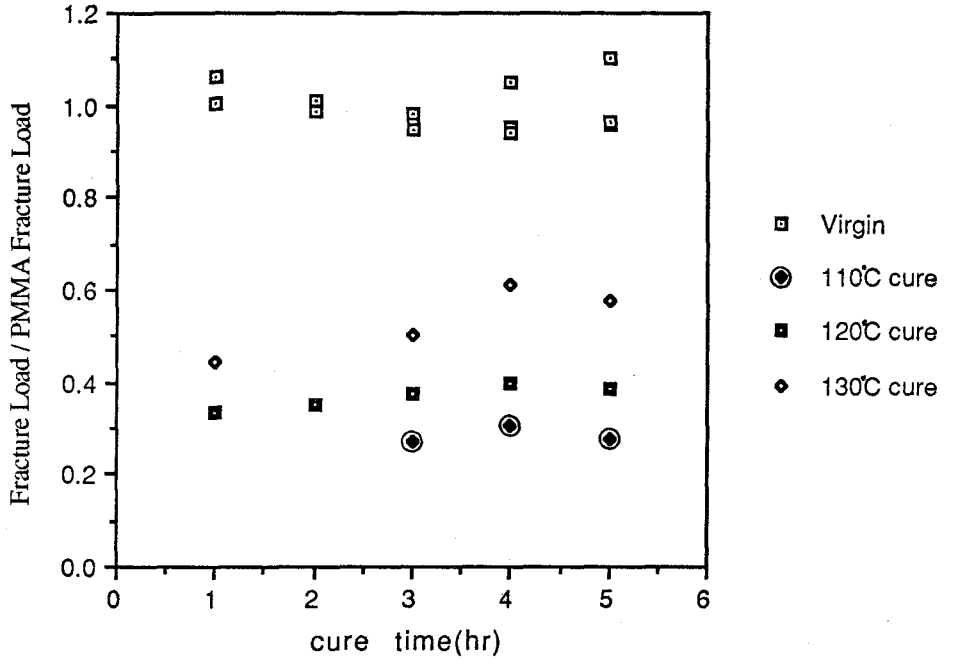

Figure (7) Strength as a function of cure time and molding temperature for virgin and interfacial PMMA specimens at 0.1% strain contact.

Shown in Figures (8) and (9) are the out-of-plane displacement contours for both a virgin and healed specimen. The measurements were taken with the Twymann-Green interferometer described in the following section. These measurements are presented here to illustrate some problems with the use of the compact fracture specimen geometry. The

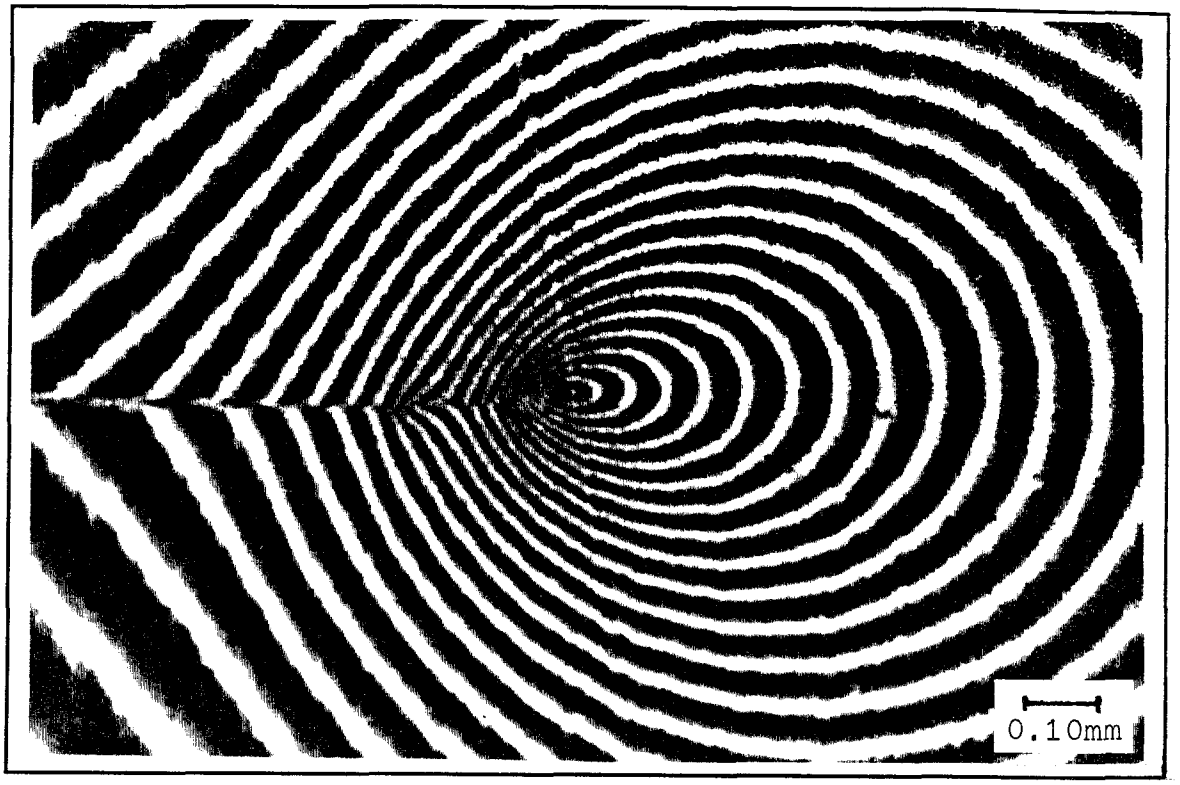

Figure (8) Out-of-plane displacement contours of a virgin PMMA specimen.

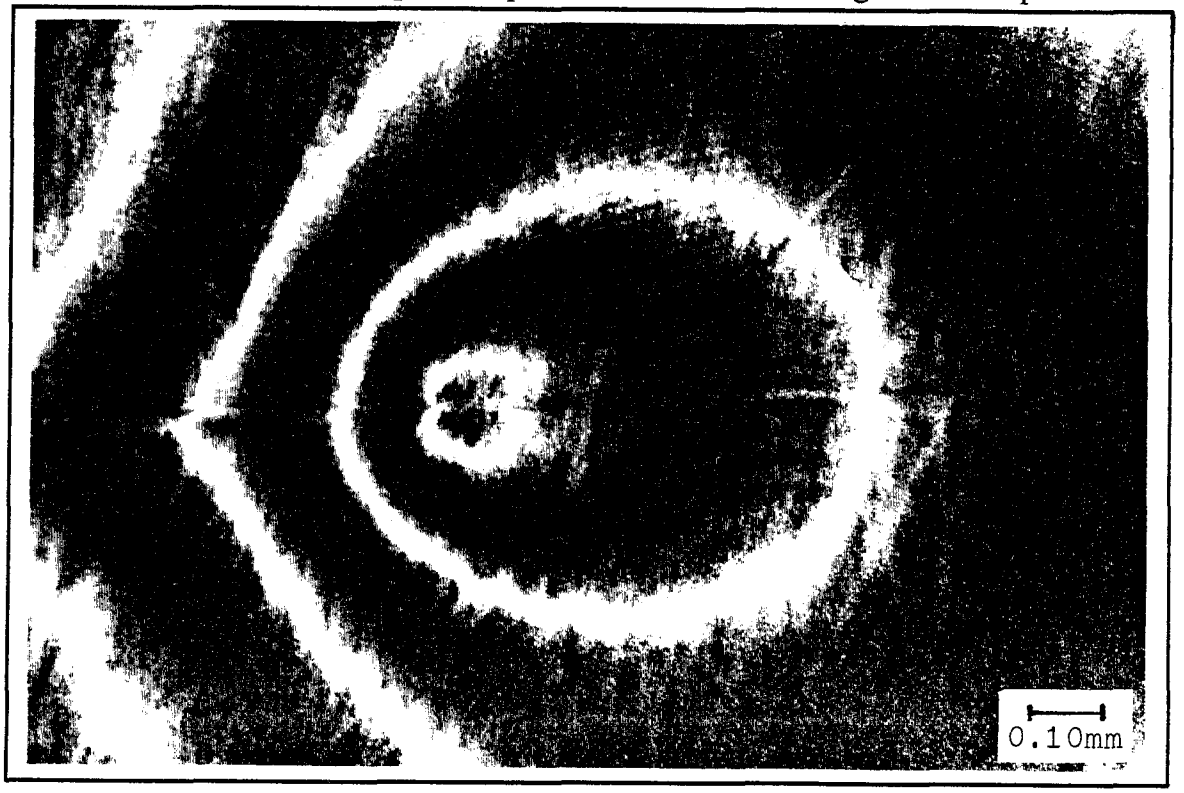

Figure (9) Out-of-plane displacement contours of a horizontal crack in a PMMA specimen healed at 110°C for 3 hours, at critical load.

thin specimen geometry is not stable, the flanges tend to twist [58]. These interferograms were painstakingly aligned to produce reasonably symmetric contours.

These photographs were taken near the critical load at which the crack starts to propagate. Consequently, the difference in fringe density at the crack tip is due to the strength difference between the two specimens. Note that in the healed specimen the interface is visible as a doubly lobed out-of-plane displacement contour at the crack-tip.

The fracture load results give confidence that the molding procedure is adequate to fully bond all individual PMMA pellets. Molding at $150^{\circ}C$ for as little as one hour is sufficient to loose visible evidence of the interface and retain the virgin material fracture load. The actual molding time for the virgin material is an order of magnitude greater. Furthermore, these tests demonstrate a method to construct weak planes and modify the local fracture process in thermoplastic specimens. Unfortunately, the compact fracture specimen's geometry sensitivity to flange buckling does not give confidence in the out-of-plane measurements. Consequently, a less-error-prone set of experiments were developed.

4.4. Test Procedures

A test procedure was used that allowed the testing of identical samples under both static and dynamic loading conditions. The testing of identical samples conserved the effort involved in slowly cooling the material to maintain flatness. The specimen geometry used for these tests is shown in Figures (10), (11), and (12). The material was molded flat and aluminized as described before to give a smooth reflective surface. The static test geometry is close to that of Single Edge Notch specimen. The reason for this configuration was so the plate would be in tension to eliminate any flange buckling problems that were present in the compact fracture specimen geometry. Furthermore, having the specimen in tension flattens any initial warpage of the surface. Single holes were used as loading points so that they could be easily filled with PMMA plugs for the dynamic tests. The location of

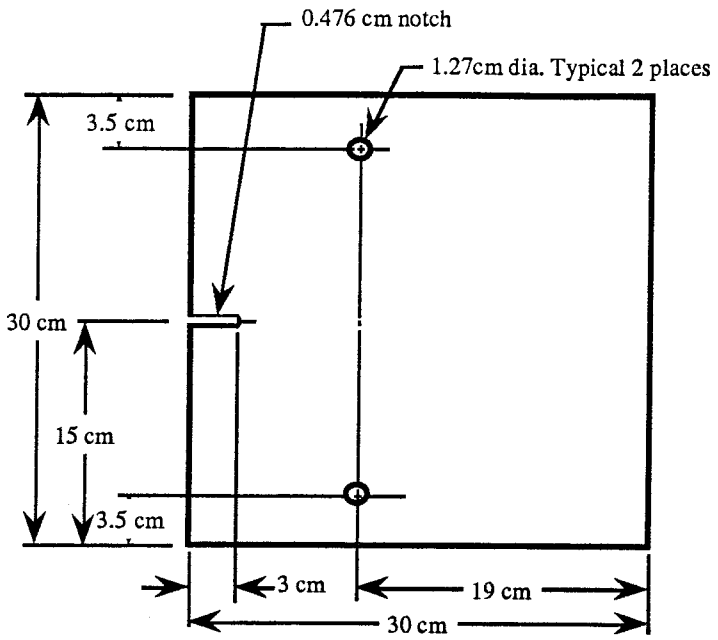

Figure (10) Specimen geometry used for the static experiments.

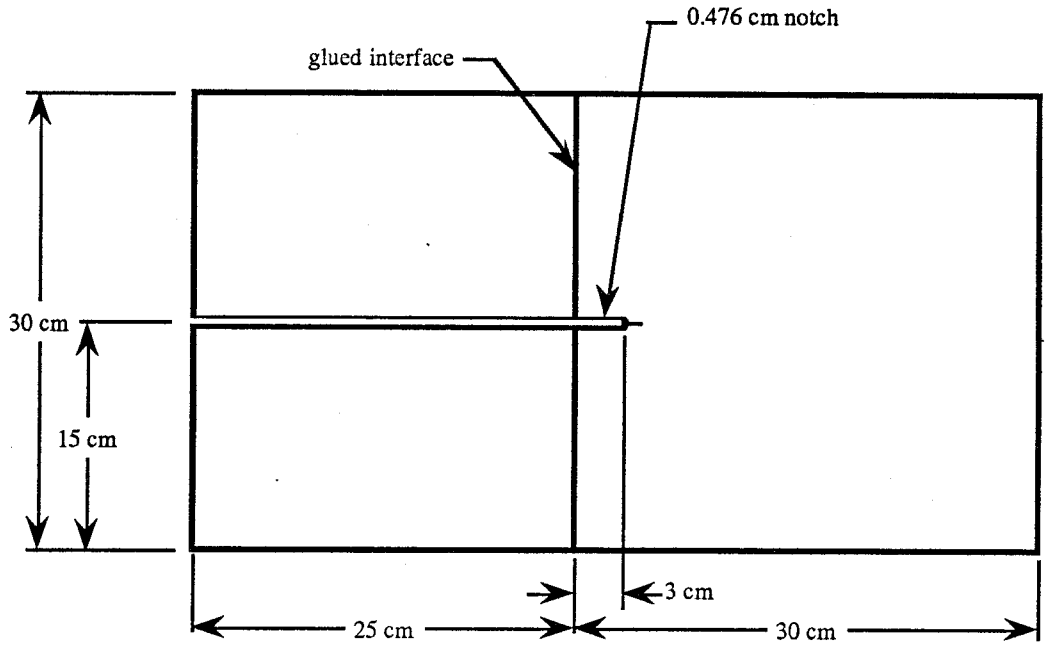

Figure (11) Specimen geometry used for the long duration dynamic experiments.

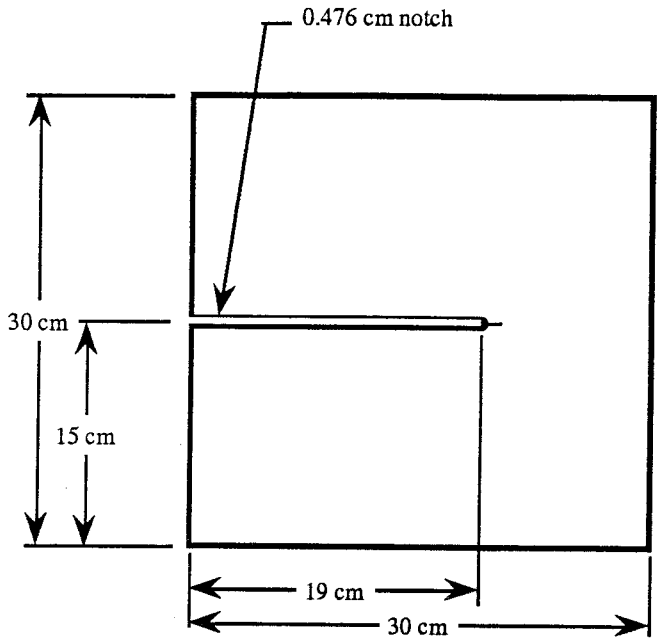

Figure (12) Specimen geometry used for the short duration dynamic experiments.

the holes were dictated by the equipment (e.g., the loading frame and optical table) available to perform the static tests in a vibration isolated environment.

The overall size and location of the notch and crack for the static tests were governed by the dynamic test requirements and economic factors. The largest mold, press, and lapping capability available before costs started to escalate was approximately 300 mm square. This size is sufficient for a thermoplastic such as PMMA with a dilatational wave speed of about 2 mm/μs and a shear wave speed of approximately 1.1 mm/μs to give a total test time of about 150 μs. This time allowed clean dynamic testing that was free of boundary wave reflections [83], thus simulating an infinite plate for the 150 μs duration of a test. The notch, 0.476 cm wide, was cut with an end-mill 30 mm into the static portion of the specimen. The width of this notch was governed by the electromagnetic loading coil to be discussed later. A chevron notch [104], approximately 3.0 mm long at both surfaces and about 0.5 mm in length at the middle of the plate was filed at the tip of the milled notch using a jewelers' file. Finally a razor blade was impacted at the base of the chevron notch

(at the center of the plate) until a crack propagated approximately 3.0 mm, the length of the entire filed section.

Once the crack was initiated using the razor, the specimen was used in the static tests. The crack was further advanced and recorded during the static tests.

After the static tests were completed two pieces of PMMA were glued to the static specimen to form the dynamic specimen. The holes used for the loading pins were filled with the same thickness of PMMA. The two legs and hole fillers were bonded to the specimen using adhesives. Two equally useful adhesives were tried, Methylene Chloride and Methylmethacrylate.

The central measurement instrument common to both the static and dynamic experiments is the Twymann-Green interferometer [58]. A schematic of the interferometer is shown in Figures (13) and (14). The interferometer consists of a collimated, coherent light source that is divided at a beam splitter. Half of the light is transmitted toward the specimen, while the other half is reflected toward the reference surface. The reference surface used was a flat mirror. The impinging light on the specimen is reflected and is distorted due to the specimen deformation. This light then propagates back toward the beam splitter, half of which is reflected toward the detector. The light reaching the reference mirror is reflected and half of this is transmitted through the beamsplitter to also reach the detector. At the beamsplitter, the light returning from the specimen and the reference mirror interfere. The information from this interference is recorded with the camera.

The information recorded at the detectors consists of fringes whose spacing represents an out-of-plane deformation of the surface of half of the wave length of the illuminating light. The details and tricks to using such an interferometer in fracture mechanics experiments where deformations and aperture requirements might be large is addressed by Pfaff [58]. The difference between the interferometers shown in

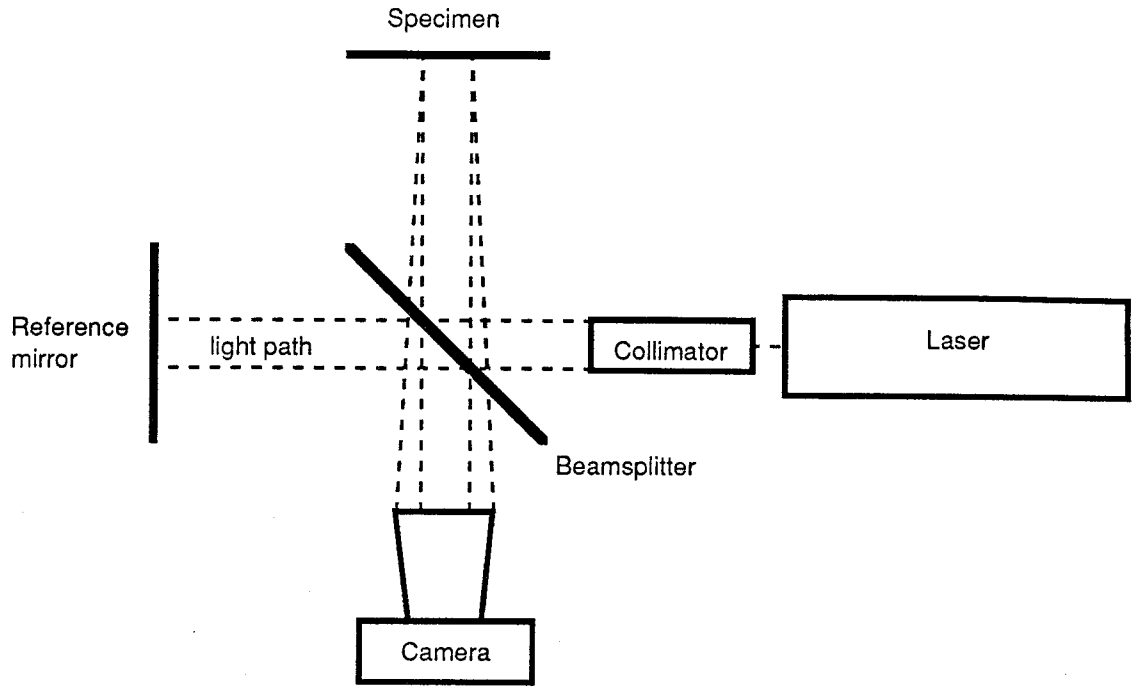

Figure (13) Schematic of the Twymann-Green Interferometer used for the static experiments.

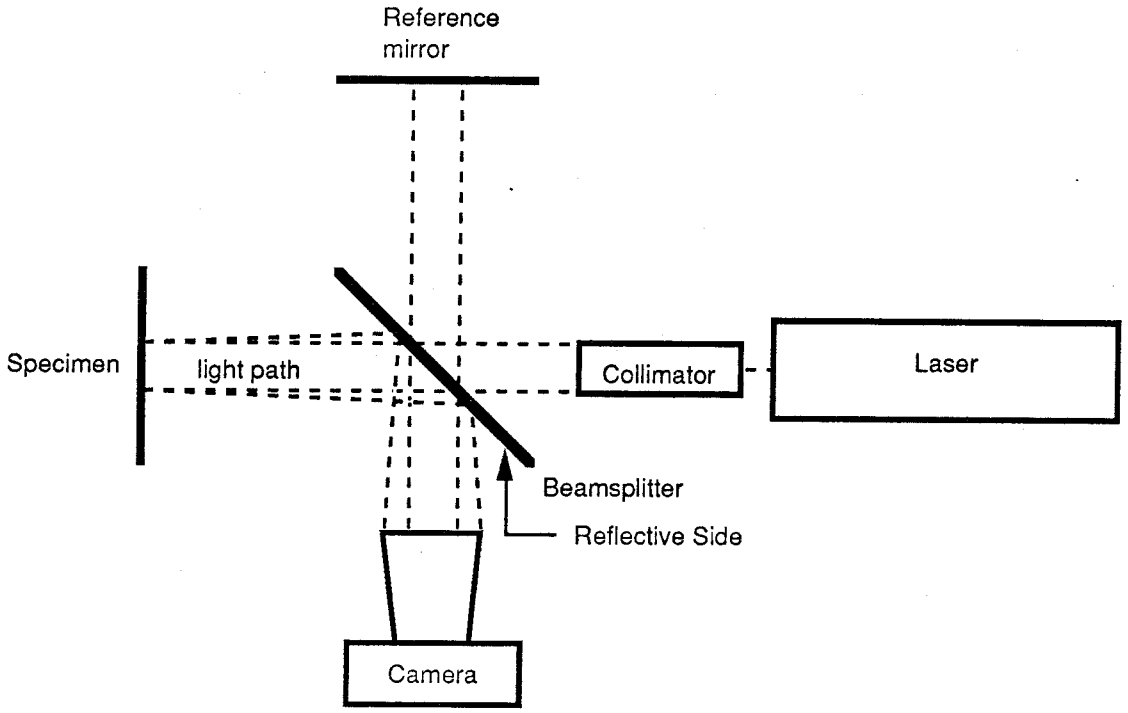

Figure (14) Schematic of the Twymann-Green interferometer used for the dynamic experiments [58].

Figures (13) and (14) is that in the later configuration the beamsplitter, specimen and reference surface are properly positioned to not introduce added distortion at large angles due to the non-unity refractive index of the glass in the beamsplitter. For the experiments reported here, the specimen thickness was chosen to be small and the optics designed so that optically large angles and large required apertures would not be encountered.

4.4.1. Static Test Procedures

The equipment used in the static tests is displayed in Figure (15). The interferometer and screw loading machine are mounted rigidly to an air isolated optical table. An electrical strain gauge load cell and linearly varying differential transformer are used to measure the load and displacement at the specimen boundaries, respectively. The isolated table is required to limit building vibrations. For this particular loading frame, although it was motorized, was hand operated to not introduce any further vibrations, thus, the loading was performed in a fixed displacement mode.

Figure (16) displays a detailed view of the interferometer and the loading frame with a specimen installed. To achieve consistent interferometric quality loading of the specimen, the loading system required some non-standard modifications. The most important step in this regard is to choose a specimen geometry that is loaded primarily in tension to minimize the flange buckling problems that are encountered with the compact specimen type geometries. Other modifications were performed to reduce unwanted shear loading at the pins. A universal joint was placed in series with the lower pin and an ball joint was placed in series with the upper loading pin to alleviate bending due to load frame misalignment. In addition, the specimen needed to be precisely aligned, to better than 0.05 mm, within the grips. This alignment was accomplished by placing spacers between the specimen and loading grip flanges to precisely center the specimen in the grip and to account for any change in specimen thickness.

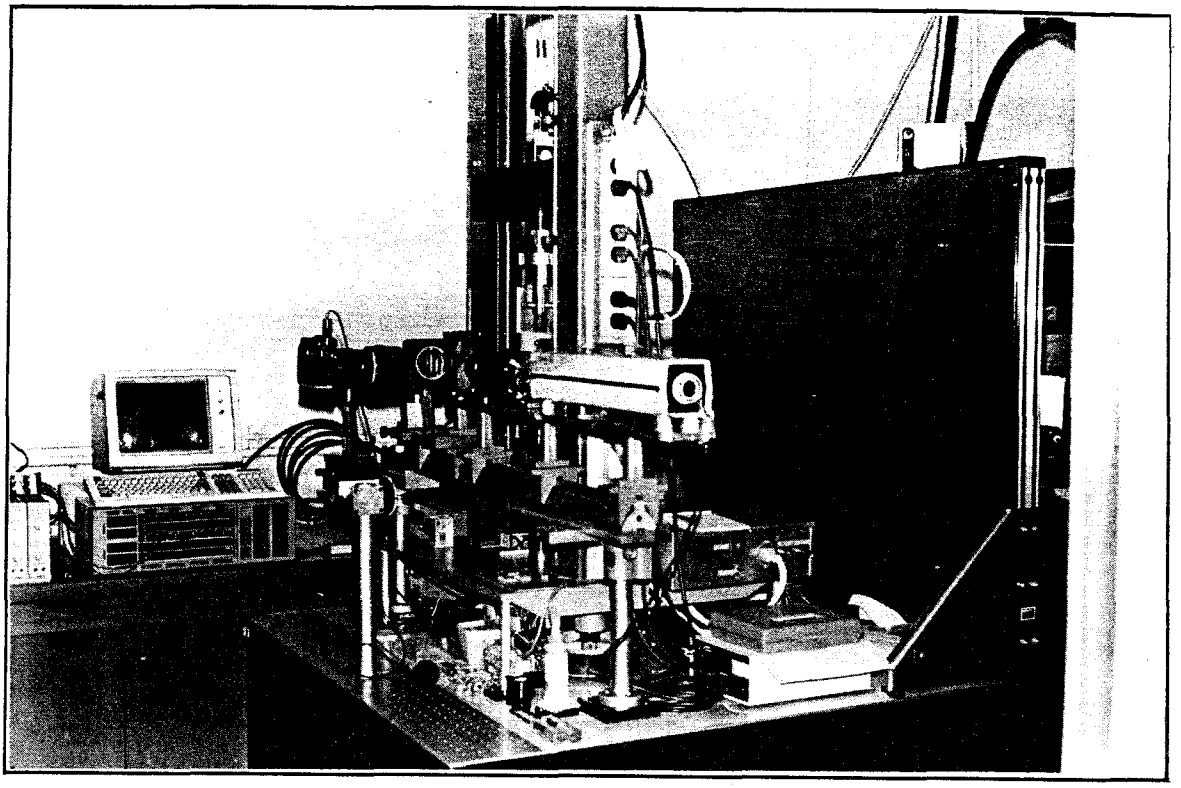

Figure (15) Static test equipment: loading frame, air isolated optical table, data acquisition computer, and an interferometer.

The interferometer was constructed to produced superior measurements by providing uniform illumination of coherent light. The laser used was a 15 mW HeNe laser. The beam from the laser was expanded, filtered and collimated by using a microscope objective, pin hole and collimating lens, respectively. The microscope objective was 80X and was not matched to the collimating lens which was a Nikon 200 mm f/2 internal focusing lens with a 52 mm exit pupil. This over expansion was accomplished at the expense of losing some light and increased exposure times to improve the uniformity of the collimated light [81]. After the light was collimated the beam was further filtered by using a Gaussian compensator. The Gaussian compensator consists of two lenses cemented together. One lens is convex and is made of a translucent glass. This lens is thicker in the

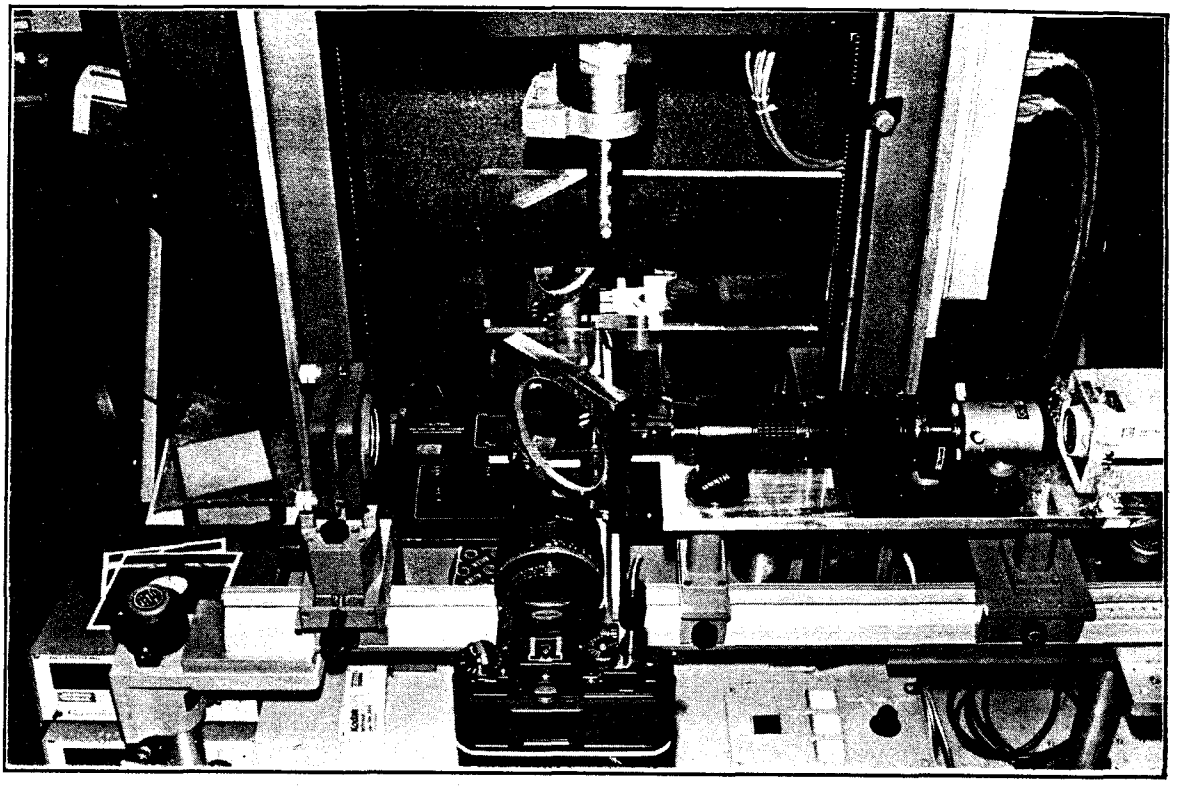

Figure (16) Detailed view of the static Twymann-Green interferometer: HeNe laser, beam expander and collimator, reference mirror and 35 mm camera-back.

middle thus absorbs more light, and compensates for the brighter central portion of a normal Gaussian beam. The second lens compensates for the refractive ability of the translucent element. The position and alignment of the microscope objective was tuned by trial and error to produce the most uniform intensity output beam. The Gaussian compensator was not fully corrected so that the the position of the collimating lens had to be adjusted slightly to compensate for the additional refraction. The resulting beam was uniform in intensity, as measured by a video camera, to better than 1% , and flat to within one-half wavelength.

The reference mirror was mounted in a tilt stage and had an aperture in the shape of an octagon that measured 40.96 mm across the flats. This octagon was used in subsequent photographic processing as a reference of integrated magnification and distortion.

A difficulty in using this interferometer for fracture mechanics specimens is the ability of the optics to collect the light. This light collection difficulty is a recurring limitation. The collection lens used for these experiments was a Nikon 105 mm f/1.8 lens with a 42 mm extension ring. The light collection capability of this system was not limited by this lens. Because the test occurred over the space of an hour, the experimenter needed access to the controls of the tilt stage of the reference mirror to account for small rigid body rotations still introduced by the load frame. This necessitated the arrangement of the elements of the interferometer as shown in Figure (13) which is different than the arrangement in Figure (14). The difference is in having the distorted beam, rather than the planar reference beam traversing the refractive portion of the beamsplitter. The distorted beam will have aberrations introduced by traversing a plate of finite thickness, with non-unity index of refraction, and oriented at a non-perpendicular angle to the beam. Beams that are planar, such as the original collimated beam and the beam returning from the reference mirror do not have this problem, they merely get displaced. Consequently, the superior orientation is that shown in Figure (14), and will image the specimen via the reflective portion of the beamsplitter. The laws of reflection will not introduce these aberrations. For the measurements reported here, the effect of the flat plate of the beamsplitter is not important because the resulting angles for the thin plate static tests are small. However, to make measurements of specimens with large surface slopes the arrangement shown in Figure (14) should be used exclusively.

After the specimen has been suitably manufactured it is centered in the grips of the static load frame using spacers. The specimen is then loaded to about half of its ultimate load. At this load the alignment of the interferometer is checked to make certain the optic axis of the interferometer is positioned properly on the specimen. The recording system is focussed on the reflective specimen surface by illuminating the surface with light from a flashlight and blocking the image to the reference mirror. The specimen is frequently collecting dust so it is a simple matter to focus on the dust that is on the specimen surface.

The reference mirror is then brought into focus. This adjustment is made by moving the mirror along the optical rail until the octagonal mask and dust on the specimen surface is brought into clear view. At this point the laser is turned on and the camera-back removed. The distorted image of the light coming from the specimen is viewed on the room wall. The upper grip, which is constrained with a ball joint was then twisted so as to produce a symmetric image. Next, the focus of the rays coming from the specimen and the reference surface are viewed through a translucent screen. The focal points are brought together by adjusting the tilt stage of the reference mirror [44]; at this point the rays coming from the specimen and the reference mirror should be centered on the optic axis of the imaging lens. A necessary test of this condition is to decrease the aperture of the lens and observe a symmetric shadowing of the image. Next, the camera-back is replaced and the specimen is viewed. The upper grip and reference mirror are adjusted until the view of the deformation is symmetric. Finally, all but about 10 N of the load is removed.

The isolation of the experiment from vibration allows an increase in exposure times. The film used to record the images from these experiments is Kodak Technical Pan Film 2415 used at an ASA rating of 25 and developed with Kodak Technidol Low Contrast Developer. This is a fine-grained black and white film. The camera-back used was a Nikon model FA in automatic exposure mode and resulted in exposure times of 1/250 s to 1/500 s.

The test commenced by the cleaning of the specimen and other optical elements with compressed gas. A photograph of the surface at the low load was taken and assumed to be the unstressed reference configuration. Bracketing of the exposures was not necessary with the automatic exposure control. The load was slowly increased by 100 N increments. After each increase it was usually necessary to tweak the upper grip in torsion and adjust the reference mirror to maintain a symmetric image with respect to the crack flank. After a symmetric interferogram was established the specimen was watched for a few minutes, after any vibration from the experimenter's adjustments had ceased, to see if anything

interesting was occurring. After every load increment of 500 N a photograph of the surface was taken. During the waiting period, the specimen was viewed with the expectation that the crack would start to propagate. After the load reached its maximum, the crack was allowed to slowly propagate for about the thickness of the plate. Once the crack had propagated this distance, a photograph of the slowly propagating crack was snapped and the load immediately reduced to near zero to prevent dynamic crack propagation. As the crack length is increased, this is an unstable specimen geometry for this material and for a fixed external displacement from a compliant load frame [23].

4.4.2. Dynamic Test Procedures

The equipment used for the dynamic tests has been collected over the years from the work of many researchers [82,83,6,58]. I will describe the salient functions and modifications. The equipment used in the dynamic experiments is displayed in Figures (17) and (18). The optical arrangement is analogous to that of the static arrangement, however, now the temporal capability of the camera system has been greatly improved. The dynamic loading mechanism is similar to that used by Smith [83], while the optical equipment is analogous to that used by Pfaff [58].

The loading mechanism is an electromagnetic loading device that can quickly load the crack flanks. A schematic of the loading coil used for this experiment is shown in Figure (19) and was suggested by Pfaff [58]. A thin copper strip cut to the width of the specimen is covered on one side with a thin layer of insulator. The strip is then folded over itself three times. Both ends of the copper strip are connected to a capacitor bank. When the capacitors discharge through the coil the set of copper strips on either side of the

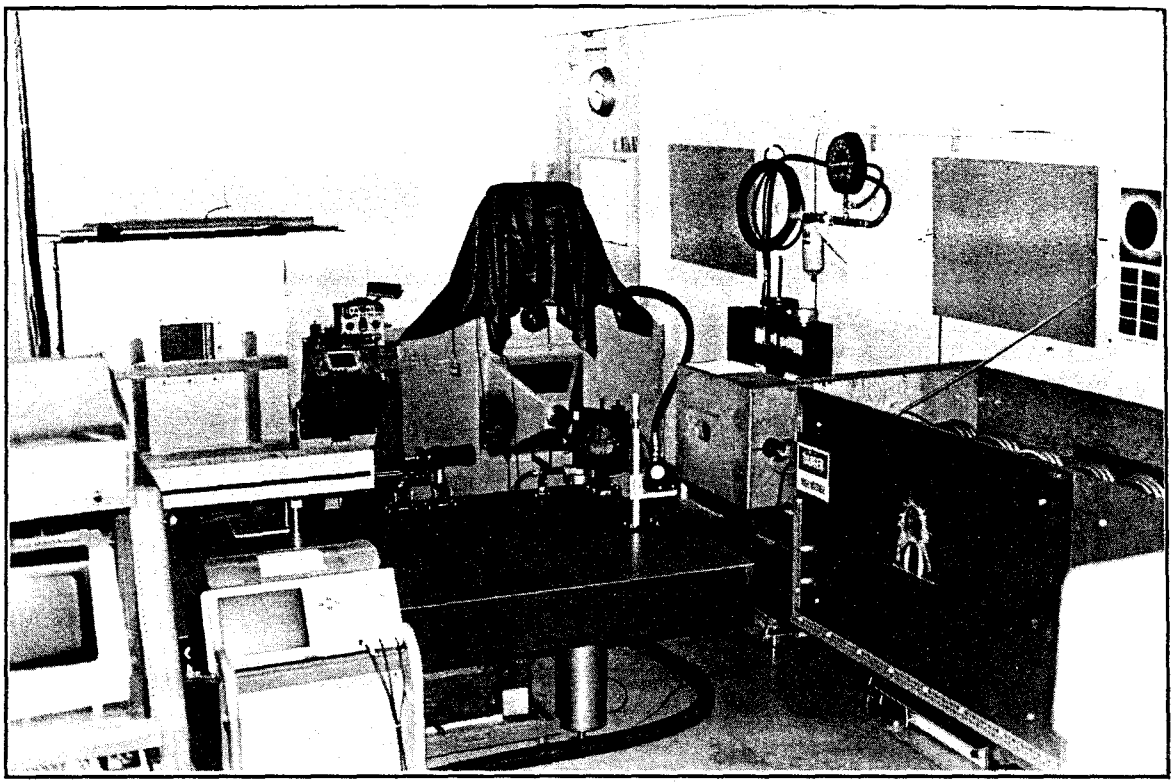

Figure (17) Dynamic test equipment: capacitor loading bank, optical table, data acquisition system, and an interferometer.

specimen are thrown apart by the electromagnetic forces. The coil tries to form a circle. The triple-wrapping of the coil effectively triples the effective current allowing the capacitor bank to operate at lower voltages for the same force output when compared with a single wrap coil. This development was important to be able to break the comparatively tough PMMA specimens.

The capacitor bank consists of capacitors with 120 kJ maximum energy storage at 20 kV. The capacitors are housed in a plywood box covered on the outside with aluminum to act as a Faraday shield. Inductors that act as a delay line are used to condition

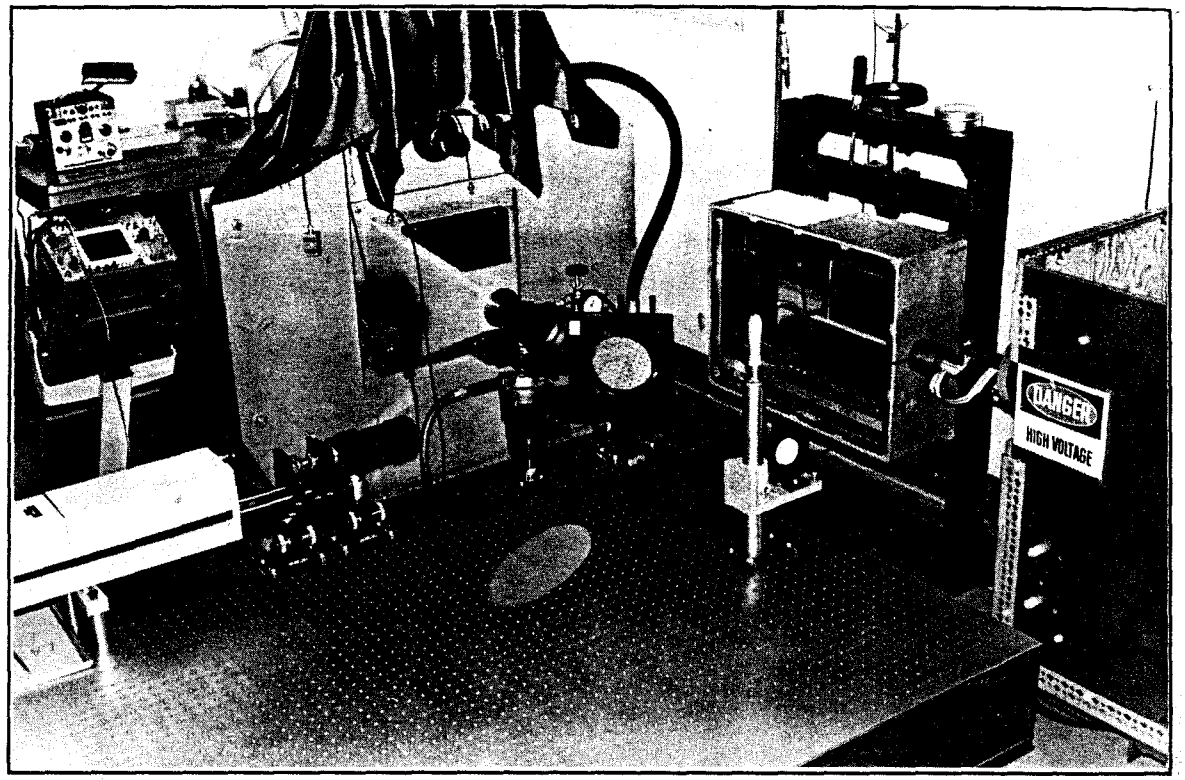

Figure (18) Detailed view of the dynamic test equipment; pulsed argon-ion laser, beam expander and collimator, beamsplitter, reference mirror, and a turbine camera.

the discharge of the capacitors to approximate a square current pulse. The inductors are 13 mm diameter copper rods, circularly wrapped to a 152 mm inside diameter, and insulated with 3 mm thick PVC tubing. The use of a triple-wrapped loading coil has the drawback of an increase in inductance, thus having a parasitic effect on the rise-time of the pulse. This increase in inductance was compensated by decreasing the inductance of the lead inductor in the capacitor bank. The capacitor bank is switched with an ignitron (a mercury liquid to vapor switch). The ignitron is triggered with a thyrotron [82] which in turn is triggered by a high voltage solid state relay. This arrangement produces an appreciable but consistent delay in the triggering of the loading. The current is measured

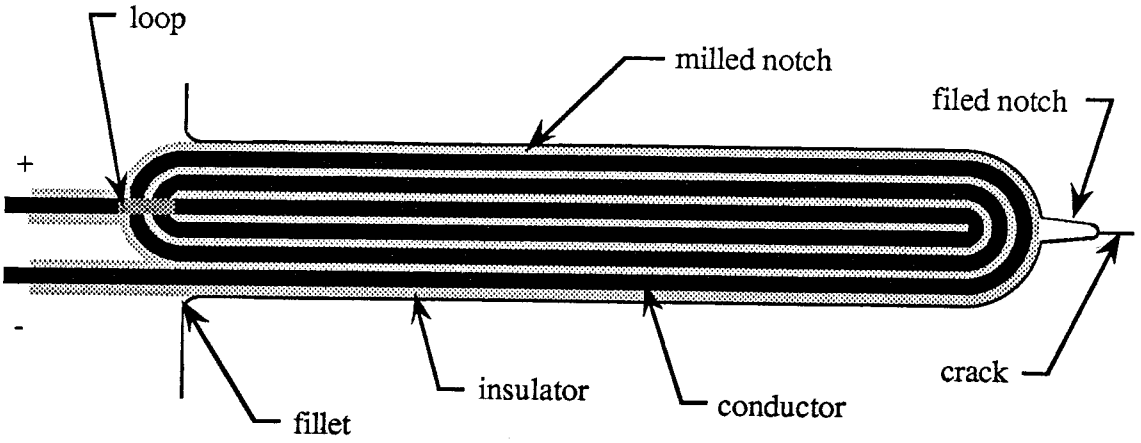

Figure (19) Schematic of the electromagnetic loading coil, 5 mm x 0.5 mm thick copper, 25 mm x 0.2 mm thick cellophane insulation.

with a Rogovski coil [83]. A typical loading pulse is shown in Figure (20). Pulses which had a superior square wave form were achieved, but after several months degraded to the pulse shown in Figure (20). It is assumed that this degradation was due to oxidation of the surface of the delay line inductor coils.

The wrapping of the coil to produce higher loads on the crack flanks to operate at lower capacitor bank voltages has other drawbacks. One problem with the coils is that they are now more difficult to manufacture. A satisfactory insulator material is translucent cellophane tape with adhesive on both sides. The coil is wrapped and simultaneously stuck together. Care must be taken to align each wrap. The triple-wrapping of the coil also tends to short out at the corners, near the end of the crack flanks. To correct this problem the crack flank corners were rounded. Another potentially more serious difficulty is that the coil is now made out of three times more material than used in a single wrap coil.

Because the Twymann-Green interferometer needs to be as close to the specimen as practical there is a possibility that the triple-wrap coil might unwind, reach out, and contact nearby equipment with high voltages. Consequently a containment vessel was constructed

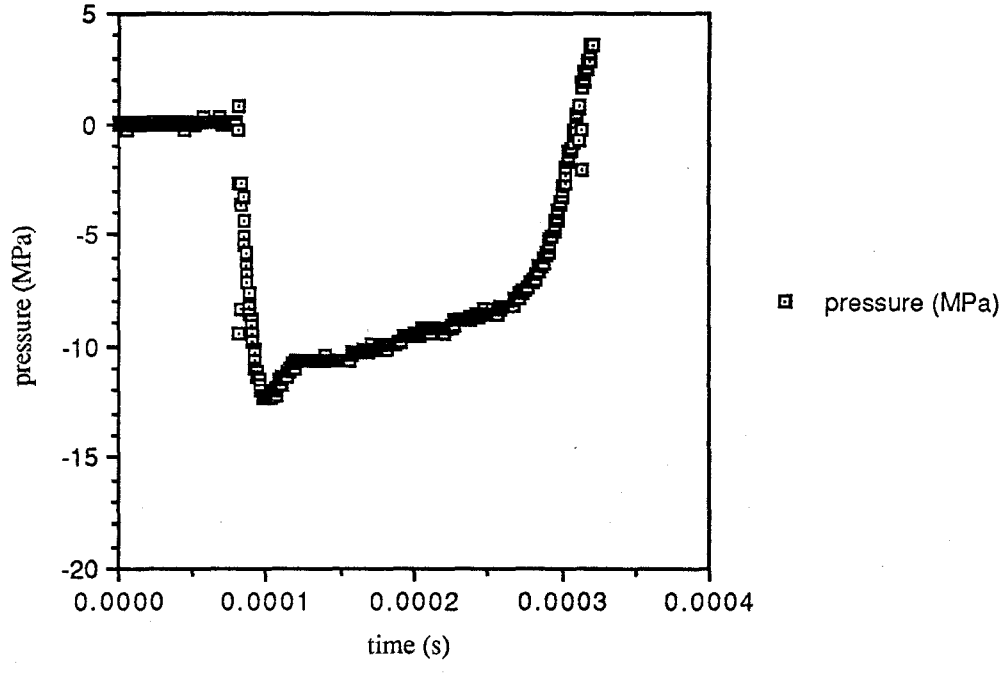

Figure (20) Typical loading pulse along the crack flanks.

out of a 12 mm thick cast aluminum electrical box, internally insulated with 25 mm of phenolic and a 4 mm thick polycarbonate impact barrier. The specimen is mounted in a jig that supports near the corners, at the periphery of the specimen. This jig is placed in the containment vessel and the cover secured with screw fasteners. The specimen is viewed through an oblong aperture 100 mm wide by 200 mm long. The loading coil exits the containment vessel through a 76 mm diameter hole. The coil is prevented from contacting the vessel by an annular ring of solid polycarbonate that is 76 mm in diameter by 152 mm long with a 25 mm centered hole. The loading coil is centered in the polycarbonate tube with two 8 mm thick sheets of neoprene.

Delay and pulse generators are used to sequence the the experiment from a single source. A mechanical shutter to the turbine camera was signalled 1 ms prior to the triggering of the loading coil to enable recording. Photographs commenced at 100.0 μs

before the start of the loading pulse. By adjusting the delays, photographic sequence and the loading pulse are synchronized to within 0.5 μs

The Twymann-Green interferometer used in this experiment is shown in figure (18). The arrangement is the interferometer shown in Figure (14) and the operation is analogous to the static interferometer already discussed except for a few differences. The light source is a pulsed 5W argon ion laser tuned to a wavelength of 514 nm. The light is expanded, filtered and collimated using an analogous arrangement as in the static case. However, here the light is not over-expanded at the microscope objective, nor is the collimated beam Gaussian compensated. The reason for this is that the dynamic tests are light limited and the loss of light though these compensation procedures cannot be tolerated. In this case the optical elements are sufficiently far apart to make use of the adjustable nature of Nikon 200 mm f/4 internal focussing collimating lens. Since the lens can adjust the collimated light to a point at a selected distance this makes alignment, matching distances, and focusing possible by focusing the impinging light on the specimen, and then moving the reference mirror and other optics to maintain the focal point at image planes.

The camera used for these tests has gone through extensive modification. The mechanical housing is essentially the same as detailed by Beebe [82], however, the optical components have gone through extensive redesign to improve the light collection capability [58]. Even with these optical improvements the camera still operates at approximately f/22 which severely limits the surface angles that can be measured. The front collection lens is a Nikon 200 mm f/2 internal focusing lens. The next optical element is a 40 mm field lens at the focal plane of the front collection lens. A Nikon 200 mm f/4 internal focusing lens focuses the image at the field lens to the film plane. The film plane is reached by reflection off a mirror oriented at 45 degrees with respect to the optic axis and mounted on a turbine. The turbine is spun with compressed gas, which in turn rotates the mirror and distributes the light along an annular film track of 1 m in diameter [82]. Because the rotating mirror

design introduces a rotation into the image, an octagon placed on the reference mirror is used as a reference orientation. Because of the flexible nature of the bayonet mounts of the Nikon optics, careful alignment of the optic axis is required.

The film used for these experiments was Kodak T-max 400 film, developed with T-max developer. The pulsing of the laser acted to shutter and freeze the images. In order to freeze the image the light must be pulsed rapidly enough in comparison with the mechanical motion. This criteria translates into essentially a Rayleigh criteria of resolution which is that the image will move less than the minimally resolvable fringe on the film plane. The mechanical motion that is the fastest for these tests was the rotation of the 45 degree mirror. To use the full width of the film, and since the Bragg cell on the laser was limited to exposures of approximately 15 ns, assuming a minimally resolvable fringe for this f/22 camera results in a minimum time between frames of approximately 20μs.

The experiment was aligned by removing all optical elements except the collimation optics. The specimen was placed in its containment vessel and closed. The entire vessel was then translated and tilted to return the beam back into the laser from the location of interest on the specimen. Next, the beam splitter was placed at 45 degrees to this path with care to make sure the reflective side is toward the camera and the specimen. The light was then focused to a point at the specimen. The reference mirror was placed and centered at the focal point on the reference leg of the beam path. The high-speed turbine camera was aligned in an iterative process by centering the light focused from the reference mirror at various apertures on the camera housing. The front optical element was installed, its centration checked by closing the lens aperture and noting a uniform closing of the aperture on the image. The location of the focal planes was checked by again focusing the light on the specimen (and the reference mirror) and checking a point focus at both the field lens position and at the film plane with the internal 200 mm f/4 lens installed. Minor adjustments of the reference mirror are performed in an iterative process to minimize the number of fringes displayed in the initial condition.

The test commenced by bringing the turbine up to speed by slowly increasing the compressed air flow through the turbine. The charging unit of the laser was then initialized and the laser power was turned on. After a few minutes when the capacitor bank was charged to full voltage the experiment was triggered and the loading proceeded. Photographs were taken every 20.0 μs starting at 100.0 μs before the loading pulse These five frames before the specimen was loaded are to ascertain the initial specimen state. The photographs were taken for 1.000 ms. After the test, the capacitor was discharged and the equipment turned off. The specimen was removed form the containment vessel, reassembled and examined.

5. Experimental Results and Discussion

The equipment described in the previous sections was used to investigate the near tip behavior of a crack propagating under Mode-I loading. Experiments were performed on slowly propagating cracks to examine the three dimensional behavior at the crack tip. Rapidly propagating cracks were studied to illuminate microstructural details under dynamic loading conditions.

5.1. Static Results

The out-of-plane displacement of the surface of a slowly propagating crack in a sheet of polymethylmethacrylate pulled in tension is shown in Figure (21). The crack was propagating with a speed of approximately 0.1 mm/s. In this case the specimen was flat to within 1μm so that the data can be directly interpreted as displacements from a flat surface. These contours are analogous to a topographical surveyors' map. By adjusting the reference mirror during the test, the sign of the deformation can be shown to be inward. The specimen was slowly loaded from zero load to the load at which the propagation occurred in about 10^3s. The loss of fringe resolution near the tip is due to difficulty in xerographic reproduction.

A digitized and enlarged view of Figure (21) is shown in Figure (22) where the field of view is about two plate thicknesses. The interferometer easily captures the surface deformation. The photograph was digitized to allow the subsequent image processing. The small-scale resolution of the digitizer was at a true spatial scale of 10μm.

To qualitatively compare all of the surface information an unmapping scheme was developed. Because the two-dimensional K-field has a central role in brittle fracture mechanics and because the method of caustics hinges on the validity of the K-field describing the surface deformation, Figure (22) was viewed from a two-dimensional K-field perspective. The crack tip was set as the origin of a cylindrical coordinate system

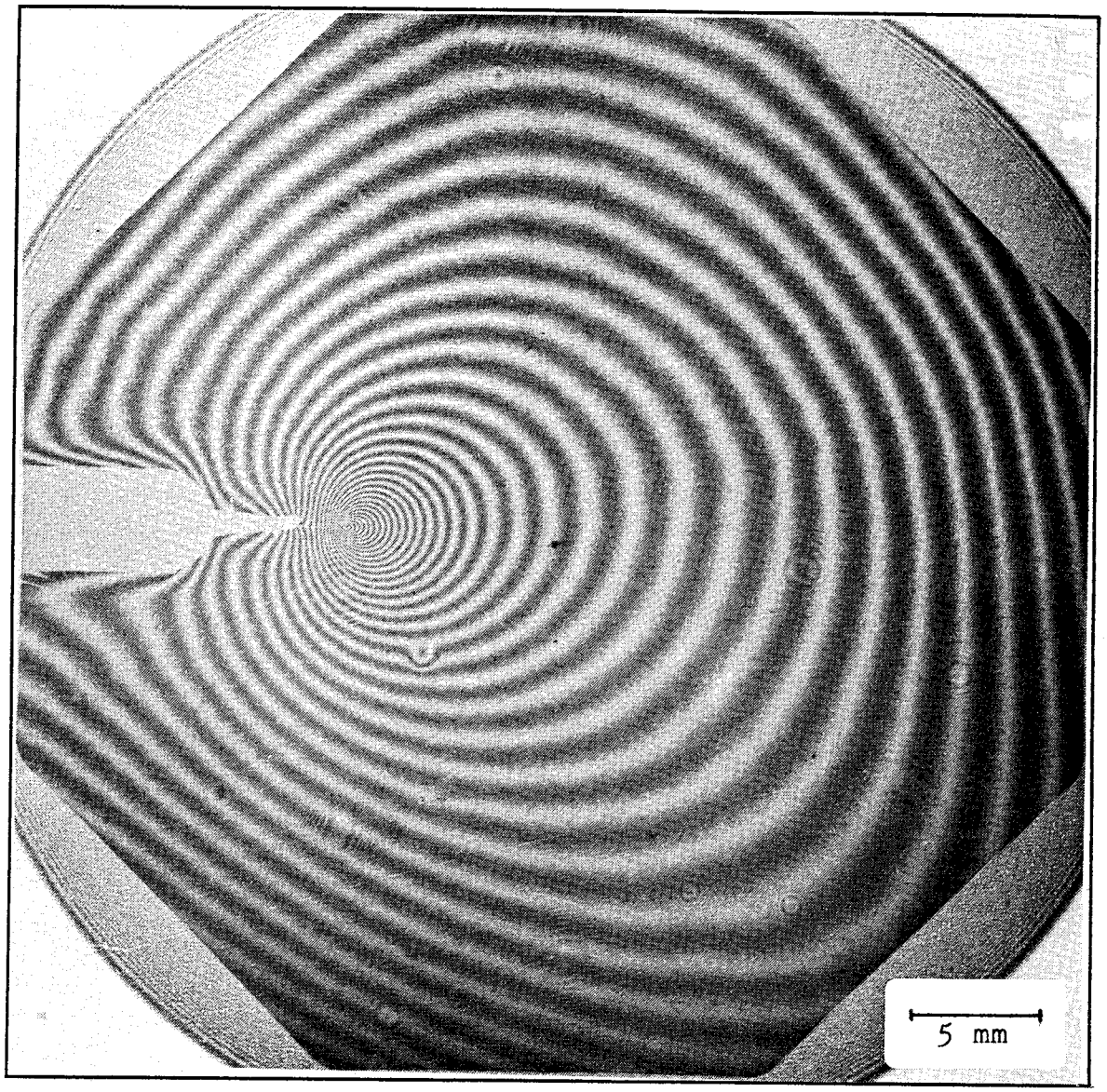

Figure (21) Interferogram of the out-of-plane displacement of a quasi-statically propagating crack in a polymethylmethacrylate sheet 4.66 mm thick. Surface contours represent displacements of 312 nm. The octagon is 40.96 mm across the flats.

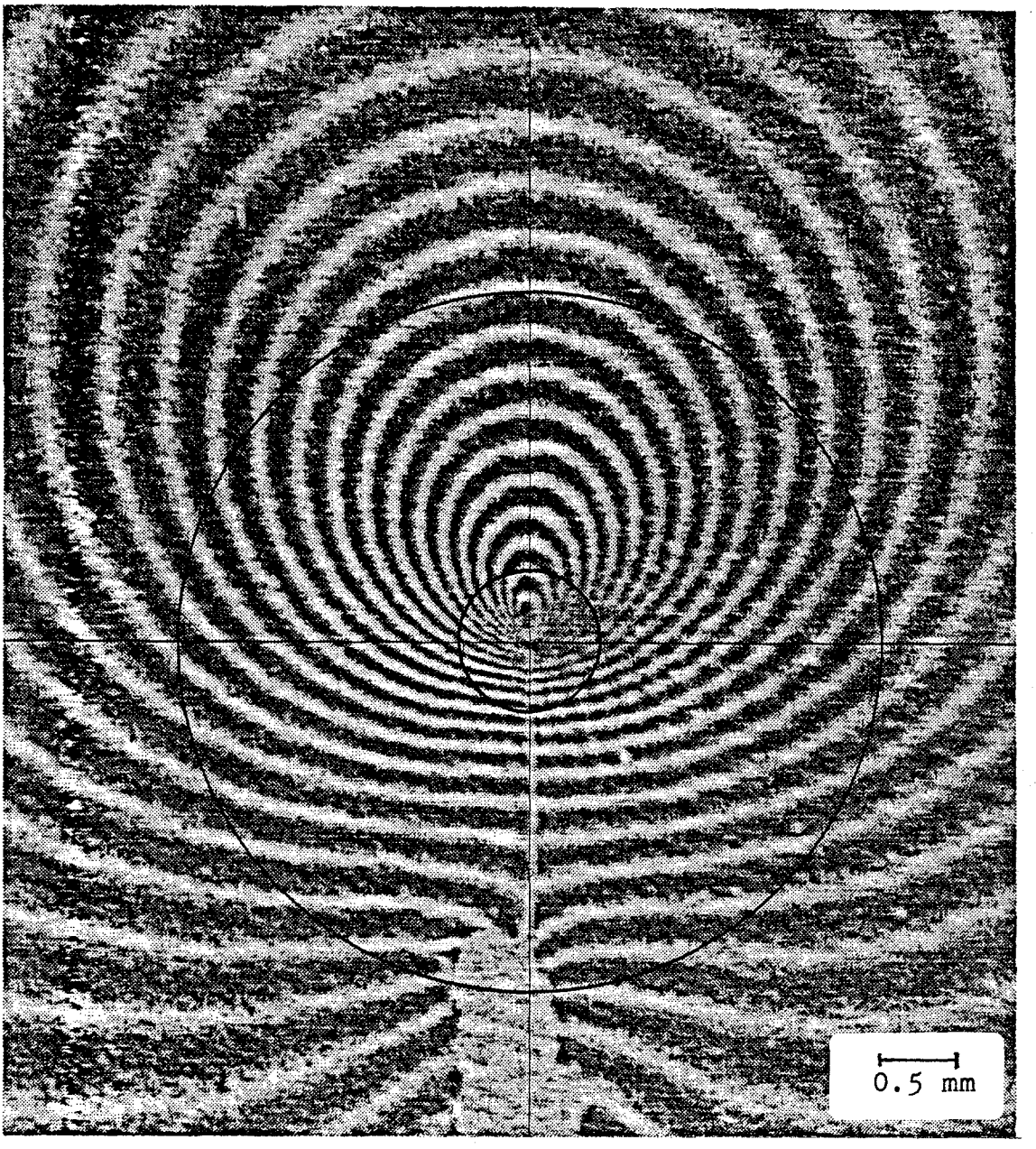

Figure (22) Digitized and enlarged interferogram of the out-of-plane displacement of a quasi-statically propagating crack in a polymethylmethacrylate sheet 4.66 mm thick. Surface contours represent displacement of 312 nm. Cross hairs are located at the intersection of the crack with the surface. Circles have radii of 0.1 and 0.5 radius/thickness, respectively.

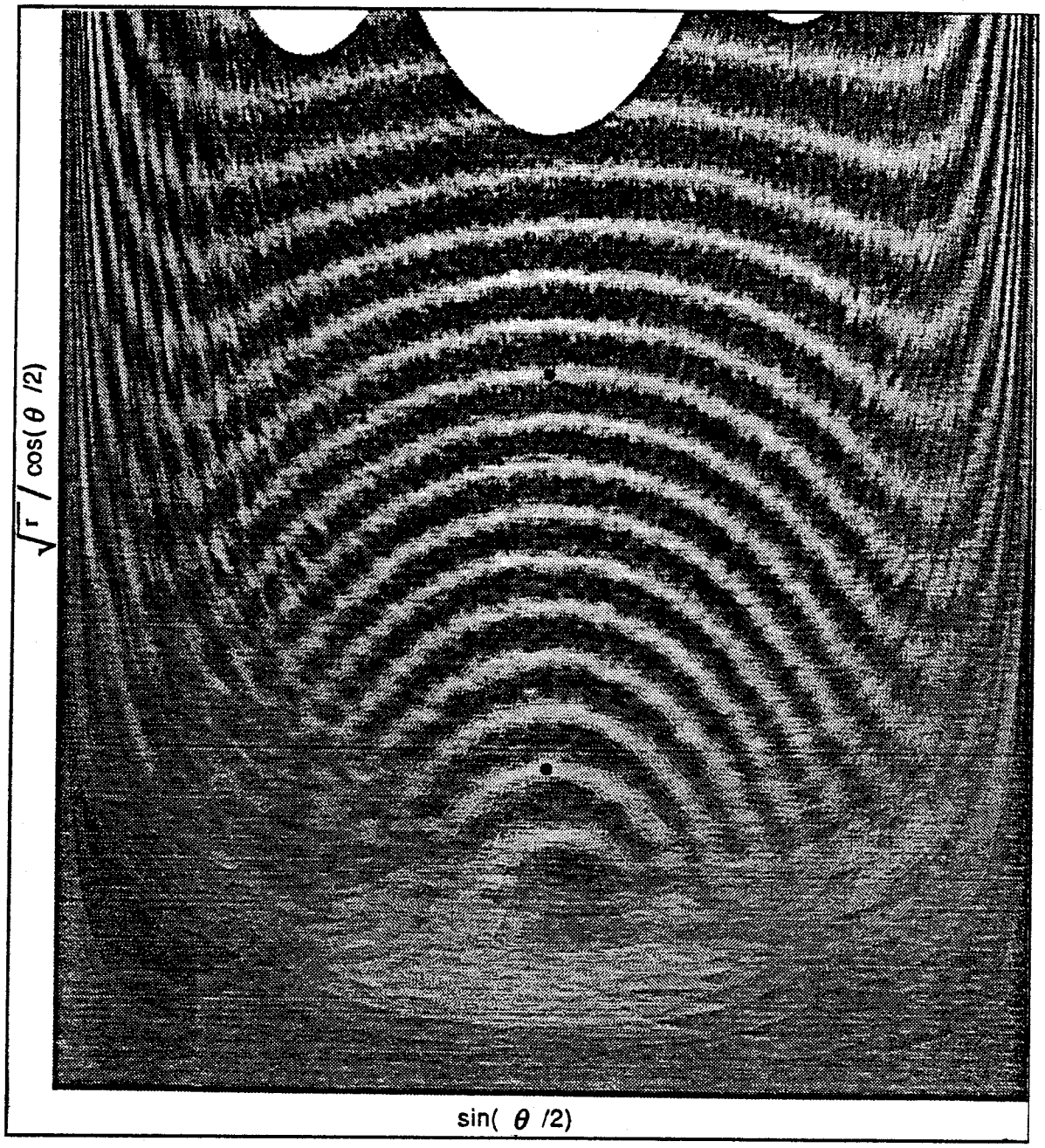

Figure (23) Qualitative comparison of out-of-plane surface with the two-dimensional K-field. Unmapped image of the out-of-plane displacement shown in Figure (22). The two dots are located directly in front of the crack tip at normalized distances of 0.1 and 0.5.

oriented so that the angular variable was zero along the crack path. That is, the crack flank is at an angle of 180 degrees. The intensities were then plotted in a new radius and angle like coordinate system based on the the two-dimensional K-field. This remapping of the data is shown in Figure (23). The abscissa is an angular measure while the ordinate has both radial and angular components. The ordinate is the inverse of the out-of-plane displacement predicted by the singular term of the two-dimensional asymptotic theory as given by equation (1).

If the singular term of the two-dimensional theory does describe the surface deformation then the contours shown in Figure (23) should be lines parallel to the abscissa. Any deviation of the lines from parallelism with respect to the abscissa is an indication of a deviation from the K-field solution. Further, the ordinate is the inverse of the out-of-plane displacement predicted from the K-field solution, not the solution. Notice that in front of the crack tip (an angle of zero) the spacing of the fringes is approximately equal as the radial distance is increased. This means that the the out-of-plane deformation in front of the crack tip can be approximated by an equation that behaves like a square root.

This qualitative comparison shows that in the region immediately surrounding the the crack tip there is no K-field region on the surface for this specimen geometry. The only region that is at all describable as K-field-like, is a region directly in front of the crack tip at a normalized distance of 0.5 to approximately 1 plate thickness from the tip.

Since the two-dimensional theory is inadequate to describe the surface deformation, a more general approach is required. Fortunately, in recent years increasing computational ability has allowed several investigations into the near tip three-dimensional elastic state of a crack. These studies were described in section 3. Figure (24) shows the normalized measured displacement from Figure (21) plotted along various radial lines vs. normalized distance from the crack front. The radial lines were chosen to cover the field from the front of the crack region to the flank and to compare with published numerical solutions. The radial distance is normalized by the plate thickness and the displacement was normalized, as

was done by Nakamura [72] and Parsons [71], by the dimensional term from the plane stress asymptotic solution. This normalization is described by equation (5). The stress intensity factor and the Young modulus to normalize the experimental data were measured for this material. Poison's ratio was taken to be 0.351 as determined by McCammond for the same molecular weight PMMA [84]. The data was corrected for a small rigid body rotation and plate bending by fitting a six term polynomial to the far field (>5 r/h) data. Finally because the region in the immediate vicinity of the crack tip is of prime interest, and the interferometer can only measure relative displacements, the data was translated to be exactly equal to Parsons and Nakamura's numerical solutions at a radial distance of zero.

Figure (24) shows that the numerical solutions approximate the measurements. The numerical problem that most closely approximates the specimen configuration is Parson's analysis of a Single Edge Notch Specimen [72]. Data from this analysis is shown at angles of 0 and 45 degrees. The other solutions are expected only to model the deformation near the crack tip. Away from the crack tip, Nakamura's solution approaches the K-field and the three point bend specimens have a compressive region in front of the crack. Other observations are that the far field (~5 r/h) comes to within approximately 9% of zero. In addition, near the crack flanks, at the angles of 135 and 140 degrees the measurements show signs that the specimen is being twisted.

A detailed view of this data is shown in Figure (25). Again, the Single Edge Notch Specimen at angles of 0 and 45 degrees agrees well with the measurements. At an angle of 140 degrees, the measurements follow the more benign deformation as predicted by the numerical solutions. However, there are some notable discrepancies. At near perpendicular angles and along the crack flank, the measurements deviate from the numerically predicted deformations.

There are several possibilities for the discrepancies shown in both the far and near field comparisons. The test was performed slowly so that a small but observable twist

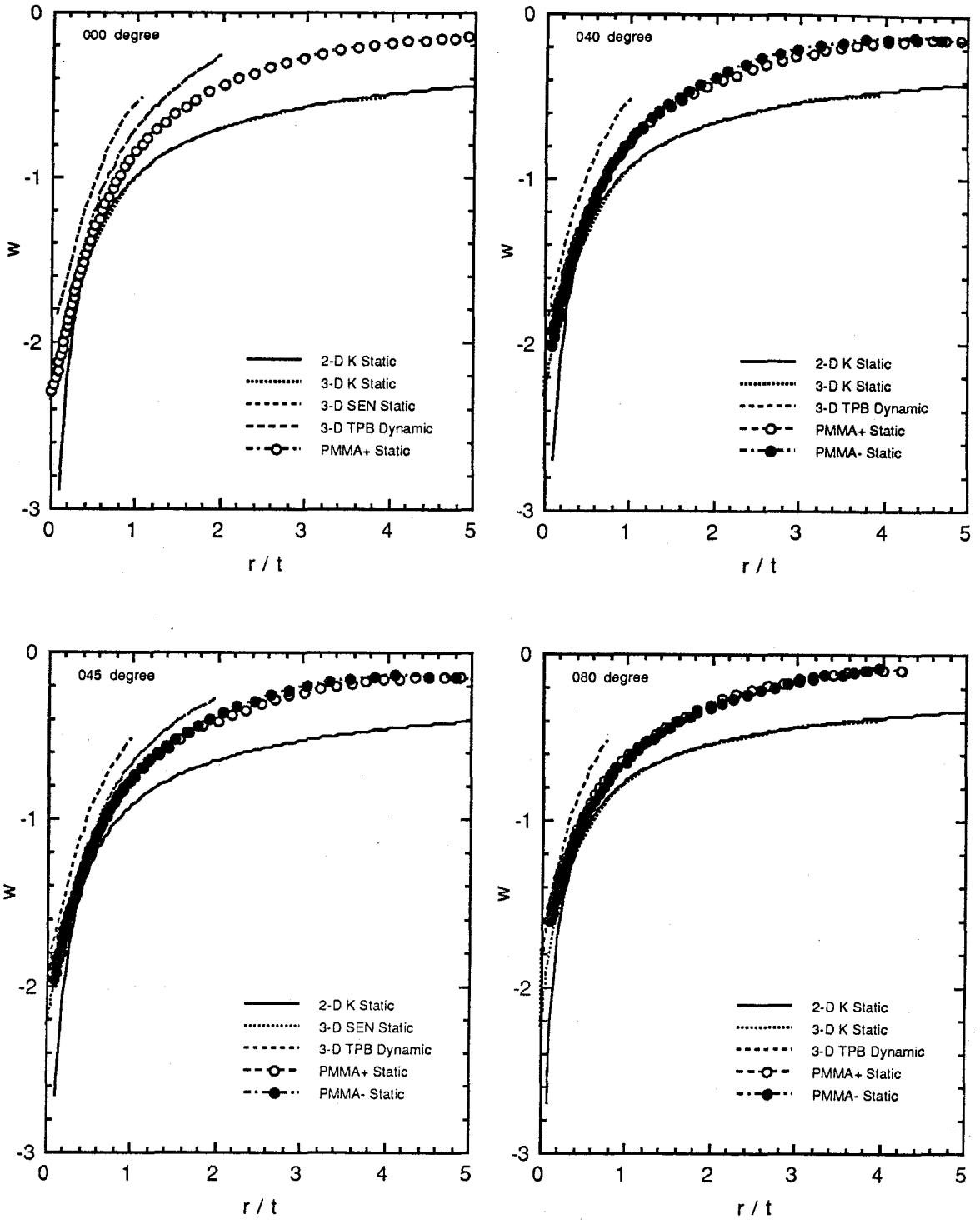

Figure (24a) Comparison of static three-dimensional numerical solutions for the out-of-plane displacements near a crack tip with experimental measurements. Displacements are shown along radial lines at angles of 0, 40, 45, and 80 degrees to ligament [59,71,72,73].

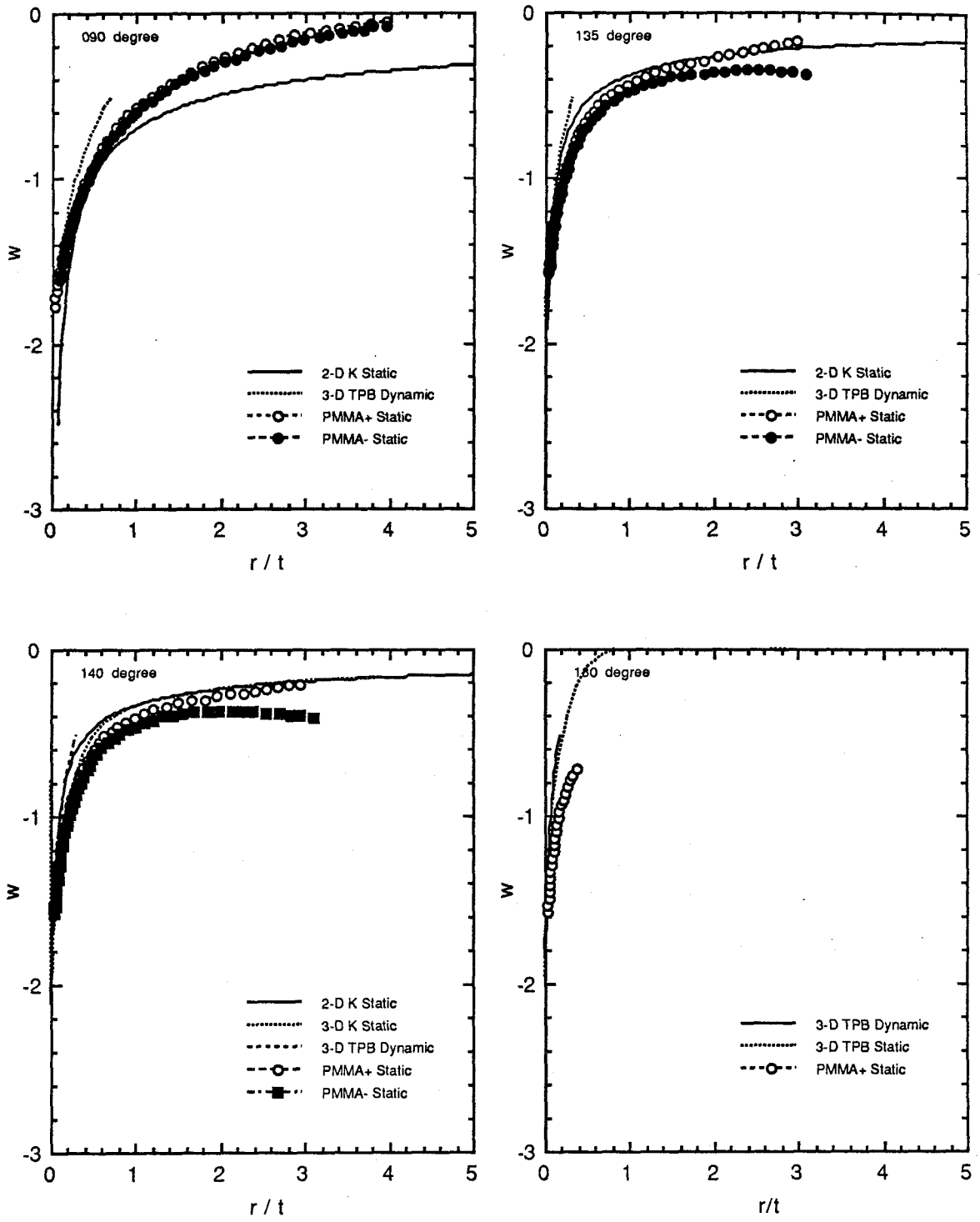

Figure (24b) Comparison of the static three-dimensional numerical solutions for the out-of-plane displacements near a crack with experimental measurements. Displacements are shown along radial lines at angles of 90, 135, 140, and 180 degrees to ligament [59,71,72,73].

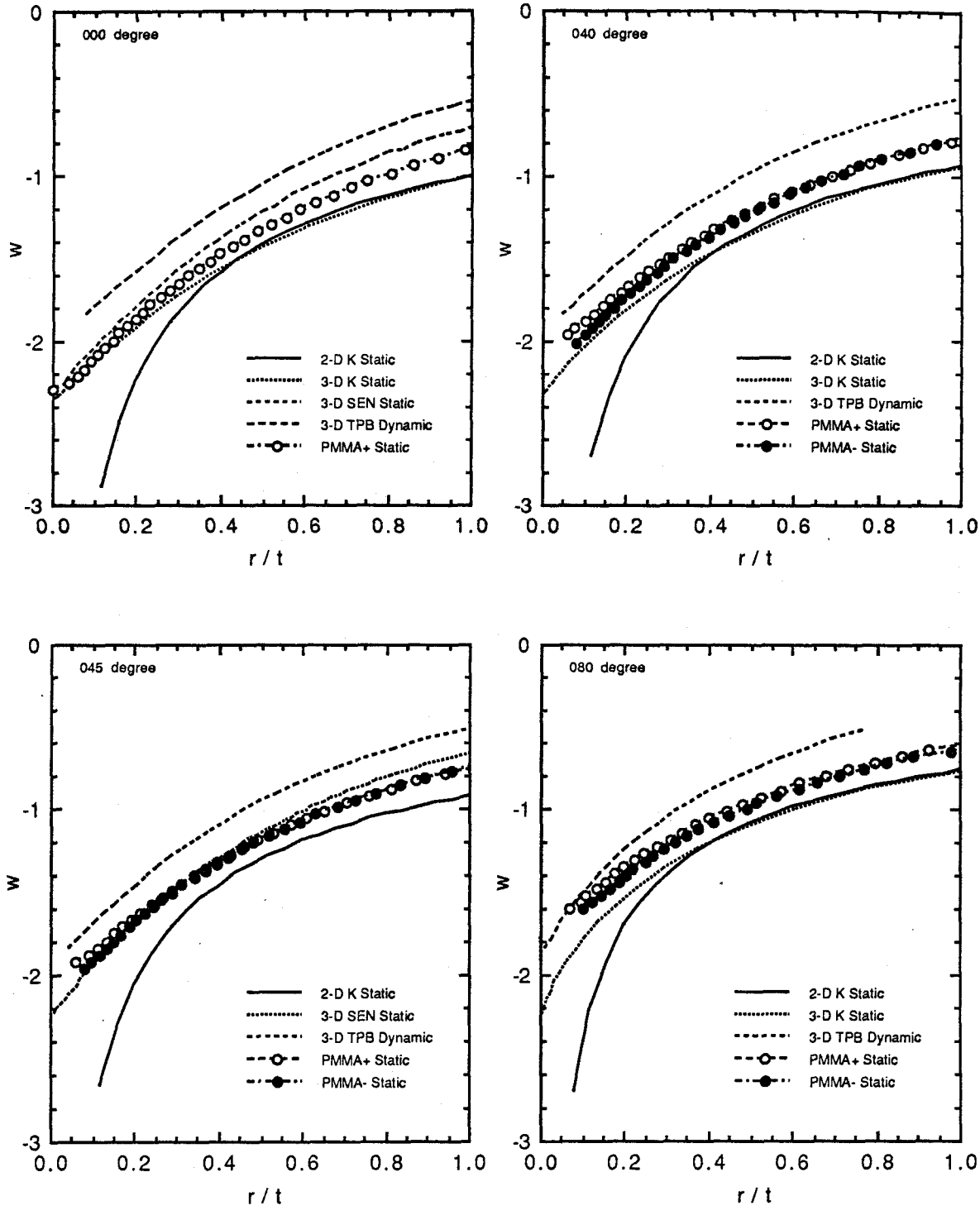

Figure (25a) Detailed comparison of the static three-dimensional numerical solutions for the out-of-plane displacements near a crack tip with experimental measurements. Displacements are shown along radial lines at angles of 0, 40, 45, and 80 degrees to ligament [59,71,72,73]

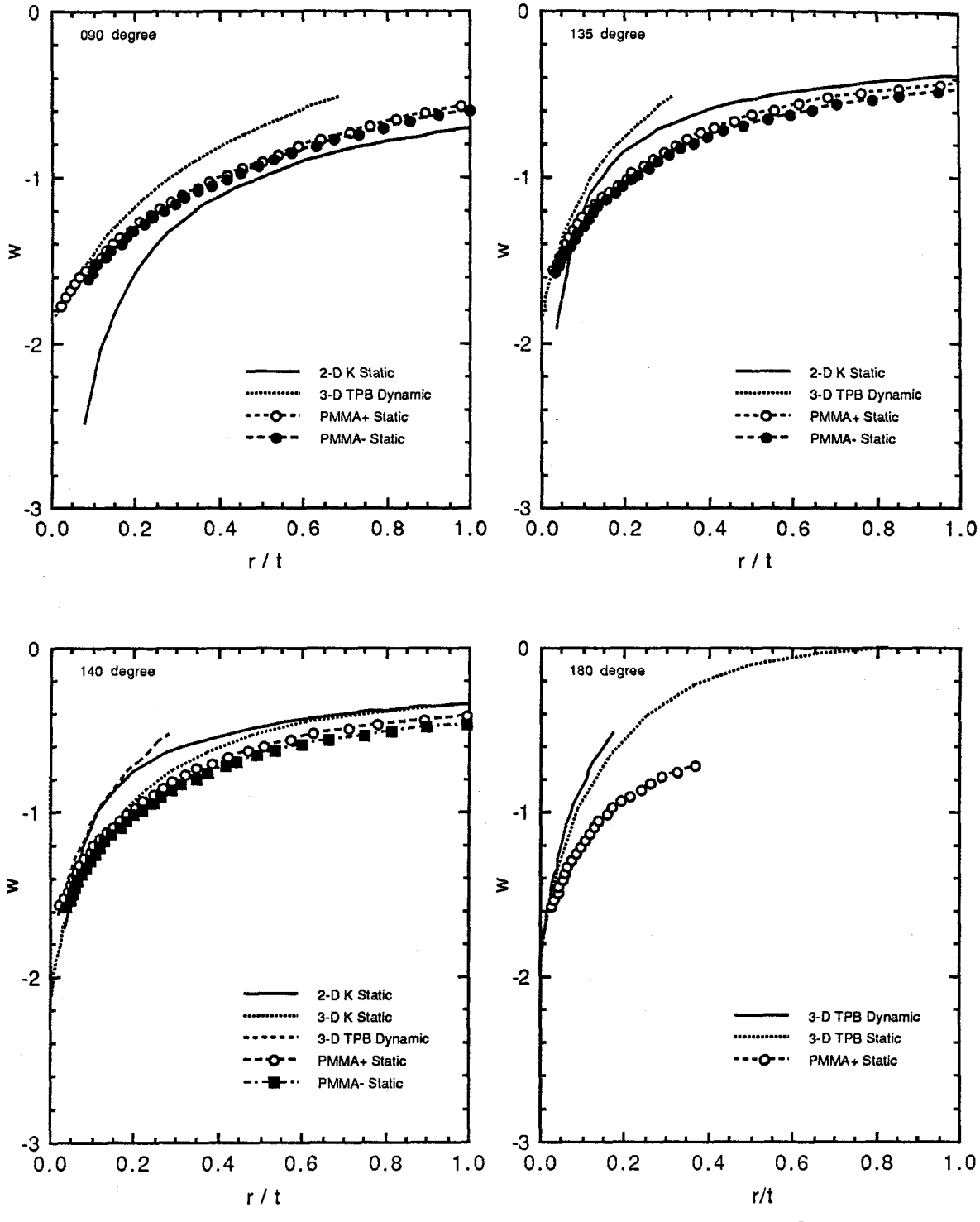

Figure (25b) Detailed comparison of the static three-dimensional numerical solutions for the out-of-plane displacements near a crack tip with experimental measurements. Displacements are shown along radial lines at angles of 90, 135, 140, and 180 degrees to ligament [59,71,72,73].

could be removed from the specimen deformation. This slow loading introduces added uncertainty of the correct Young's modulus used in the measurement normalization. Other normalization errors to account for a 9% discrepancy in total deformation could arise though the other parameters such as Poisson's ratio. The near field data has an added complication, in that the crack front for the measurement was not straight but had a radius of curvature/thickness of approximately 1.14. Thus, at the center of the specimen, the crack front was 0.1 times the thickness further advanced than on the surface. All of the numerical solutions are for straight crack fronts.

The surface deformation for this specimen is not modeled by the K-field, but is approximated by the three-dimensional solution. This is not to say that the K-field would never approximate a surface deformation. The choice of a suitable experimental configuration could produce a surface K-field deformation. Here, a plate with a size to thickness of ratio of greater than 50, the surface K-field is shown to be illusive. The strong presence of three-dimensionality in a region within the plate thickness is consistent with other investigations [6,58]. Consequently, investigations that require K-field behavior near the surface using typical specimen geometries must be inaccurate.

5.2. Dynamic Results

Inadequate measurement techniques, due both to spatial limitations of the method and interpretation through two-dimensional analysis, and microstructural effects have been blamed for unexplained behavior as cracks rapidly tear though a material [6]. This unexplained behavior includes both the apparent non-unique crack propagation speed as a function of crack fracture parameter and the terminal crack velocities that are below what is theoretically possible in simple elastic materials [8]. Using Twymann-Green interferometry, the through-the-thickness averaging of photoelasticity and the limited spatial

capability of shadowgraphic techniques are avoided and complete surface deformations can be recorded to illuminate (at least on the surface of the plate) the near tip behavior.

Figure (26) displays the out-of-plane displacement for a long duration dynamic specimen, Figure (11), being torn in two, by the dynamic experimental method described in section 4. This set of figures covers the first 100μs of the experiment from the start of the loading pulse The loading record is given in Figure (20) with 0 μs starting along with the loading pulse. The first figure, (26a), is the specimen surface before the loading pulse arrives. This surface is not particularly flat, and is what is to be expected if no special care is taken to flatten the specimen using a mold. This troublesome initial surface shape interferes with immediate qualitative evaluation of the surface deformation in the subsequent frames, but for the quantitative comparison, this shape can be subtracted from the data.

Keeping the specimen flat from the mold at the start of the test was improved in subsequent measurements by several means. Since the more interesting fracture behavior occurs at the higher propagation velocities the smaller short time loading specimen could be used, as shown in Figure (12). This specimen geometry does not require gluing of legs along the crack flank, and elimination of this step improves flatness at the expense of a decrease in total test time. The copper loading strip is also responsible for this initial deformation, both due to its construction and installation. Constructing the strip and then compressing it with weights on a flat surface for several weeks, allows the copper coil to creep and straighten. Installation of the copper strip and subsequent gluing in place, was performed while the specimen was not situated in an interferometer. Changing this procedure by careful placement of the test assembly in the containment vessel while the glue (holding the loading strip in the notch) was still not dry, allowed some adjustment of the initial shape while being measured with the interferometer.

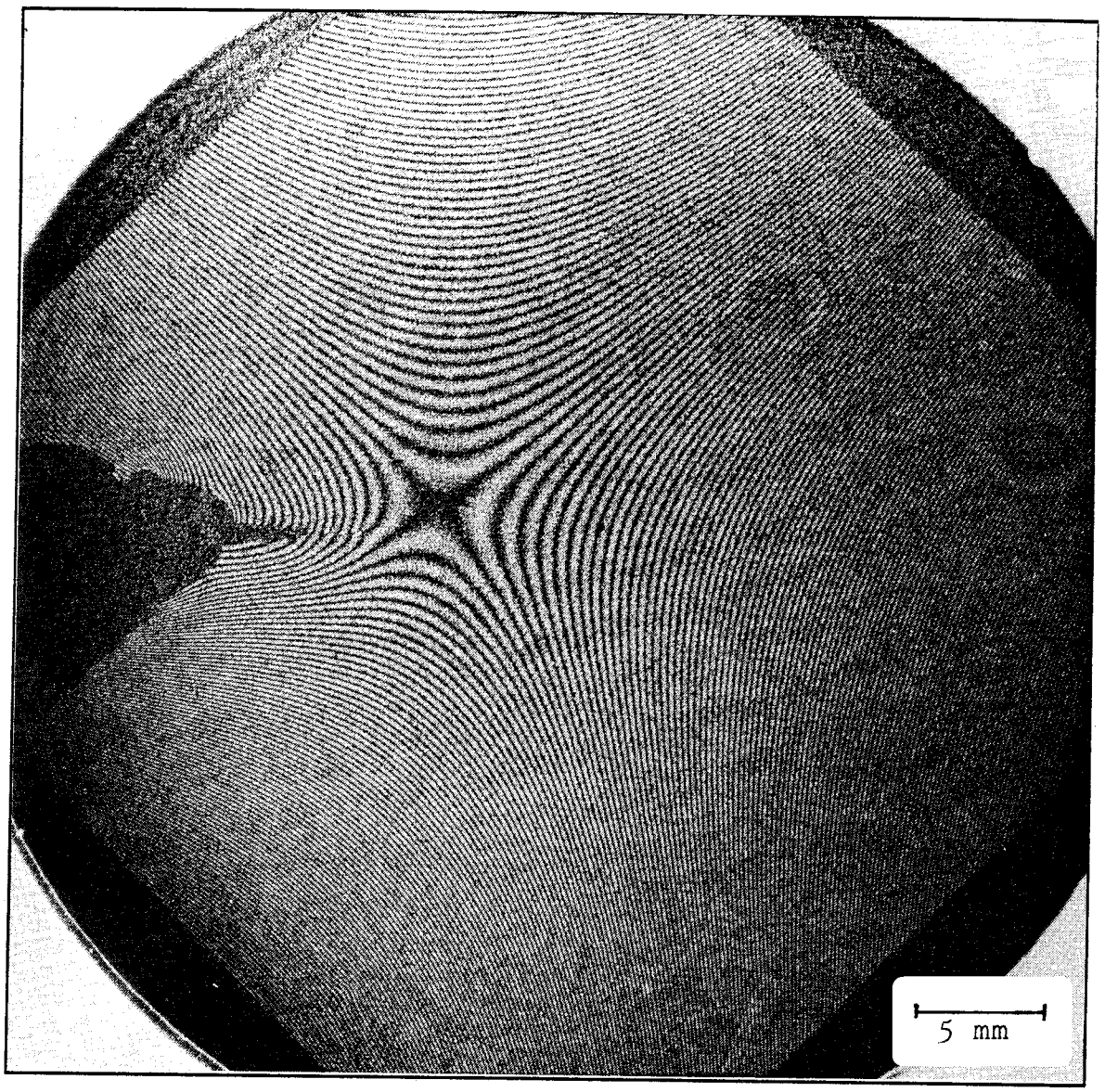

Figure (26a) Interferogram of the out-of-plane displacement of the initial surface deformation at 0 μs, crack in a polymethylmethacrylate sheet 4.59 mm thick. Surface contours represent displacements of 257 nm. The octagon is 40.96 mm across the flats.

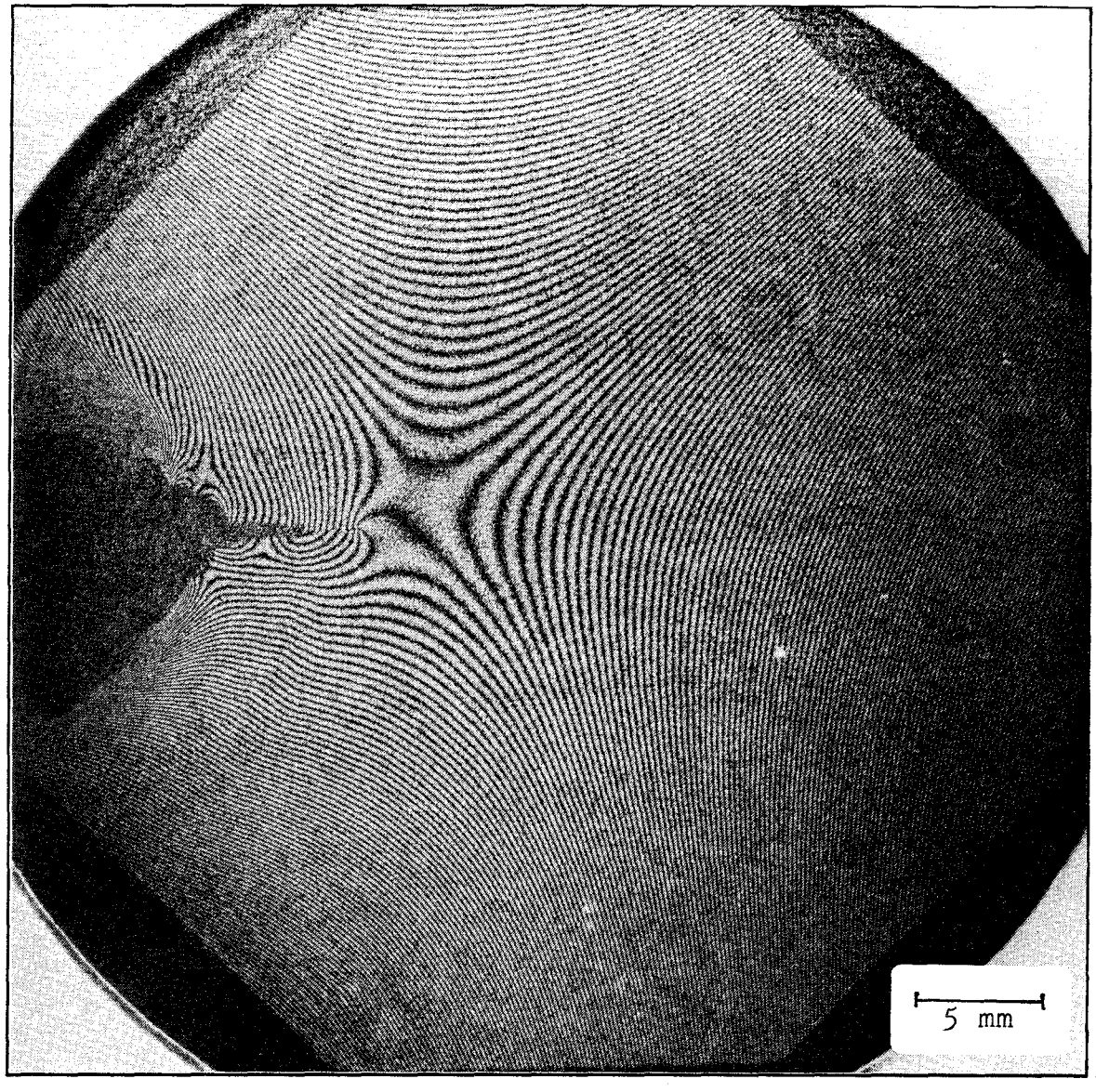

Figure (26b) Interferogram of the out-of-plane displacement of the surface deformation of a crack in a polymethylmethacrylate sheet 4.59 mm thick, under dynamic loading conditions at 20 μs. Surface contours represent displacements of 257 nm. The octagon is 40.96 mm across the flats.

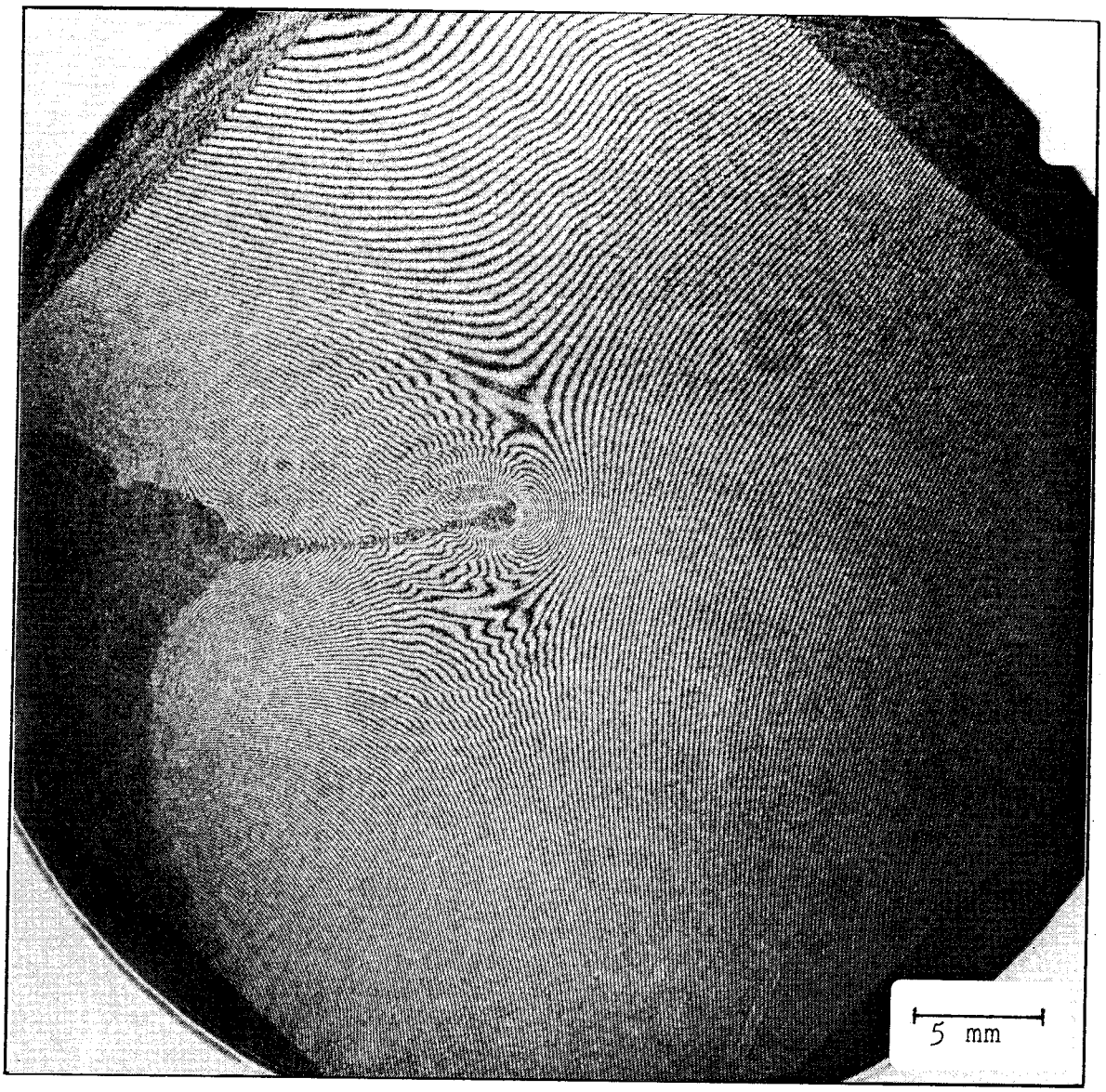

Figure (26c) Interferogram of the out-of-plane displacement of the surface deformation of a crack moving at 0.5 m/s in a polymethylmethacrylate sheet 4.59 mm thick, at 40 μs. Surface contours represent displacements of 257 nm. The octagon is 40.96 mm across the flats.

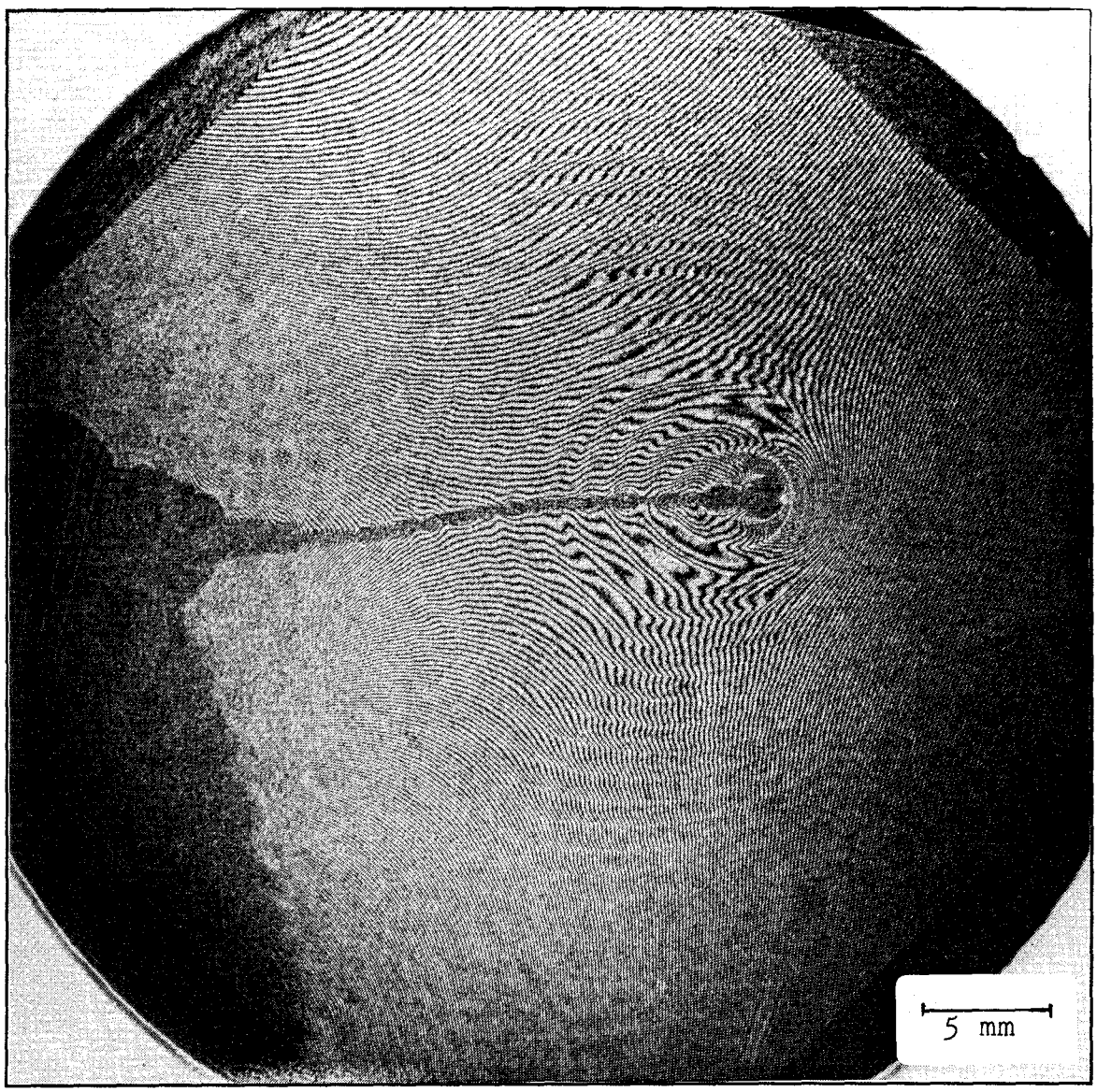

Figure (26d) Interferogram of the out-of-plane displacement of the surface deformation of a crack moving at 0.5 m/s in a polymethylmethacrylate sheet 4.59 mm thick, at 60 μs. Surface contours represent displacements of 257 nm. The octagon is 40.96 mm across the flats.

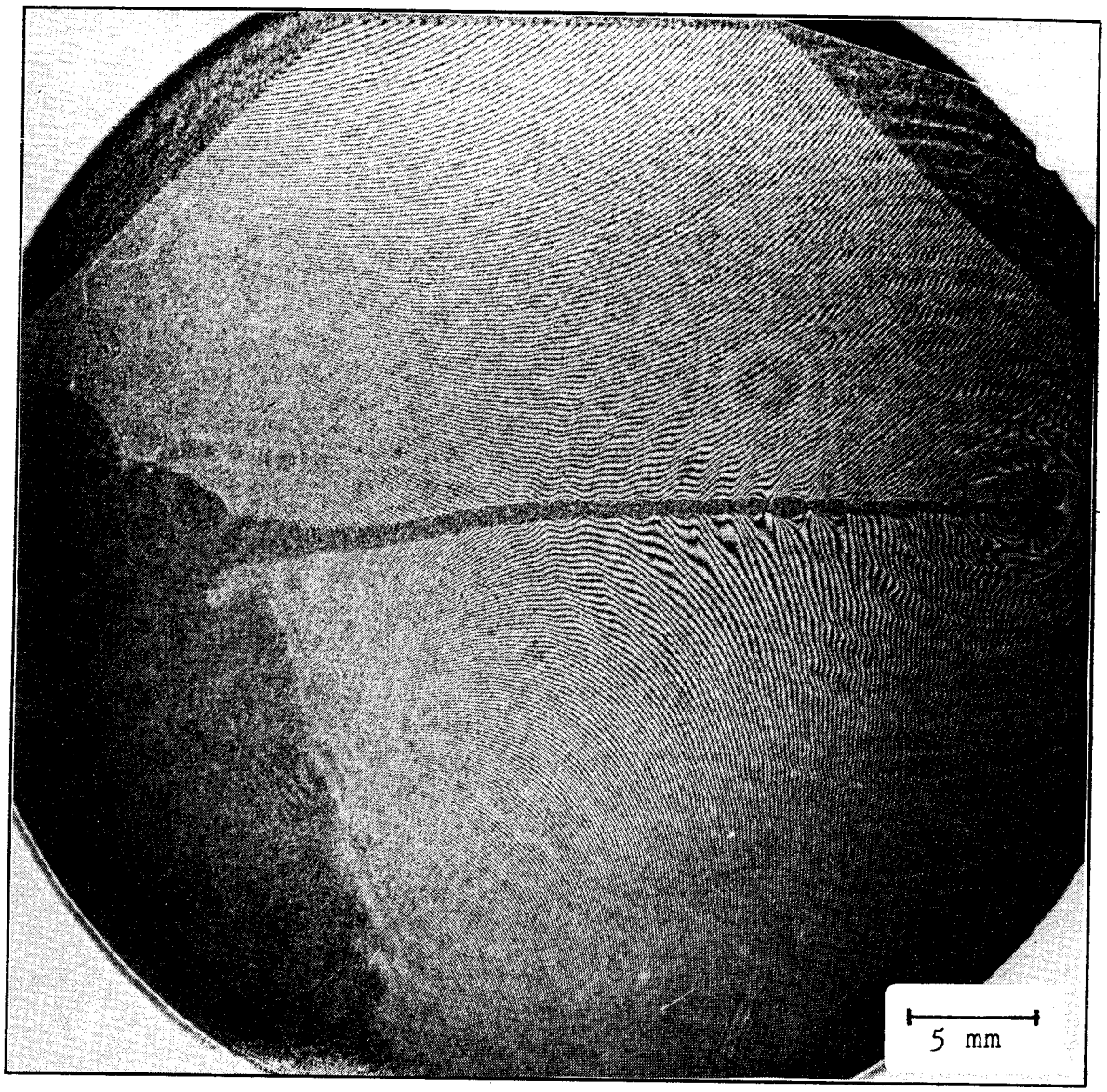

Figure (26e) Interferogram of the out-of-plane displacement of the surface deformation of a crack moving at 0.5 m/s in a polymethylmethacrylate sheet 4.59 mm thick, at 80 μs. Surface contours represent displacements of 257 nm. The octagon is 40.96 mm across the flats.

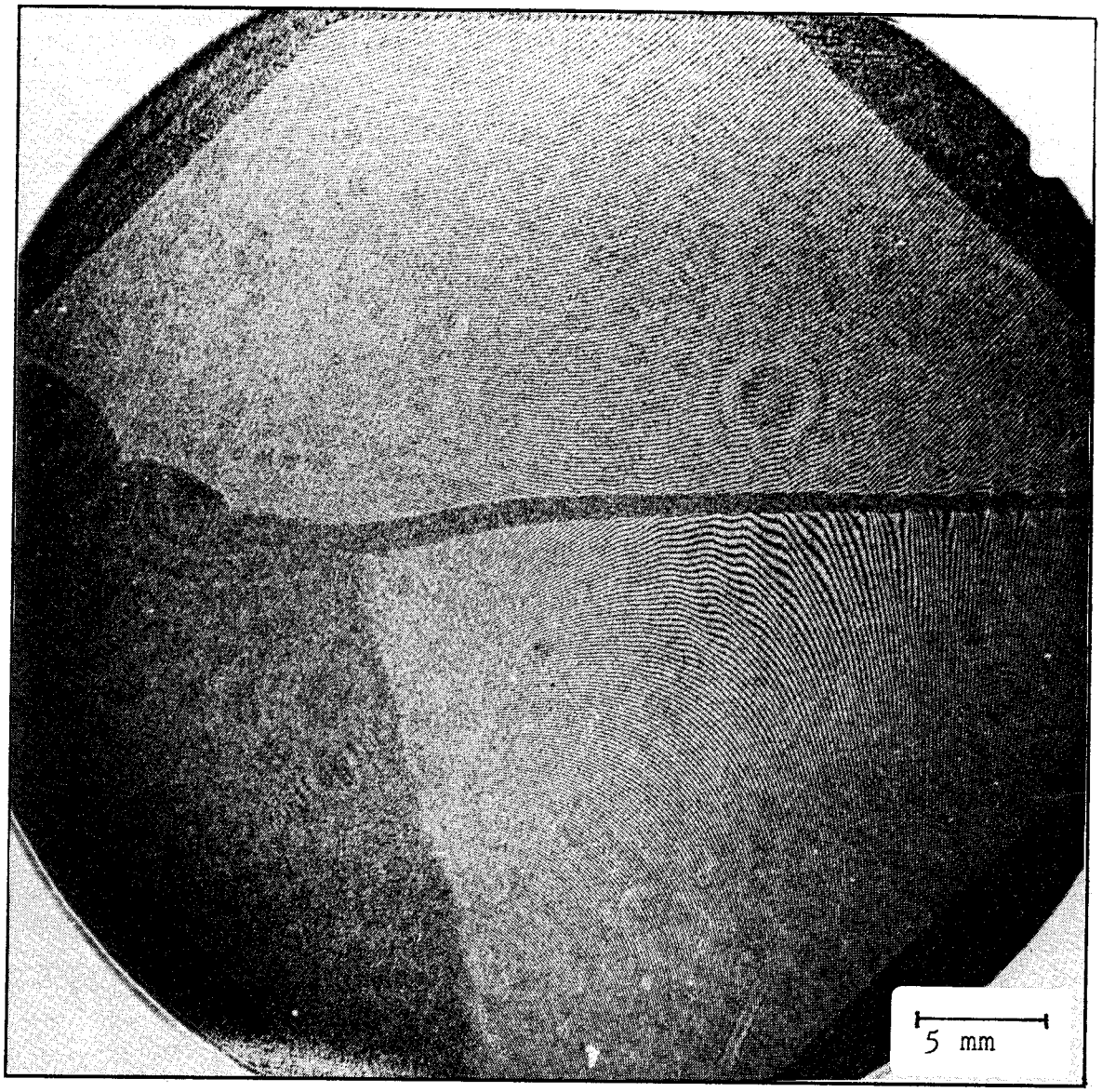

Figure (26f) Interferogram of the out-of-plane displacement of the surface deformation of the flanks of a crack moving in a polymethylmethacrylate sheet 4.59 mm thick, at 100 μs. Surface contours represent displacements of 257 nm. The octagon is 40.96 mm across the flats.

Figure (26b), shows the surface shape at approximately the peak of the loading pulse. To get an idea of scale, a dilatational wave in this material travels at about 2 mm/μs and has had enough time to propagate from the loading surfaces to just outside the field of view between frames.

In the next figures, (26c) through (26e), the crack is seen to be propagating. The final figure, (26f), shows the crack flanks moving apart. Based on the crack propagation figures, the average crack velocity is approximately 0.5 mm/μs. Associated with the crack propagating, small ripples appear to radiate from the crack tip. Base on the crack speed and the Doppler shift of the ripples with respect to the crack front, these waves propagate out at approximately 1.0 mm/μs, about the shear or the Rayleigh wave speed of the material [85]. Before investigating the origin of the surface ripples, the overall deformation is examined.

Echoing the procedure used to examine the static interferogram, the out-of-plane displacements from Figure (26c) were determined by digitizing the image, counting fringe crossings, normalizing, and are displayed in Figure (27). Several questions arise as to the correct material properties to use in the normalization, and to the effect of the crack tip motion on the surface displacement. This material has weak rate dependent properties. Quick microsecond loading has revealed an increase in the fracture toughness with propagation velocities [88], and an increase in the material modulus [89,90]. The effect of loading rate on Poisson's ratio is not known. The increase in the apparent fracture toughness of the propagating crack is approximately three times the static value at a crack velocity of 0.5 mm/μs. Since the increase in the modulus of the material is of the same order of magnitude as the increase in the fracture toughness, and since these two quantities offset each other in the normalization the static material properties were used.

Studies of the effect of crack tip velocity on the measured stress intensity factor have been performed using planar theories [93,94], however, a three-dimensional investigation near the tip of a moving crack corresponding to the static work, is lacking.

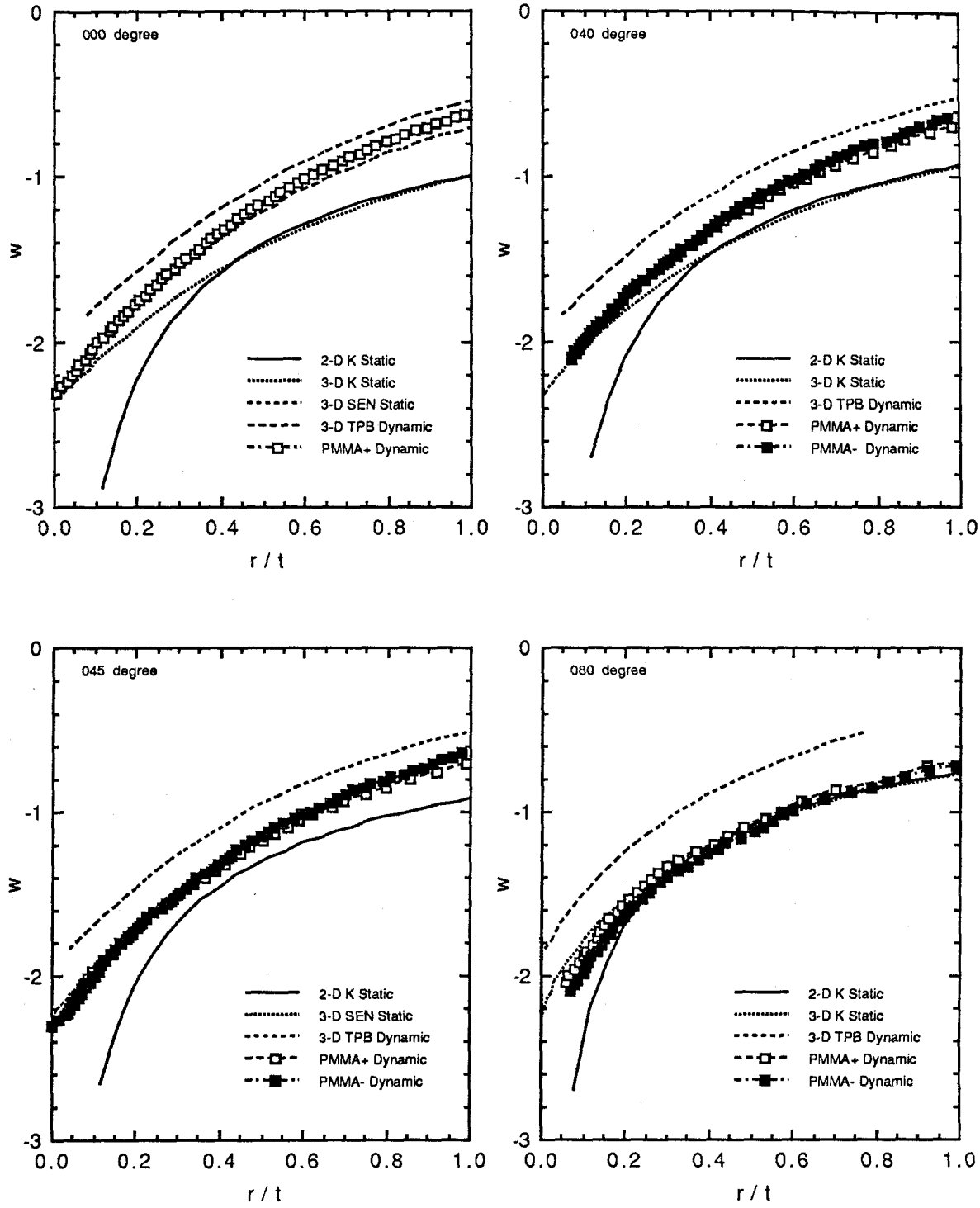

Figure (27a) Comparison of the out-of-plane displacements of a dynamically propagating crack, in Figure (26c), with the static three-dimensional numerical solutions. The crack is propagating at about 45% of the shear wave speed. Displacements are shown along radial lines at angles of 0, 40, 45, and 80 degrees to ligament [59,71,72,73].

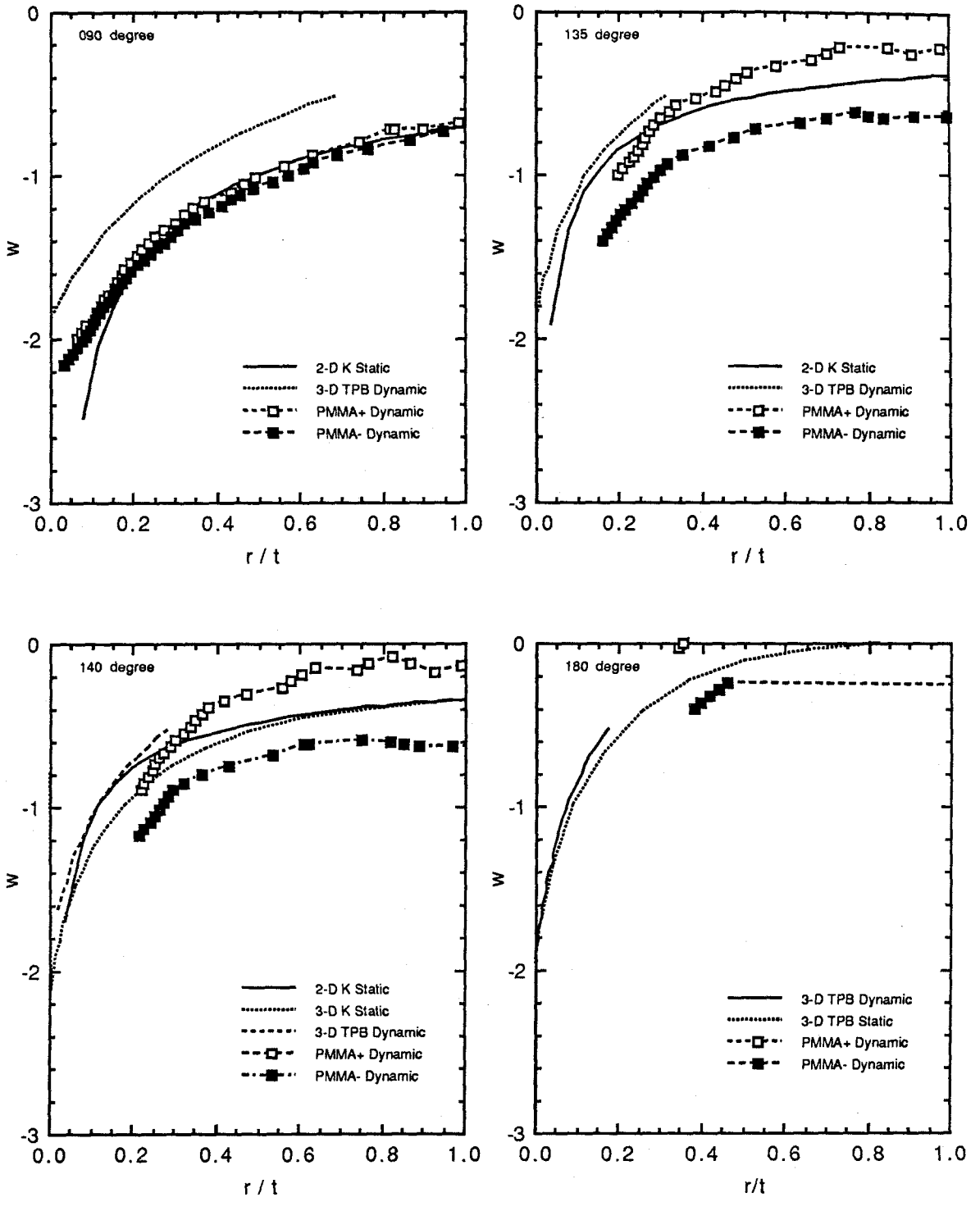

Figure (27b) Comparison of the out-of-plane displacements of a dynamically propagating crack, in Figure (26c), with the static three-dimensional numerical solutions. The crack is propagating at about 45% of the shear wave speed. Displacements are shown along radial lines at angles of 90, 135, 140, and 180 degrees to ligament [59,71,73].

The effect of the surrounding dynamic elastic field on the stress intensity factor at a propagation speed of 0.5 mm/μs, from the two-dimensional analysis, is about five percent of the total deformation [93]. Since the assumption on the material properties involve higher errors, greater than ten percent, this dynamic effect was ignored.

As can be seen from Figure (27), the near tip experimental data closely follows the static numerical predictions. As with the static data, the dynamic results have the correct smaller deformation in front (along 0 degrees), and a larger deformation behind the crack than predicted from the static singular asymptotic approximation. This close agreement is surprising in light of the assumptions on the material properties. The dynamic data appears to closely match the numerical curves even in the region within one-tenth of the plate thickness. This is attributed to a straight crack front as is evident by the fracture morphology. The different values for positive and negative angles with respect to the crack tip is attributed to specimen twisting from the loading coil. However, even with this twist, the experimental data falls on either side of the numerical simulation.

A detailed view of the interferogram of Figure (26c) is shown in Figure (28). The fracture surfaces corresponding to this location are displayed in Figure (29). As shown in Figure (28), a crack is propagating though an amorphous material at about one-half of the shear wave velocity. At this speed, waves are radiated away from the moving crack tip with approximately the shear wave velocity. These surface ripples are apparently generated periodically at a rate of one every 0.8 microseconds, implying that a surface wave is produced for every 0.4 mm of crack advance. The morphology of this fracture process has a corresponding 0.4 mm periodic, approximately straight, ripple structure that is on average parallel with the plate normal. The surface waves indicate that crack advance in a statically amorphous material, under sufficiently severe loading, occurs by a non-steady process with a particularly large length scale. This process may even be discontinuous.

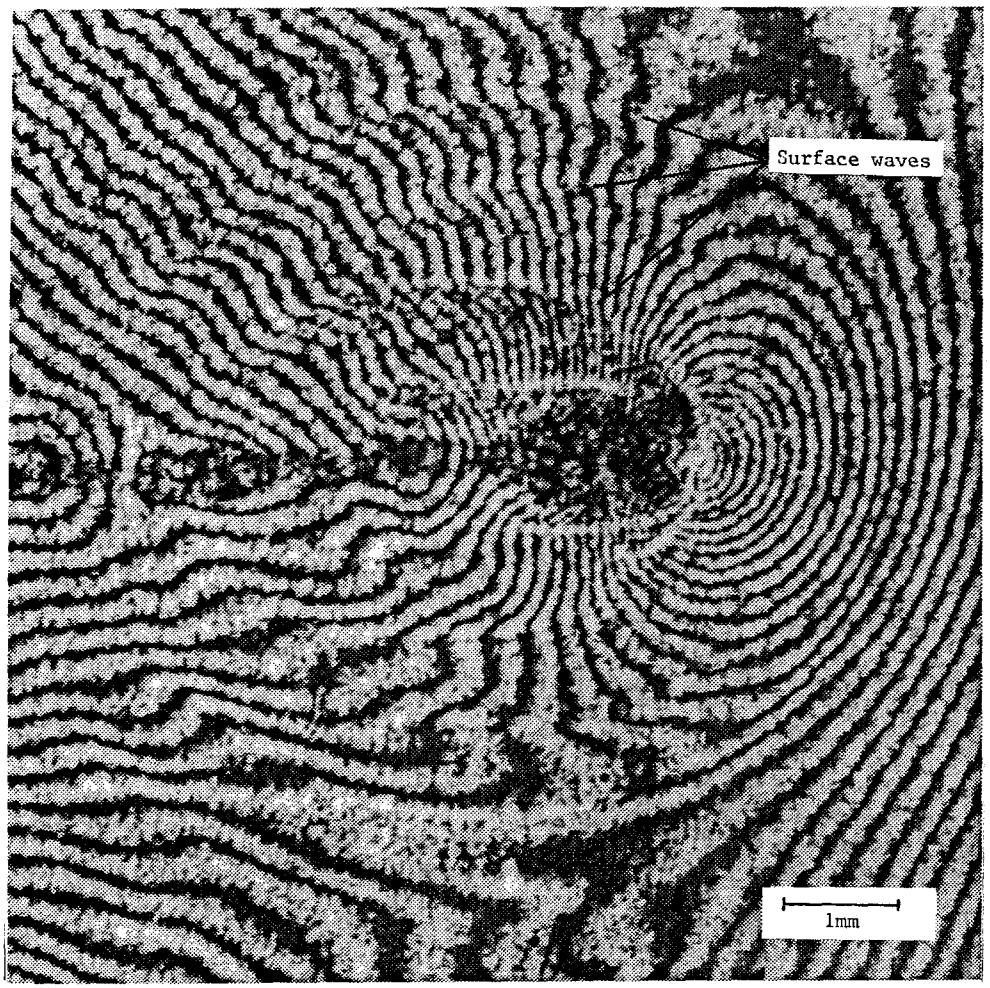

Figure (28) Detailed view of Figure (26c), an interferogram of the out-of-plane surface displacement of a crack moving at 0.5 mm/μs in a 4.59 mm thick plate of polymethylmethacrylate. Contours represent a 257 nm change in elevation. Surface ripples are propagating at approximately 1 mm/μs.

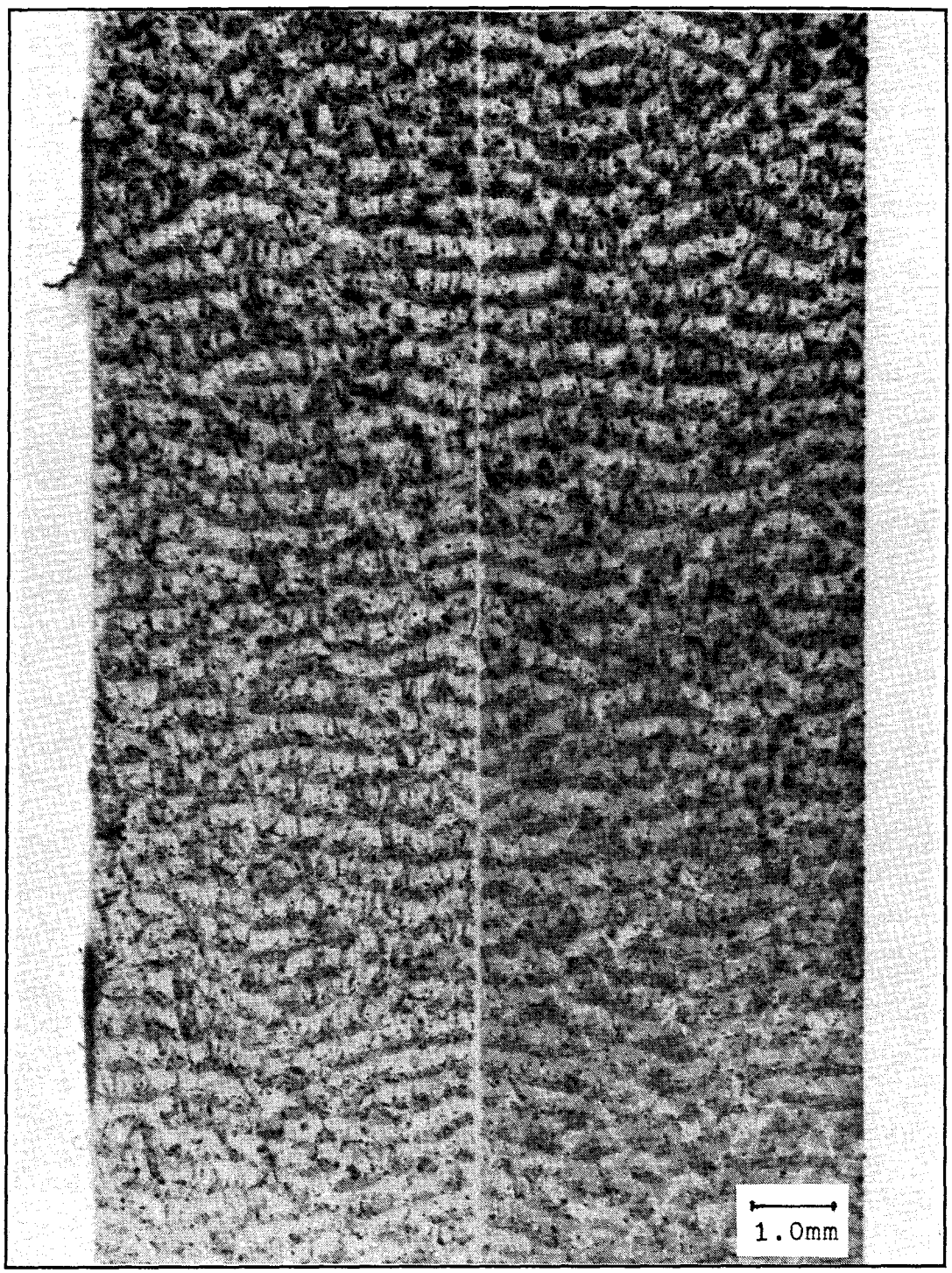

Figure (29) Fracture morphology of both separated halves of the specimen shown in Figure (28). This surface was produced by a crack propagating at 0.5 mm/μs in a 4.59 mm thick plate of polymethylmethacrylate.

The fracture morphology of PMMA has been extensively studied primarily at slower rupture velocities [95,96,97,98]. The ripple markings are not present at these slow speeds. This morphology is not unique to this experiment or specimen geometry. Cotterell [100] correlated the morphology of PMMA with crack velocity and noticed the periodic surface markings at velocities above 0.5 mm/μs and below a crack branching velocity of approximately 0.7 mm/μs. The periodic markings are also apparent, but not explicitly mentioned, in other experiments [96]. These periodic markings are different from Wallner lines [34], as the fracture markings are approximately parallel with the plate normal, and there are no periodic surface initiation points.

Upon re-examination of previous work involving PMMA and an analogous infinite plate loading arrangement [88], the periodic ripple fracture morphology is present at velocities above 0.3 mm/μs. However, the distance between ripples, the ripple wavelength, does not correlate with crack speed as is shown in Figure (30). The ripple wavelength does tend to increase with increasing stress intensity factor as is shown in Figure (31).

As the load magnitude (and loading rate in these experiments) is increased the ripple wavelength becomes longer and eventually the crack branches into multiple cracks. Figure 32 shows the out-of-plane displacements for a branching crack. This test is the same as that displayed in Figure (27), except the maximum load is increased 1.5 times.

Figure (31a) shows the initial surface displacement and Figure (31b) the surface after the initial dilatational wave has propagated out of the field-of-view. At 40 μs, the crack is propagating and at 60 μs the crack has already branched. At 80 μs the crack branches again. The remaining figure, (31f), shows the aftermath of the cracks propagating through the material. This sequence of photographs demonstrates the inadequate temporal resolution of the present detector system. As the cracks propagate, surface ripples are generated along with the corresponding periodic fracture morphology. The last two frames show a crack that started and stopped within 40μs.

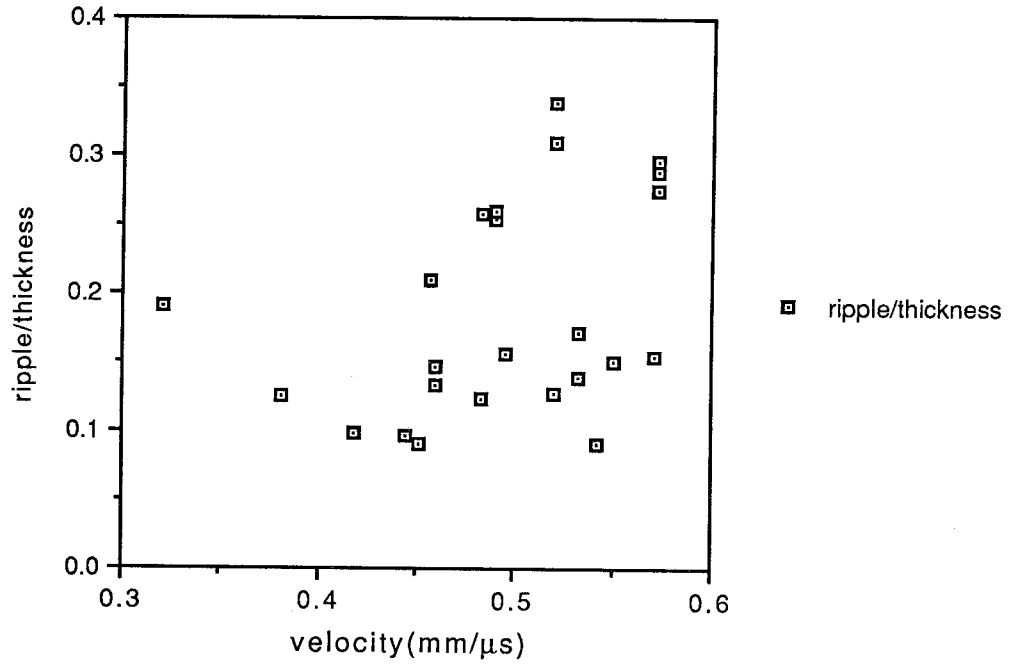

Figure (30) Fracture morphology size vs. crack velocity for PMMA.

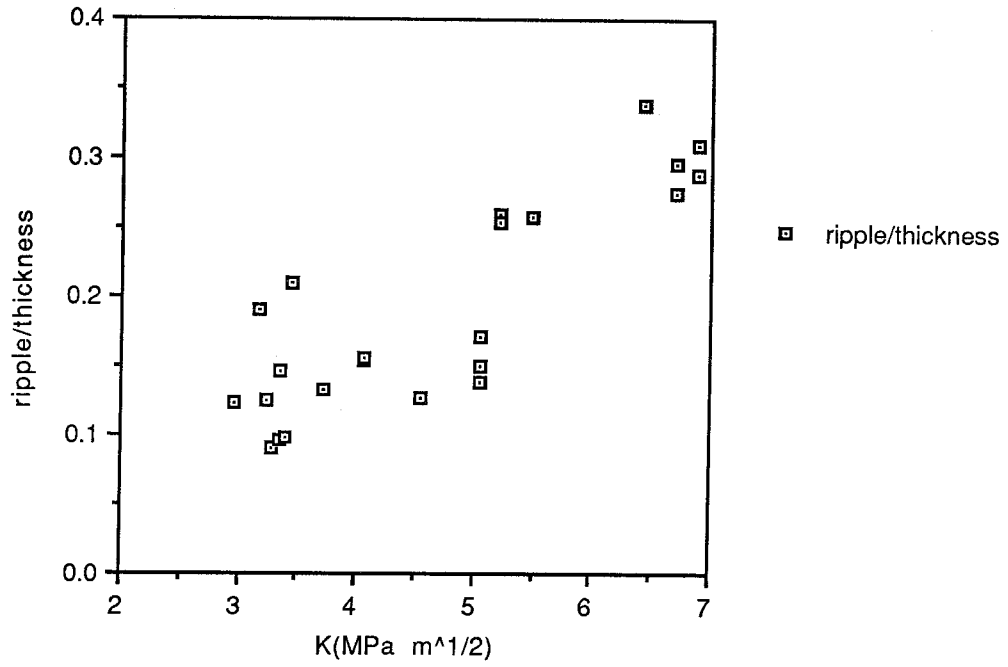

Figure (31) Fracture morphology size vs. stress intensity factor for PMMA.

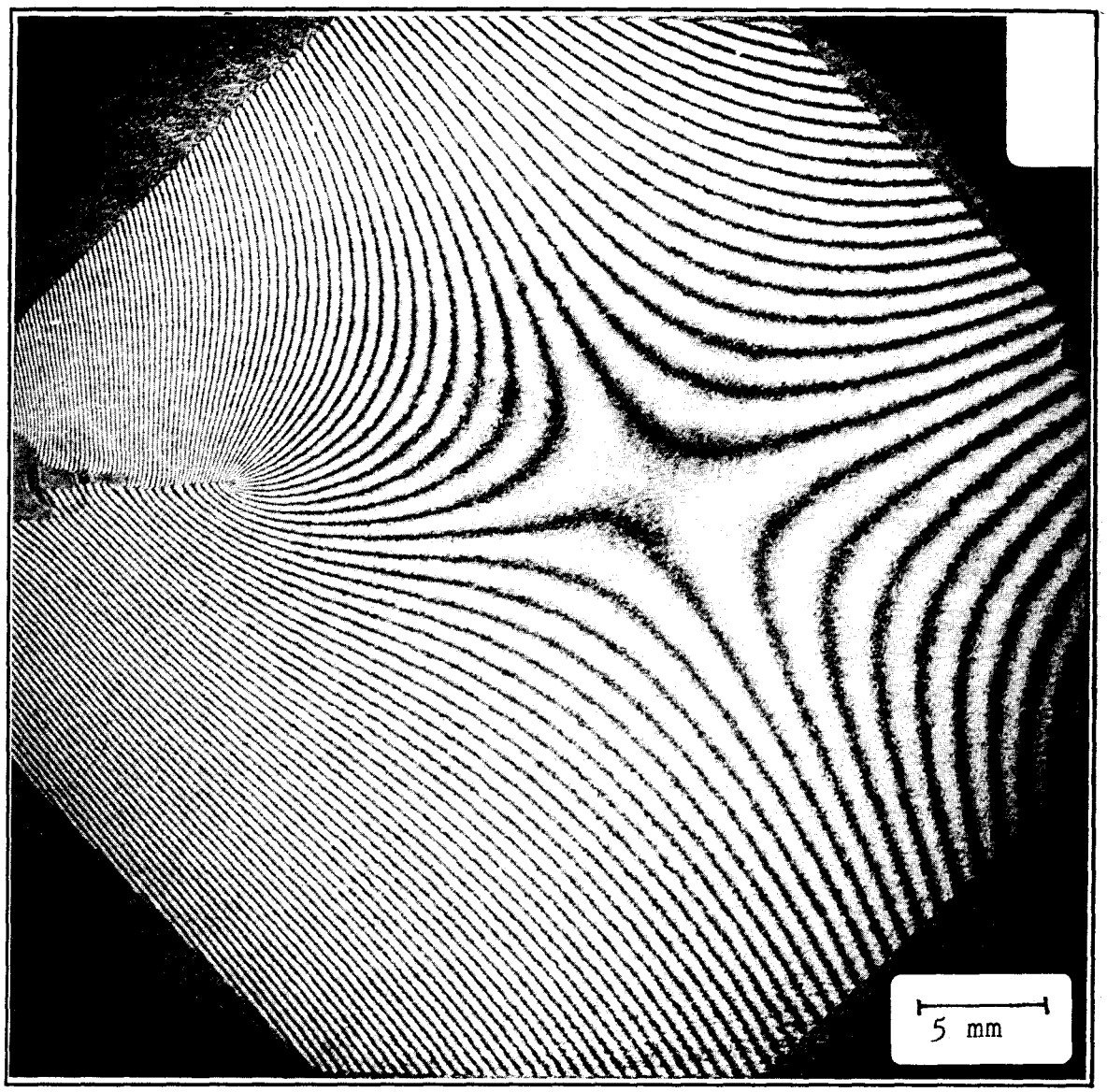

Figure (32a) Interferogram of the out-of-plane displacement of the initial surface deformation at 0 μs, crack in a polymethylmethacrylate sheet 4.42 mm thick. Surface contours represent displacements of 257 nm. The octagon is 40.96 mm across the flats.

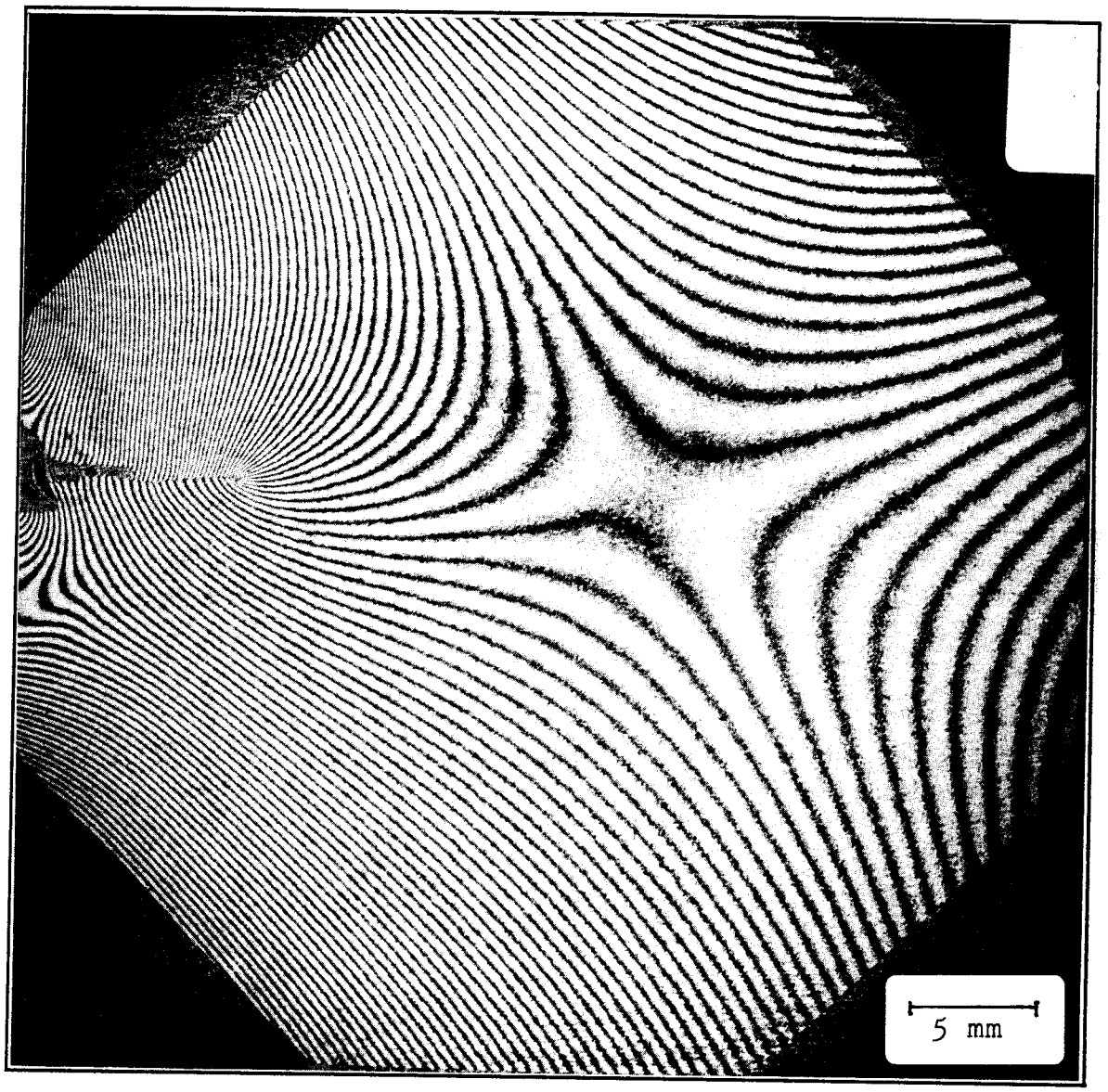

Figure (32b) Interferogram of the out-of-plane displacement of the surface deformation of a crack in a polymethylmethacrylate sheet 4.42 mm thick, under dynamic loading conditions at 20 μs. Surface contours represent displacements of 257 nm. The octagon is 40.96 mm across the flats.

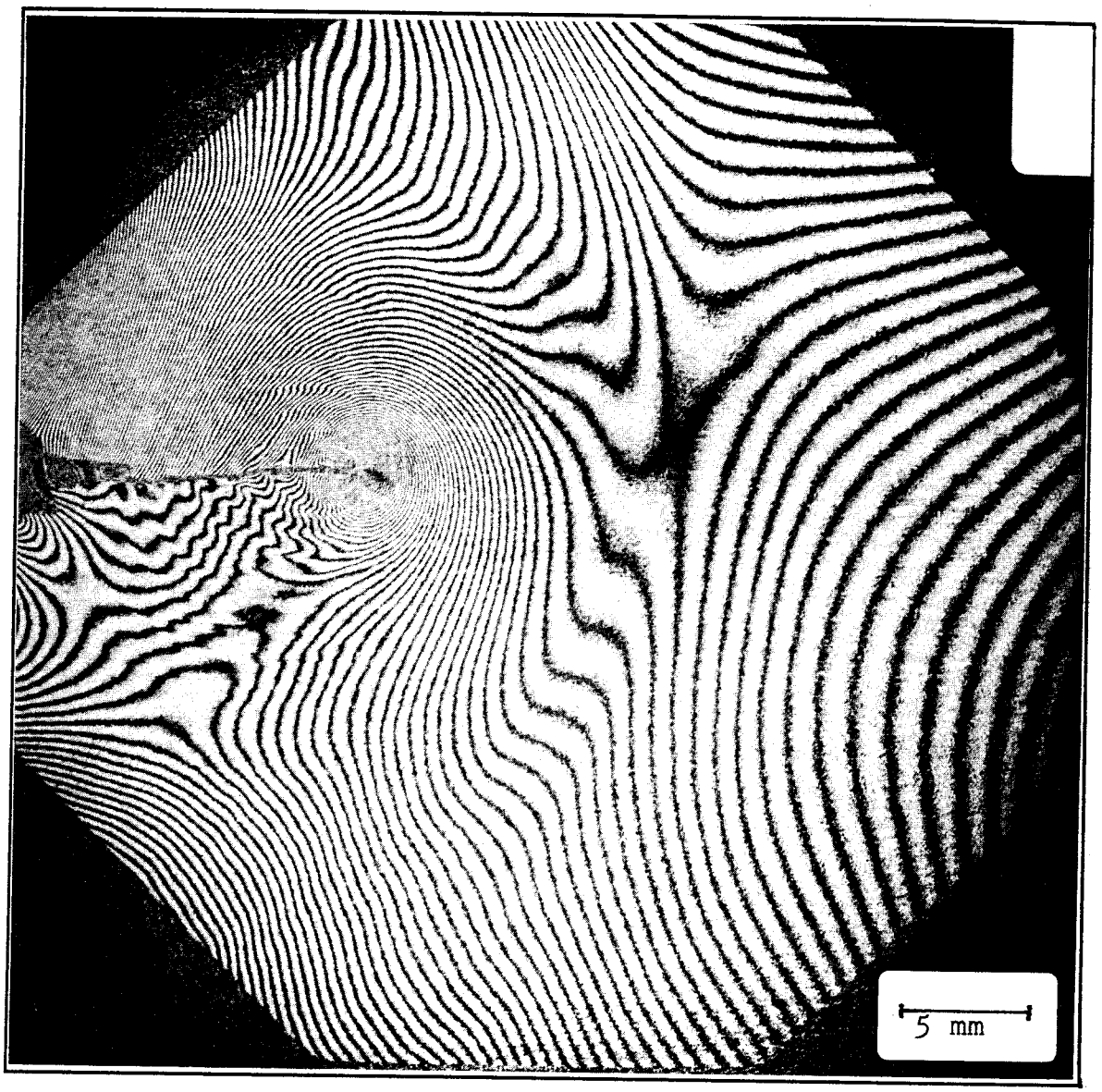

Figure (32c) Interferogram of the out-of-plane displacement of the surface deformation of a crack moving at in a polymethylmethacrylate sheet 4.42 mm thick, at 40 μs. Surface contours represent displacements of 257 nm. The octagon is 40.96 mm across the flats.

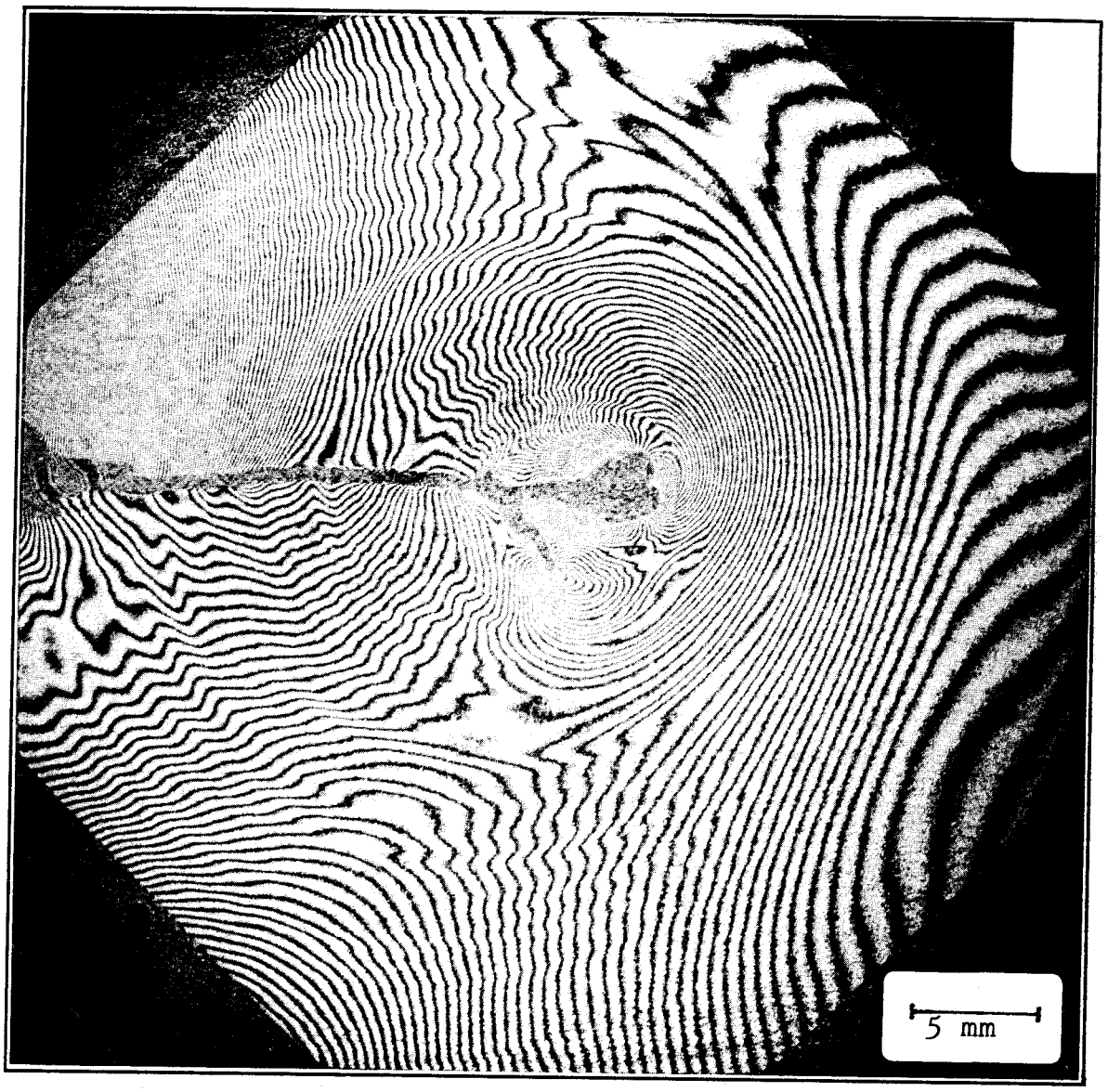

Figure (32d) Interferogram of the out-of-plane displacement of the surface deformation of a crack branching in a polymethylmethacrylate sheet 4.42 mm thick, at 60 μs. Surface contours represent displacements of 257 nm. The octagon is 40.96 mm across the flats.

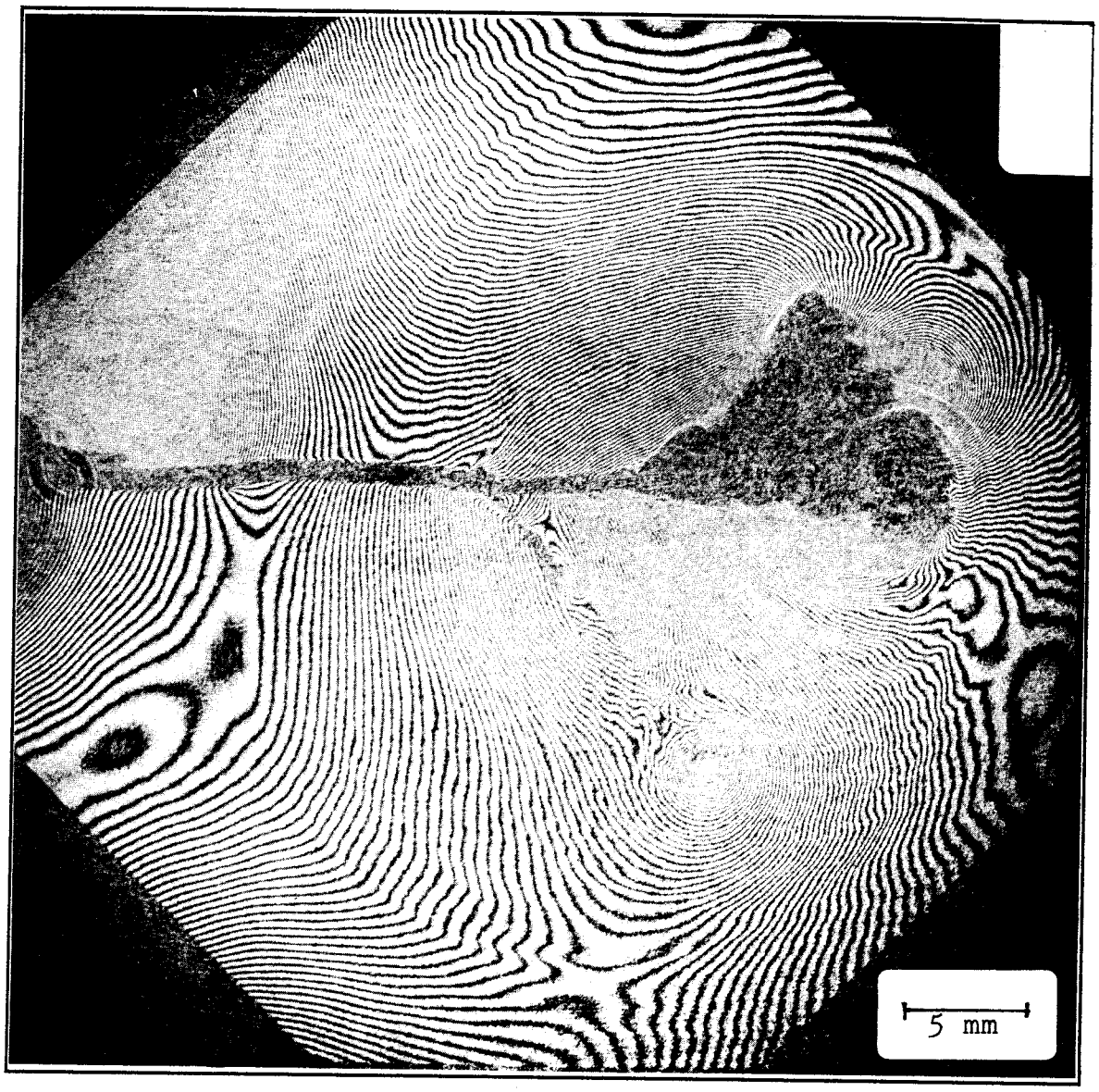

Figure (32e) Interferogram of the out-of-plane displacement of the surface deformation of a crack branching in a polymethylmethacrylate sheet 4.42 mm thick, at 80 μs. Surface contours represent displacements of 257 nm. The octagon is 40.96 mm across the flats.

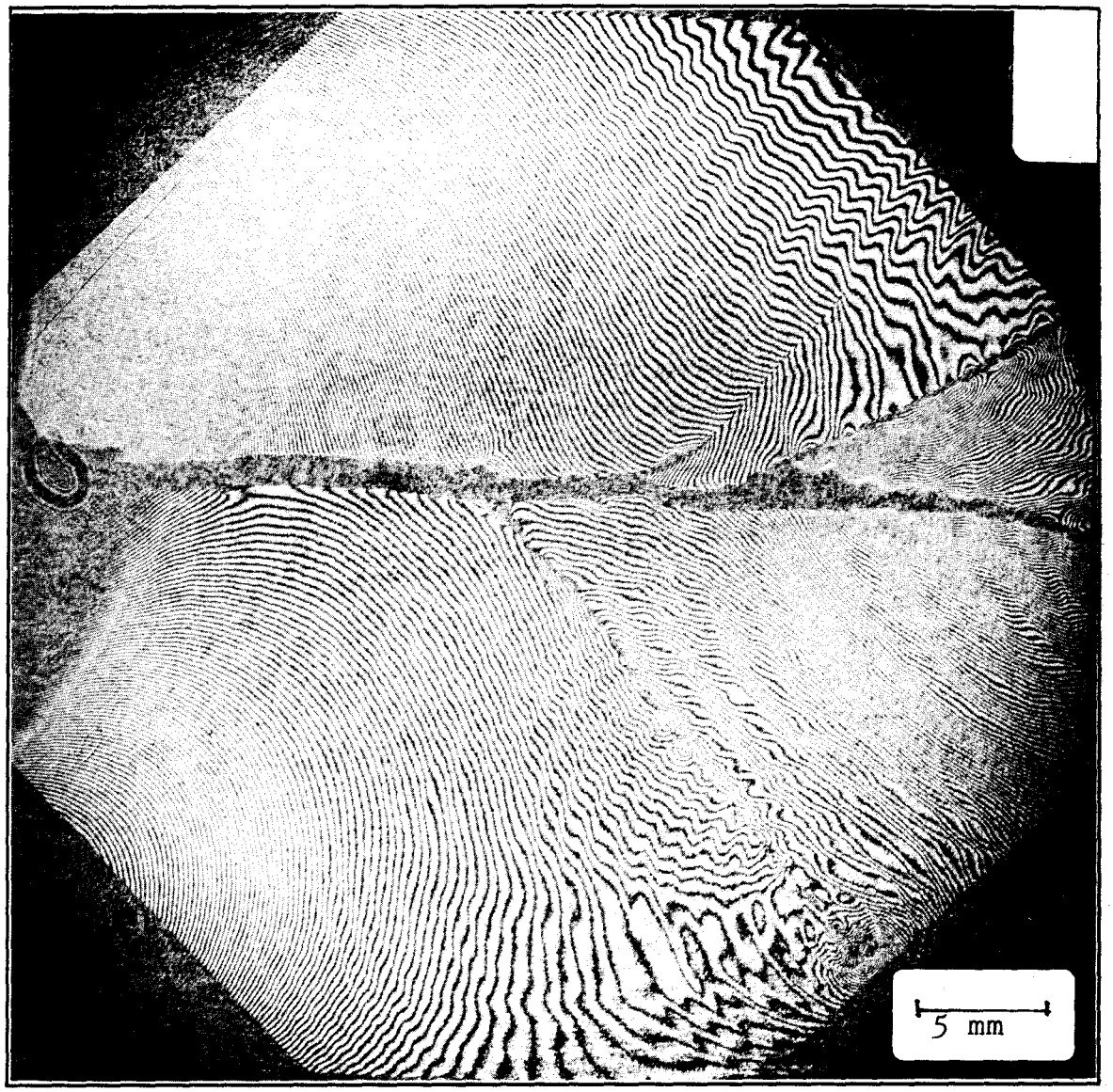

Figure (32f) Interferogram of the out-of-plane displacement of the surface deformation of the flanks of cracks moving in a polymethylmethacrylate sheet 4.42 mm thick, at 100 μs. Surface contours represent displacements of 257 nm. The octagon is 40.96 mm across the flats.

These dynamic fracture results on the thermoplastic PMMA, corrobarate the results on the thermoset polymer Homalite-100 [6,21,36]. Near the crack branching speed, the surface roughness increases with increasing magnitude of deformation at the crack tip not with the average crack tip velocity. Furthermore, if the intensity of deformation is sufficiently severe, cracks are observed to start and unsuccessfully propagate. This is consistent with the hypothesis that as the crack velocity is augmented due to increased deformation, weak spots in the material fail preceding the crack front. The net effect is to blunt the crack tip due to unbroken ligaments, slow down the crack [103], and enable other cracks to compete for surrounding energy and propagate.

There are some differences between the two material systems. The fracture morphology of PMMA at the near branching velocities is on a scale that is at least an order of magnitude larger than that in the Homalite-100. This fact is attributed to the greater toughness of the thermoplastic. The Homalite-100 propagation mechanism is theorized to be a haphazard collection of coalescing small voids and cracks while the PMMA appears to become periodic and fairly uniform through the thickness.

There is at present no explanation as to the reason why a crack in PMMA propagates in a non-steady, periodic fashion with a particular length scale. At the crack several scales can be identified. In this relatively low molecular weight polymer, craze zones are approximately 10 μm. This distance (i.e., 10 μm) is approximately the same size as the zone of heating due to temperature rise measurements [100,101,102]. Both of these sizes are much smaller than the millimeter size ripples seen on the fracture surface. The only other intentional scale is the specimen thickness. A possible mechanism here would be that a standing wave is established bouncing symmetrically from the center of the specimen to the specimen surface and returning back to the specimen center. This mechanism would require that the wave speed locally at the crack tip be double that of the

surrounding material; however, this would not account for the ripples being approximately parallel with the plate normal. The temporal resolution of the experiment was not sufficient to resolve these details of the sub-microsecond crack propagation phenomena.

5.3 Interfacial Results

The proposed reason for a crack branching and propagating at velocities much lower than the Rayleigh wave speed of the material is that small cracks and voids open preceding the main crack front and blunt it [6]. If the spatially disperse nature of this failure process is suppressed then the rupture should behave more ideally brittle. This more brittle behavior should be apparent as both an increase in the crack propagation velocity [8] and a suppression of the non-steady behavior. To test this hypothesis a dynamic interfacial specimen was constructed using the thermal curing techniques used to calibrate the thermoplasitc molding process. The specimen was constructed for a short duration dynamic test as is shown in Figure (13). The specimen was cured at 130 $^{\circ}C$ for 4 hours yielding a strength of approximately 60% of the original material strength based on the curing calibration. This healing resulted in an interface approximately 0.005 mm thick as measured optically in transmission. The specimen was loaded using a pulse comparable to that in Figure (20). This test is analogous to the test shown in Figure (27), except that a weak material plane has been introduced. The results of this test are shown in Figure (33).

The time sequence of photographs corresponds to those described in Figures (27) and (32). However, here the specimen is flatter due to the absence of glued-on legs along the crack flank and because of improvements in constructing and installing the copper loading strip. The crack starts at approximately the same time as in the virgin material test. However, the crack velocity is much greater, about 0.9 mm/μs. The crack is seen to be propagating through two frames.

Comparison of the normalized surface deformation, as was done previously for the dynamic specimens shows that the character of the near tip surface behavior is maintained even at this crack velocity. Here the stress intensity factor used in the normalization has been reduced by 40% to account for the weakened specimen and the corresponding smaller deformation. Indeed, the presence of the interface localizes the failure process, suppresses the surface rippling and the crack velocity is augmented.

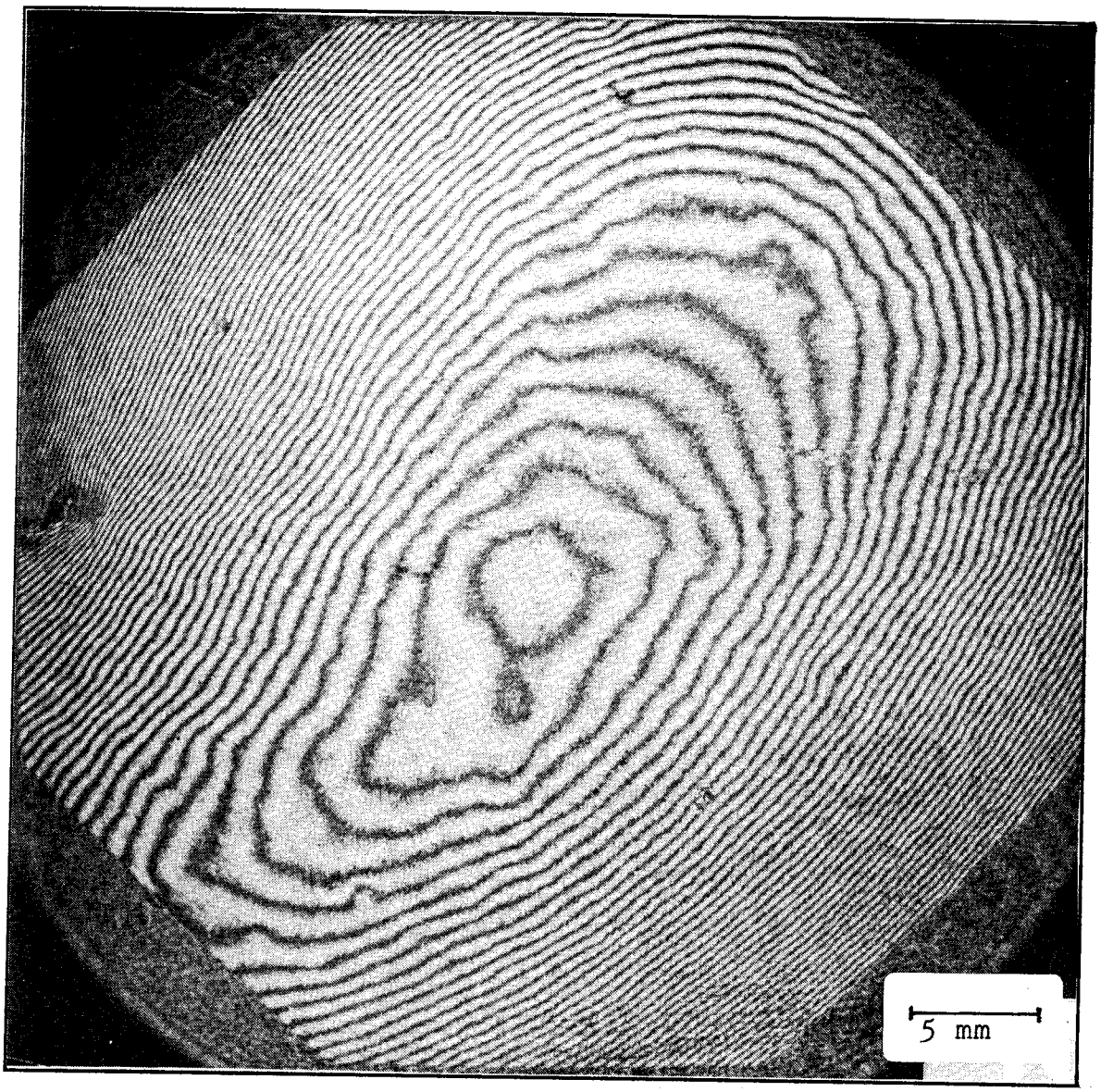

Figure (33a) Interferogram of the out-of-plane displacement of the initial surface deformation at 0 μs, crack in a polymethylmethacrylate sheet 4.71 mm thick, with a weak interface. Surface contours represent displacements of 257 nm. The octagon is 40.96 mm across the flats.

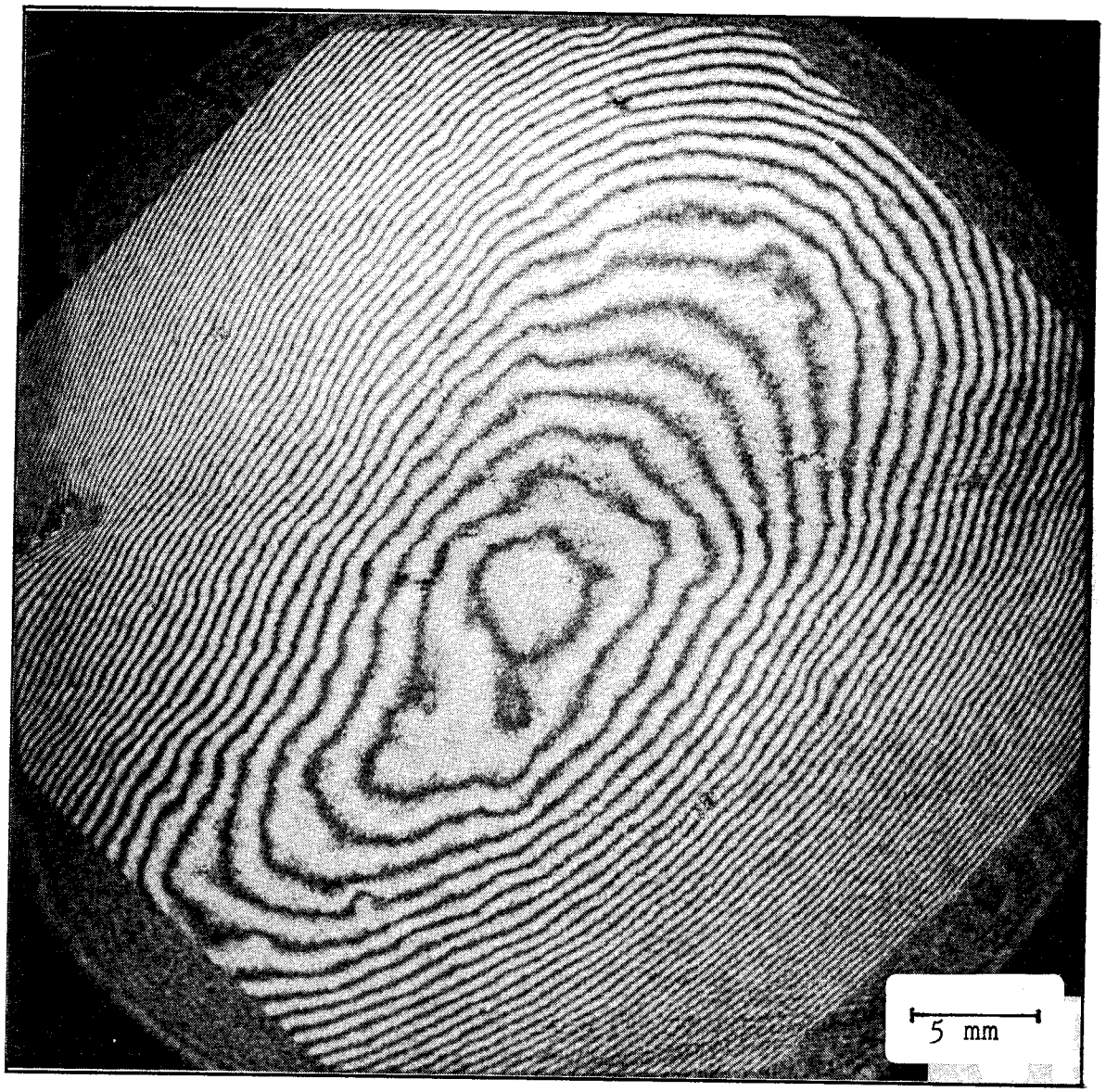

Figure (33b) Interferogram of the out-of-plane displacement of the surface deformation of a crack in a polymethylmethacrylate sheet 4.71 mm thick, with a weak interface, under dynamic loading conditions at 20 μs. Surface contours represent displacements of 257 nm. The octagon is 40.96 mm across the flats.

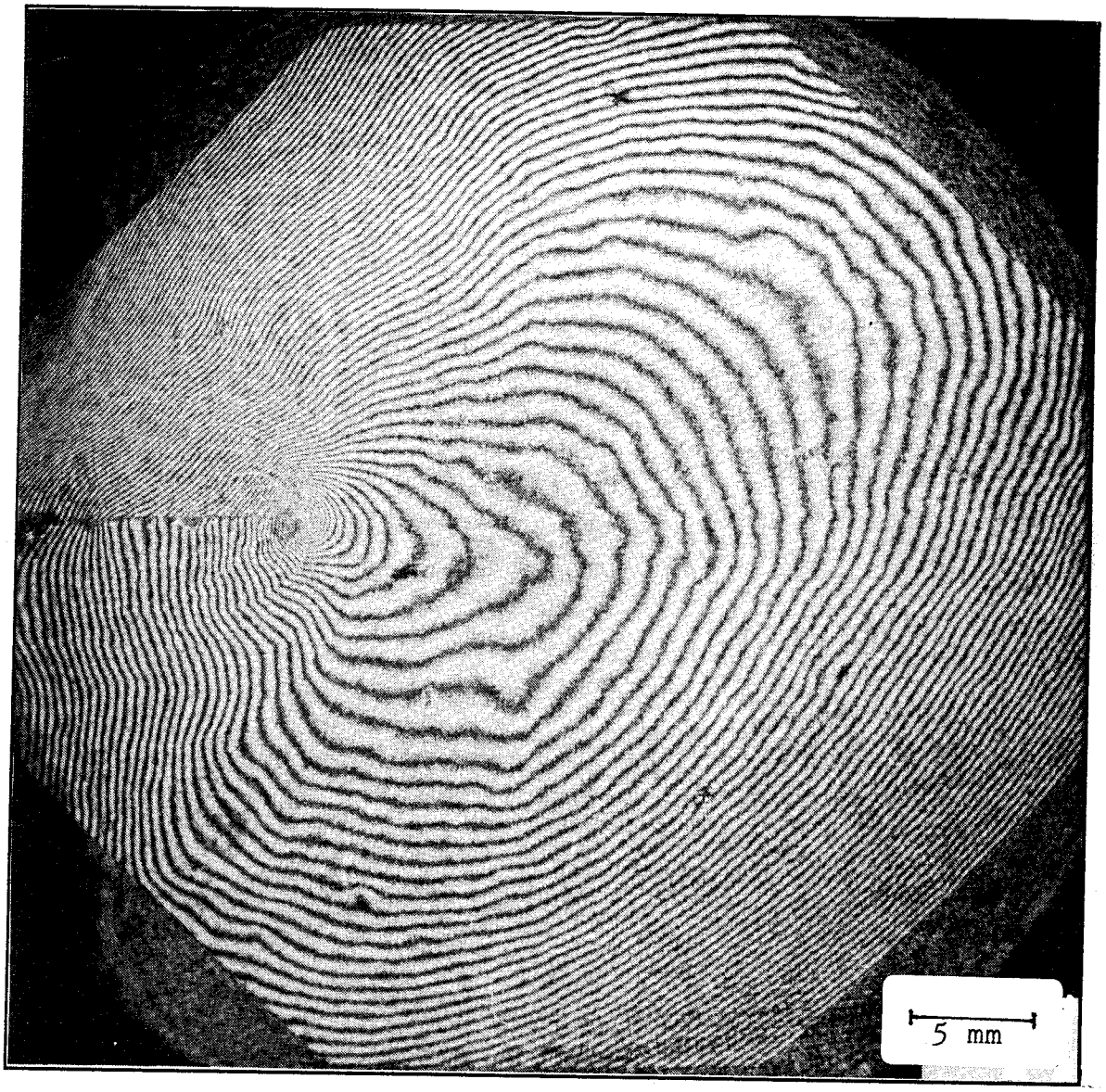

Figure (33c) Interferogram of the out-of-plane displacement of the surface deformation of a crack moving at 0.9 mm/μs, along a weak interface, in a polymethylmethacrylate sheet 4.71 mm thick, at 40μs. Surface contours represent displacements of 257 nm. The octagon is 40.96 mm across the flats.

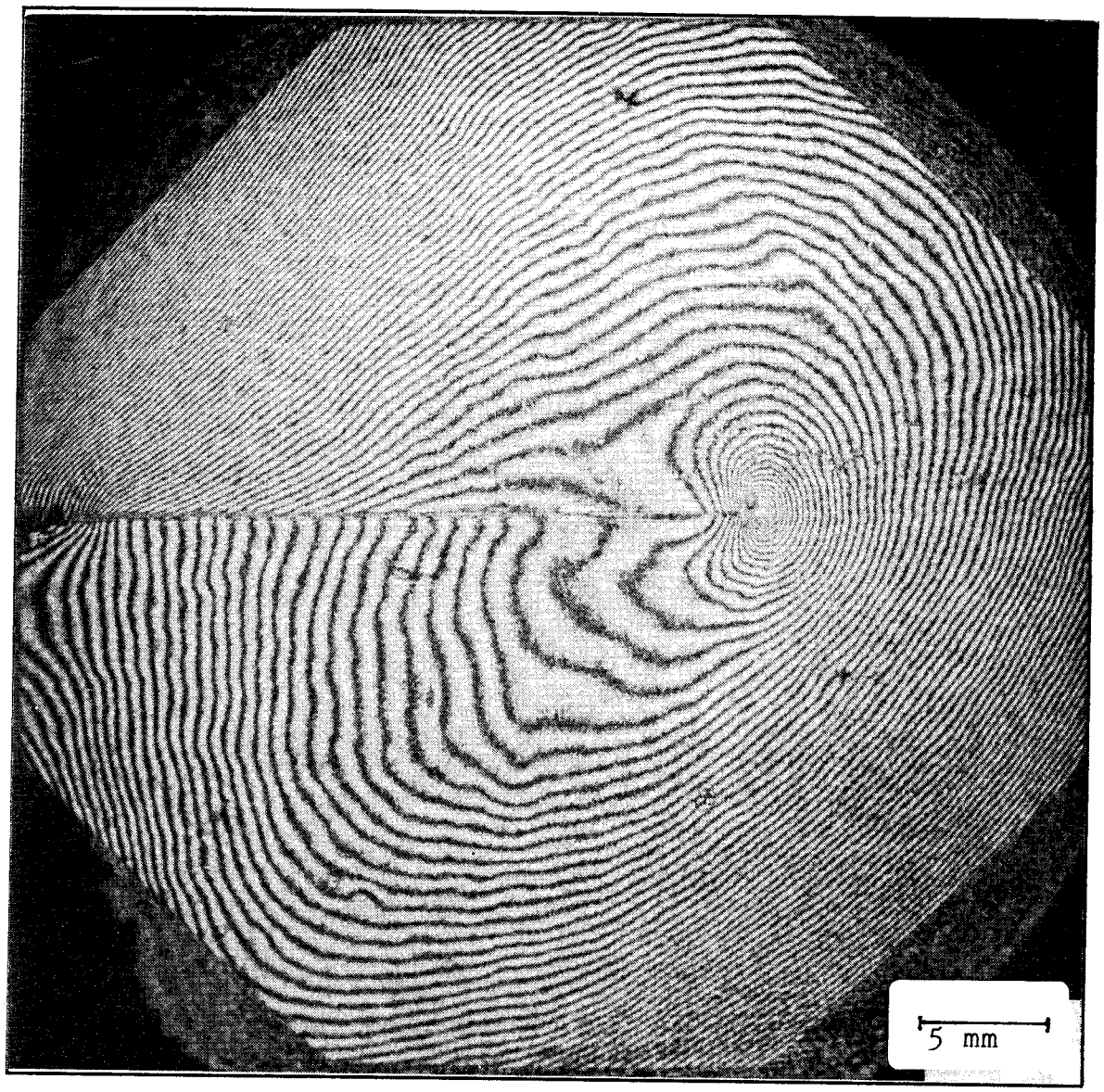

Figure (33d) Interferogram of the out-of-plane displacement of the surface deformation of a crack moving at 0.9 mm/μs, along a weak interface, in a polymethylmethacrylate sheet 4.71 mm thick, at 60μs. Surface contours represent displacements of 257 nm. The octagon is 40.96 mm across the flats.

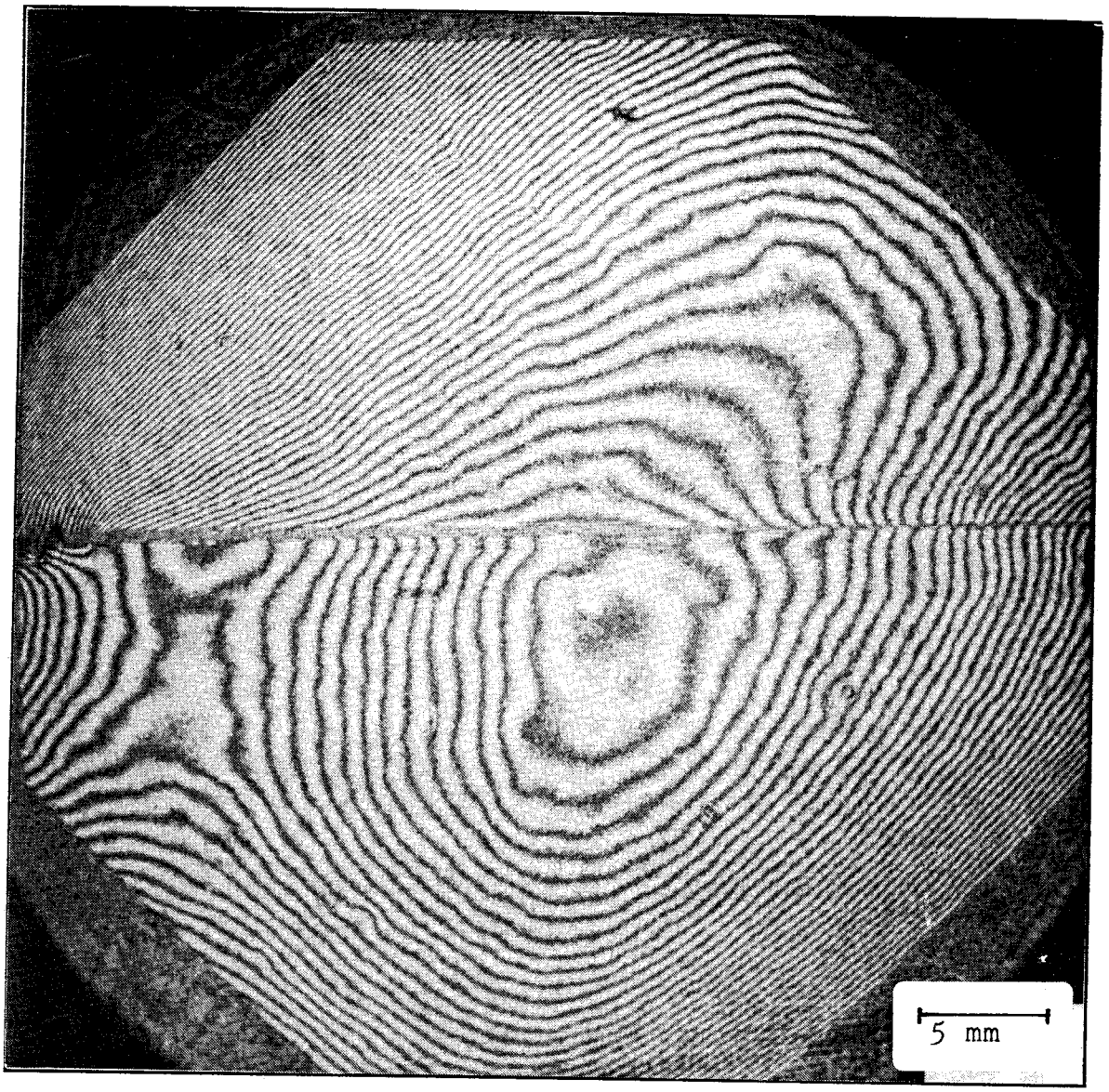

Figure (33e) Interferogram of the out-of-plane displacement of the surface deformation of the flanks of a crack moving in a polymethylmethacrylate sheet 4.71 mm thick, at 80 μs. Surface contours represent displacements of 257 nm. The octagon is 40.96 mm across the flats.

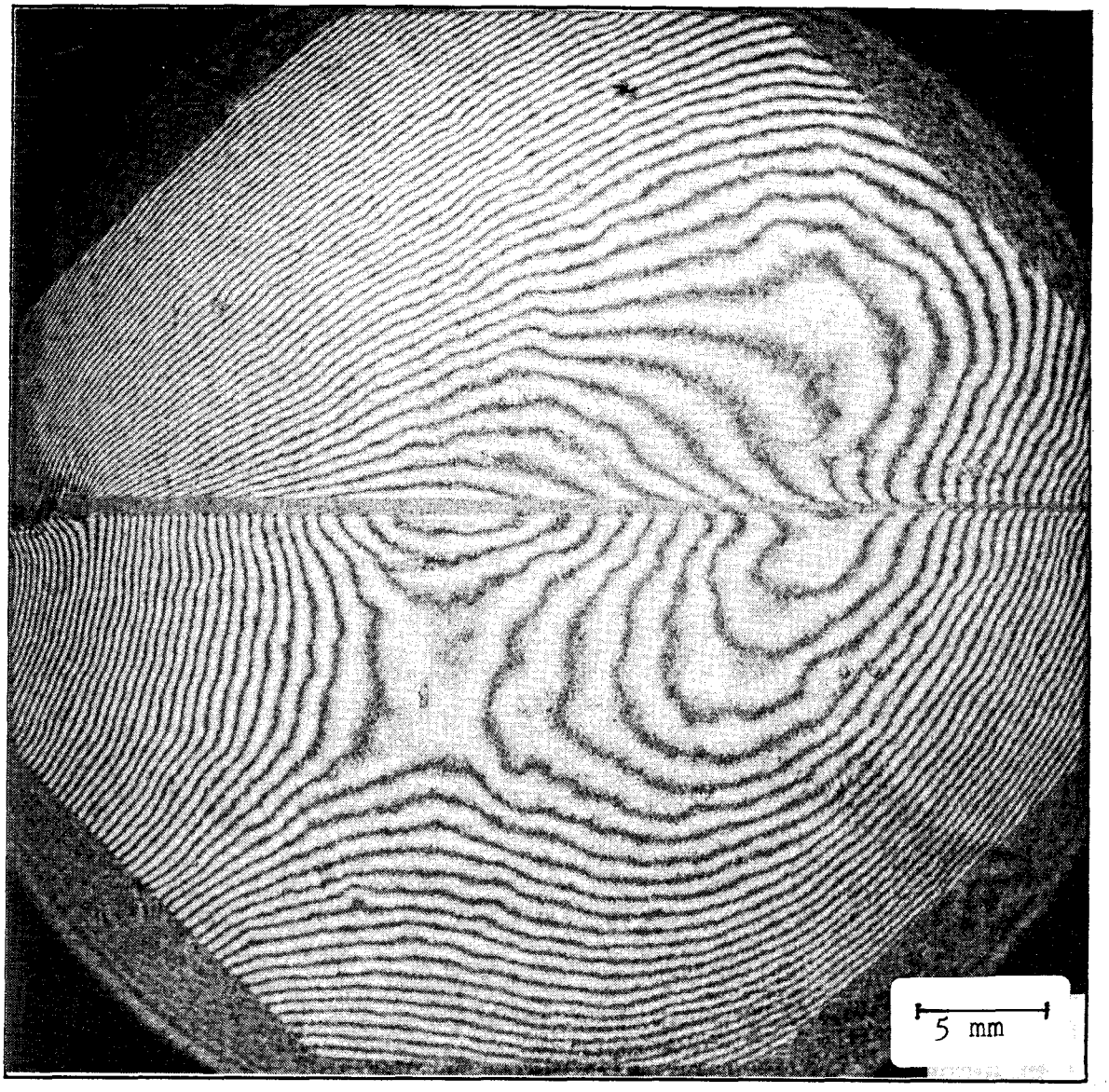

Figure (33f) Interferogram of the out-of-plane displacement of the surface deformation of the flanks of a crack moving in a polymethylmethacrylate sheet 4.71 mm thick, at 100 μs. Surface contours represent displacements of 257 nm. The octagon is 40.96 mm across the flats.

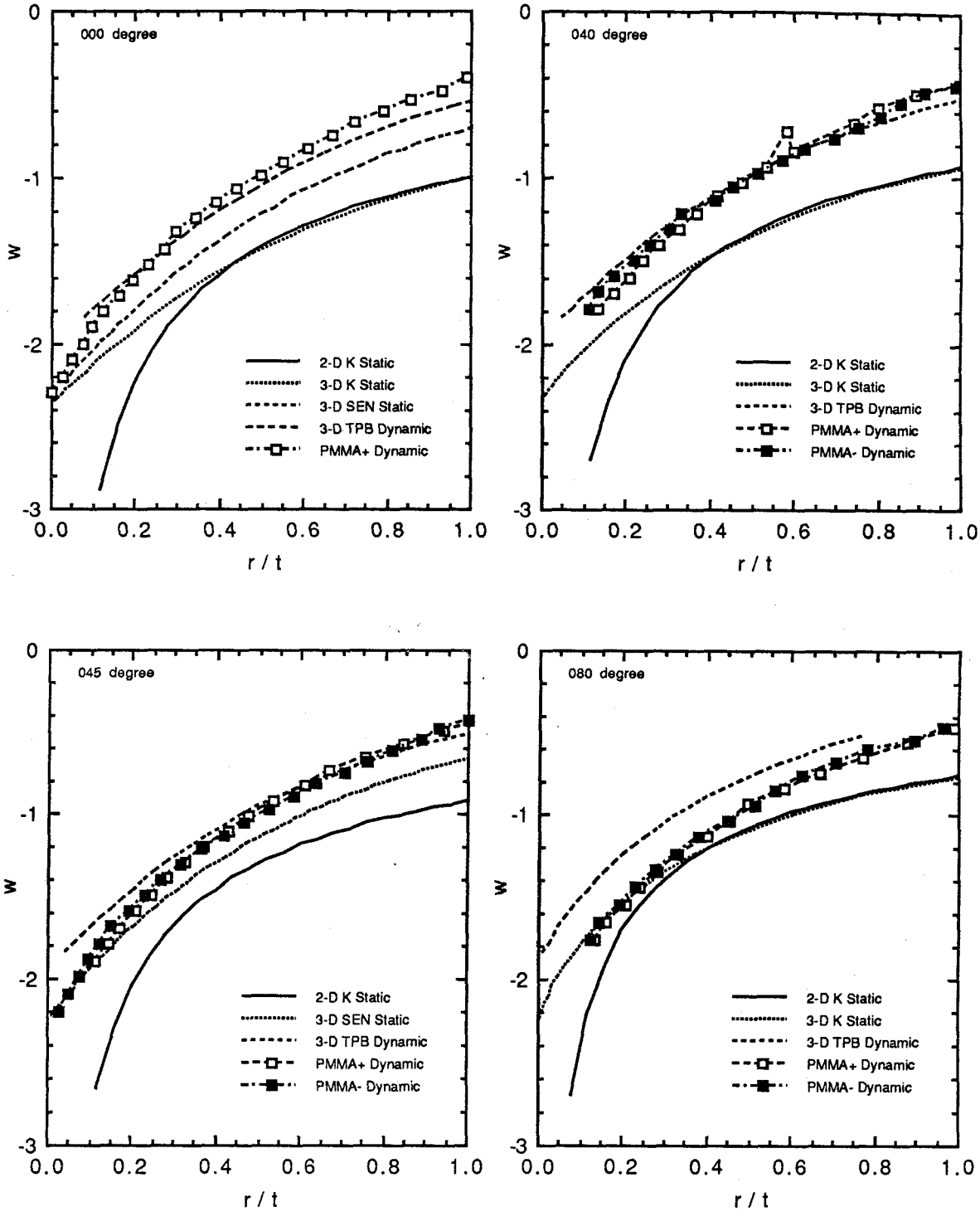

Figure (34a) Out-of-plane displacement at various radial angles for a specimen with a weakly healed (60%) interface. Crack is propagating at about 90% of the shear wave speed in the plate. Specimen is PMMA with non-dimensional displacement determined from static values. Displacements at radial angles of 0, 40, 45 and 80 degrees.

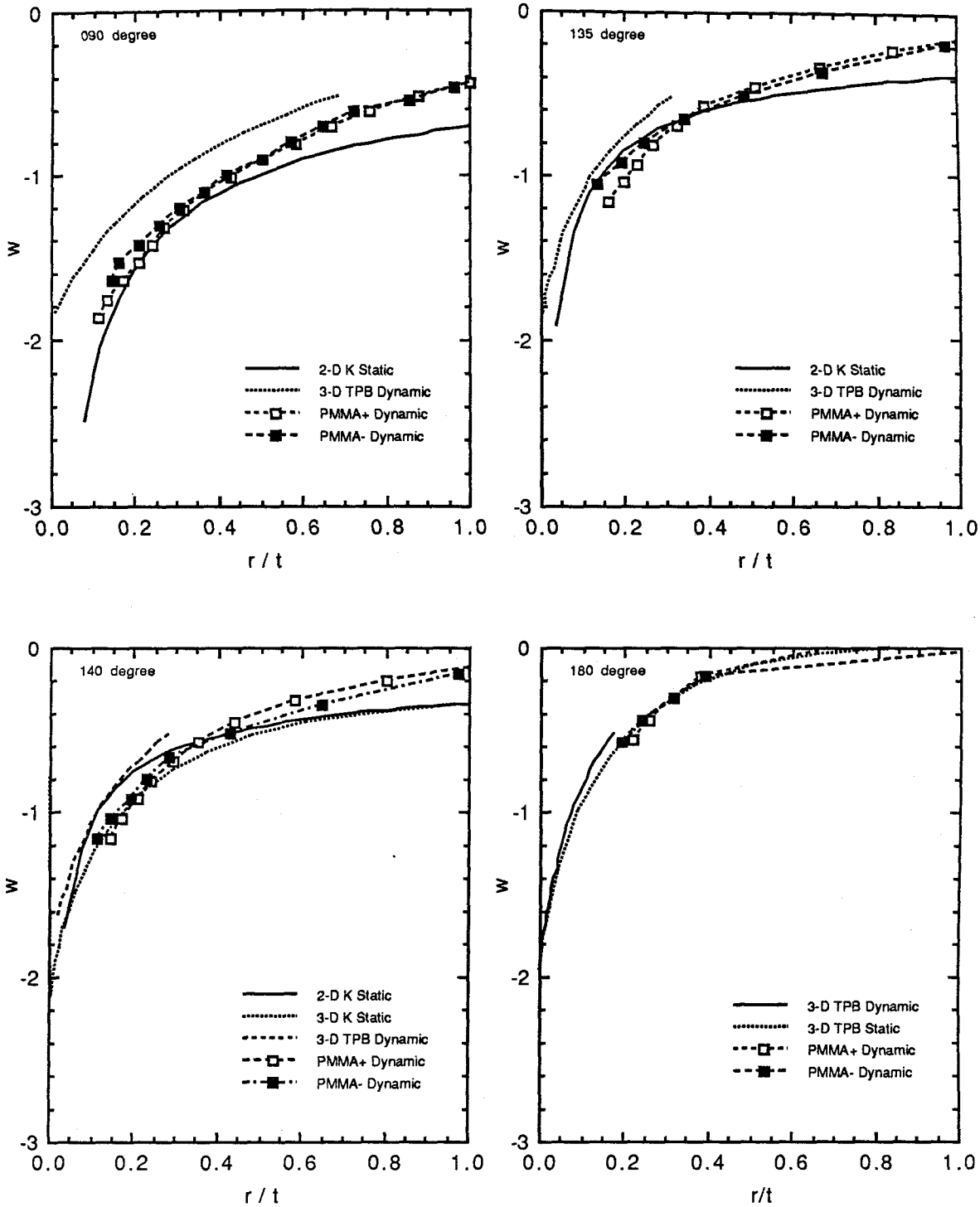

Figure (34b) Out-of-plane displacement at various radial angles for a specimen with a weakly healed (60%) interface. Crack is propagating at about 90% of the shear wave speed in the plate. Specimen is PMMA with non-dimensional displacement determined from static values. Displacements at radial angles of 90, 135, 140 and 180 degrees.

6. Conclusions

The two-dimensional plane stress asymptotic solution is not a reliable model of the out-of-plane surface deformation near the tip of a brittle crack in a plate under Mode-I loading conditions. Thus, experimental techniques which make use of this model are suspect. The use of the reflective shadowgraphic techniques such as caustics and the Stress Intensity Factor Tracer used in reflection, is unjustified in typical experimental arrangements. These techniques suffer from requiring interferometric quality distance measurements to maintain accuracy as the crack tip is approached. Furthermore, any method which relies on the surface surrounding a crack to dimple as predicted by the two-dimensional plane stress asymptotic solution requires a special, and as yet unspecified specimen geometry. The out-of-plane deformation in three point bend and single edge notch specimens have measurable three-dimensional character that agrees in slope with numerical simulations.

Normalizing the magnitude of the numerically predicted surface dimple at the crack front with a stress intensity factor derived quantity, results in agreement of only ten percent. This discrepancy leads one to suspect the validity of a single parameter fracture criteria (e.g., the stress intensity factor) or the wisdom of using "standard" specimen geometries that ostensibly isolate the crack tip from boundary conditions. Since these difficulties arise in simple geometries, there is little confidence that the true three-dimensional character of a crack is isolated from boundary effects in more involved practical problems.

The slope of the out-of-plane deformation of brittle cracks under Mode-I loading has the character of the three-dimensional elastic solutions. This result is true for both

slowly propagating and dynamically propagating cracks. A crack that propagates sufficiently fast in PMMA does so in a non-steady, periodic fashion. The scale of this local failure process correlates with the local intensity of deformation, and not with the average crack velocity. This result supports a void nucleation and coalescence crack propagation mechanism that limits the crack velocity because of the blunting effect of multiple fracture sites. In further support of this mechanism, this non-steadiness can be inhibited and the crack velocity augmented by introducing a weak material plane. This weak plane inhibits the surrounding nucleation by decreasing the local stress required to propagate a crack, and thus reduces the number of multiple fracture sites and thereby shrinks the failure zone.

7. References

[1] Irwin, G.R., "Structural Aspects of Brittle Fracture," Applied Materials Research, Volume 3, No. 2, April 1964, pp. 65-81.

[2] Rice, J.R., "A Path Independent Integral and the Approximate analysis of Strain Concentration by Notches and Cracks," Journal of Applied Mechanics, Volume 35, 1968, pg. 379.

[3] Freund, L.B., and Clifton, R.J., "On the Uniqueness of Plane Elastodynamic Solutions for Running Cracks," Journal of Elasticity, Volume 4, No. 4, December 1974, pp. 293-299.

[4] "Standard Method of Test for Plane-Strain Fracture Toughness of Metalic Materials," ASTM E 399-74, 1974, Part 10.

[5] Lai, M.O., and Ferguson, W.G., "The Inadequacy of the Plane-Strain Fracture Toughness Test Requirements," Engineering Fracture Mechanics, Volume 13, 1980, pp. 285-292.

[6] Ravi-Chandar, K.,"An Experimental Investigation into the Mechanics of Dynamic Fracture," Doctoral Dissertation, California Institute of Technology, Pasadena, California, 1982

[7] Larsson, S.G., and Carlsson, A.J., "Influence of Non-Singular Stress Terms and Specimen Geometry on Small-Scale Yielding At Crack Tips in Elastic-Plastic Materials," Journal of the Mechanics and Physics of Solids, Volume 21, 1973, pg. 263.

[8] Freund, L.B., Journal of Elasticity, Volume 2, 1972, pg. 341.

[9] Ma. C.C., and Freund, L.B., "The Extent of the Stress Intensity Factor Field During Crack Growth Under Dynamic Loading Conditions," Journal of Applied Mechanics, Volume 53, 1986, pp. 303-310.

[10] Ravi-Chandar, K., and Knauss, W.G., "On the Characterization of the Transient Stress Field Near the Tip of a Crack," Journal of Applied Mechanics, Volume 54, 1987, pp. 72-77.

[11] Atkinson, C.,"Stress Singularities and Fracture Mechanics," Applied Mechanics Reviews, Volume 32, 1979, pp. 123-135.

[12] Freund, L.B.,"Dynamic Crack Propagation," in the Mechanics of Fracture, edited by Erdogan, ASME-AMD 19, 1976, pp. 105-134.

[13] Rice, J.R.,"Elastic-Plastic Fracture Mechanics," in the Mechanics of Fracture, edited by Erdogan, ASME-AMD 19, 1976, pp. 23-53.

[14] Panasyuk, V.V, Anrejkiv, A.E., and Stadnik, M.M., "Three-Dimensional Static Crack Problems Solution (A Review)," Engineering Fracture Mechanics, Volume 14, 1981, pp. 245-260.

[15] Aravas, N., and McMeeking, R.M.,"Microvoid Growth and Failure in the Ligament between a Hole and a Blunt Crack Tip," International Journal of Fracture, Volume 29, 1985, pp. 21-38.

[16] Aboudi, J., and Achenbach, J.D., "Numerical Analysis of Fast Mode-I Fracture of a Strip of Viscoplastic Work-Hardening Material," International Journal of Fracture, Volume 21, 1983, pp. 133-147.

[17] Popelar, C.H., and Hoagland, R.G., "On The Nature of Crack Propagation and Arrest in a Damaging Material," Engineering Fracture Mechanics, Volume 23, 1986, pp. 131-144.

[18] Ravichandran, G., and Clifton, R.J., "Dynamic Fracture Under Plane Wave Loading," International Journal of Fracture, Volume 40, 1989, pp.157-201.

[19] Rolfe, S.T., and Barsom, J.M, "Fracture and Fatigue Control in Structures, Applications of Fracture Mechanics," Prentice Hall, Englewood Cliffs, New Jersey, 1977, pg. 31.

[20] Irwin, G.R., Dally, J.W., Kobayashi, T., Fourney, W.L., Etheridge, M.J., and Rossmanith, H.P., "On the Determination of the a-K Relationship for Birefringent Polymers," Experimental Mechanics, 1979, pp. 121-128.

[21] Kobayashi, A.S., and Mall, S., "Dynamic Fracture Toughness of Homalite-100," Experimental Mechanics, Volume 18, 1978, pp.11-18.

[22] Dally, J.W., Fourney, W.L., and Irwin, G.R.,"On the Uniqueness of K-a Relation," International Journal of Fracture, Volume 27, 1985, pp. 159-168.

[23] Takahashi, K. and Arakawa, K., "Dependence of Crack Acceleration on the Dynamic Stress-Intensity Factor in Polymers," Experimental Mechanics, 1987, pp. 195-200.

[24] Vasudevan, N., and Knauss, W.G.," An Approximate Analysis of the Effect of Micro-Fractures on the Caustic of a Dynamically Moving Crack Tip," SM Report 86-10, Graduate Aeronautical Laboratories, California Institute of Technology, 1986.

[25] Smith, C.W., McGowan, J.J, and Jolles, M. " Effects of Artificial Cracks and Poison's Ratio Upon Photoelastic Stress-Intensity Determination," Experimental Mechanics, May 1976, pp. 188-193.

[26] Stock, T.A.C., "Stress Field Intensity Factors for Propagating Brittle Cracks," International Journal of Fracture, Volume 3, June 1967, pp. 121-129.

[27] Betser, A.A., Kobayashi, A.S., Lee, O.S., and Kang, B.S.J.,"Crack-tip Dynamic Isochromatics in the Presence of Small-Scale Yielding," Experimental Mechanics, April 1982, pp. 132-138.

[28] Hausler, E., "Shadow Optical Investigations of Elastic Shock Waves in Perspex Sheets," Journal of Mechanics and Physics of Solids, Volume 11, 1963, pp. 243-248.

[29] Schardin, H., "Velocity effects in Fracture," in Fracture, Averbach et al. (eds.), John Wiley and Sons, New York, New York, 1959.

[30] Manoog, P., "Anwendungen der Schattenoptik zur Untersuchung des Zerreissvorgags von Platten", Dissertationsschrift an der Universitat Freiburg, 1964.

[31] Theocaris, P.S.,"Reflected Shadow Method for the Study of Constrained Zones in Cracked Plates", Applied Optics, Volume 10, No. 10, October 1971, pp. 2240-2247.

[31a] Kalthof, J.F., et al. VDI Berichte Nr. 313., 1978, pg.791.

[32] Kim, K.-S., "A Stress Intensity Factor Tracer," Journal of Applied Mechanics, Volume 52, 1985, pp. 291-297.

[33] Theocaris, P.S., " Diffused Light Interferometry for Measurement of Isopachics," Journal of Mechanics and Physics of Solids, Volume 11, 1963, pp. 181-195.

[34] Green, A.K., and Pratt, P.L., " Measurement of the Dynamic Fracture Toughness of Polymethylmethacrylate by High-Speed Photography," Engineering Fracture Mechanics, Volume 6, 1974, pp. 71-80.

[35] Lee, O.S., and Kobayashi, A.S., " Crack Tip Plasticity of a Tearing Crack," in Fracture Mechanics: Sixteenth Symposium, ASTM STP 868, Kanninen, M.F.,and Hopper, A.T., editors, American Society for Testing and Materials, Philadelphia, 1985, pp.431-450.

[36] Kobayashi, A.S., Wade, B.G., Bradley, W.B. and Chiu, S.T., "Crack Branching in Homalite-100 Sheets," Engineering Fracture Mechanics, Volume 6, 1974, pp. 81-92.

[37] Manoog, P.,"Investigation of the Rupture of a Plexiglas Plate by means of an Optical Method Involving High-Speed Filming of the Shadows Originating Around Holes Drilled in the plate," International Journal of Fracture Mechanics, Volume 2, 1966, pp. 604-613.

[38] Theocaris, P.S.,"Local Yielding Around a Crack Tip in Plexiglas," Journal of Applied Mechanics, June 1970, pp. 409-415.

[39] Beinert J., and Kalthoff J.F., "Experimental Determination of Dynamic Stress-Intensity Factors by Shadow Patterns," in Mechanics of Fracture, Volume VII, G. Sih, Sijthoff and Noordhoff, 1981, pp 281-330.

[40] Zehnder, A.T., "Dynamic Fracture Initiation and Propagation in Metals: Experimental Results and Techniques," Doctoral Dissertation, California Institute of Technology, Pasadena, California, 1987.

[41] Kim, K.-S., "Dynamic Fracture Under Normal Impact Loading of the Crack Faces," Journal of Applied Mechanics, Volume 52, 1985, pp. 585-592.

[42] Evans, W.T., and Luxmoore, A., "Measurement of In-Plane Displacements Around Crack Tips by a Laser Speckle Method," Engineering Fracture Mechanics Volume 6, 1974, pp. 735-743.

[43] Reidmuller, J., "Experimental Determination of the Energy Density Distribution around a Crack Tip under Mixed Mode Loading," Institut fur Festkorpermechanik der Fraunhofer-Gesellschaft, e.V. 78 Freiburg i.Br., Rosastr. 9, August 1975.

[44] Schultheisz, C.R., Doctoral Dissertation, California Institute of Technology, Pasadena, California, 1990.

[45] Dudderar, T.D., and O'Regan, R., "Measurement of the Strain Field near a Crack Tip in Polymethylmethacrylate by Holographic Interferometry," Experimental Mechanics, 1971, pp. 49-56.

[46] Ennos, A.E., and Virdee, M.S., "Application of Reflection Holography to Deformation Measurement Problems," Experimental Mechanics, 1982, pp. 202-209.

[47] Liepmann, H.W., and Roshko, A., "Elements of Gasdynamics," John Wiley and Sons Inc., New York, New York, 1957, pg 157-162.

[48] Theocaris, P.S., and Gdoutos, E., "Verification of the Validity of the Dougdale-Barrenblatt Model By the Method of Caustics," Engineering Fracture Mechanics,Volume 6, 1974, pp. 523-535.

[49] Rosakis, A.J., and Freund, L.B., " The Effect of Crack-Tip Plasticity on the Determination of Dynamic Stress-Intensity Factors by the Optical Method of Caustics," Transactions of the ASME, Volume 48, June 1981, pp. 302-308.

[50] Shockley, D.A., Kalthoff, J.F., Klemm W., and Winkler, S., "Simultaneous Measurements of Stress Intensity and Toughness for Fast-Running Cracks in Steel," Experimental Mechanics, 1983, pp.140-145.

[51] Rosakis, A.J., and Ravi-Chandar K., "On Crack-Tip Stress State: An Experimental Evaluation of Three-Dimensional Effects," International Journal of Solids and Structures, Volume 22, Number 2, 1986, pp 121-134.

[52] Nigam, H., and Shukla, A., "Comparison of the Techniques of Transmitted Caustics and Photoelasticity as Applied to Fracture", Experimental Mechanics, June 1988, pp.123-135.

[53] Manajan, R.V., and Ravi-Chandar, K., "Experimental Determination of Stress-Intensity Factors Using Caustics and Photoelasticity," Experimental Mechanics, Volume 29, No. 1, 1989, pp. 6-11.

[54] Williams, M.L.,"On the Stress Distribution at the Base of a Stationary Crack," Journal of Applied Mechanics,Volume 24, 1957, pp. 109-114.

[55] Rosakis, A.J., and Zehnder, A.T., "On the Method of Caustics: An Exact Analysis Based on Geometrical Optics", Journal of Elasticity, Volume 15, 1985, pp. 347-367.

[56] Kamath, S.M., and Kim, K.S.,"Coherent-Light-Shadow Spot of a Crack Under Mode-I Loading: Theory and Experiment," Experimental Mechanics, December 1986, pp. 386-393.

[57] Rosakis, A.J., Zehnder, A.T., and Narasimhan, R.,"Caustics by Reflection and Their Application to Elastic-Plastic and Dynamic Fracture Mechanics," SPIE Conference on Photomechanics and Speckle Metrology, San Diego, California, August 16-20, 1987.

[58] Pfaff, R.D., Doctoral Dissertation, California Institute of Technology, Pasadena, California, 1990.

[59] Krishnaswamy, S., "On the Domain of Dominance of the Asymptotic Elastodynamic Crack-Tip Fields," Doctoral Dissertation, California Institute of Technology, Pasadena, California, 1989.

[60] Alblas, J.E.,"Theory of the Three-Dimensional Stress State in a Plate with a Hole," Thesis, H.J. Paris, Amsterdam, 1957: NASA TT F-10, 451.

[61] Benthem, J.P.,"State of Stress at the Vertex of a Quarter-Infinite Crack in a Half-Space," International Journal of Solids and Structures, Volume 13, 1977, pp. 479-492.

[62] Folias, E.S.,"On the Three-Dimensional Theory of Cracked Plates," Transactions of ASME, E42(3), 1975, pp. 663-674.

[63] Cruse, T.A., and Vanburen, W., " Three-Dimensional Elastic Stress Analysis of Fracture Specimen with an Edge Crack," International Journal of Fracture Mechanics, Volume 7, No. 1, 1971, pp. 1-15.

[64] Tseng, A.A., "A Three-Dimensional Finite Element Analysis of The Three Point Bend Specimen," Engineering Fracture Mechanics, Volume 13., 1980, pp.939-943.

[65] Raju, I.S., and Newman, J.C. Jr.,"Three-Dimensional Finite-Element Analysis of Finite-Thickness Fracture Specimens," NASA, TN D-8414, 1977.

[66] Villarreal, G., Sih, G.C., and Hartranft, R.J., " Photoelastic Investigation of a Thick Plate with a Transverse Crack," Journal of Applied Mechanics, Volume 4., 1975, pp. 9-14.

[67] Levy, N.,Marcal, P.V., and Rice, J.R, "Progress in Three-Dimensional Elastic-Plastic Stress Analysis for Fracture Mechanics," Nuclear Engineering and Design, Vol. 17, 1971, pp. 66-75.

[68] Soleki, J.S., and Swedlow, J.L., "On the Three-Dimensional Implications of LEFM: Finite Element Analysis of Straight and Curved Through-Cracks in a Plate," in Fracture Mechanics: Sixteenth Symposium, ASTM STP 868, Kanninen, M.F., and Hopper, A.T., editors, American Society for Testing and Materials, Philadelphia, 1985, pp. 535-553.

[69] Wellman, G.W., Rolfe, S.T., and Dodds, R.H, " Three-Dimensional Elastic-Plastic Finite Element Analysis of Three-Point Bend Specimens," in Fracture Mechanics: Sixteenth Symposium, ASTM STP 868, Kanninen, M.F., and Hopper, A.T., editors, American Society for Testing and Materials, Philadelphia, 1985, pp. 214-237.

[70] Burton, W.S., Sinclair, G.B., Solecki, J.S., and Swedlow, J.L., "On the implications for LEFM of the three-dimensional aspects in some crack/surface intersection problems," International Journal of Fracture, Volume 25, 1984, pp. 3-32.

[71] Parsons, I.D., Hall, J.F., and Rosakis, A.J., " A Finite Element Investigation of the Elastostatic State Near a Three Dimensional Edge Crack," GALCIT Report SM86-29, California Institute of Technology, 1986.

[72] Nakamura T., and Parks D.M., "Three-Dimensional Field Near the Crack Front of a Thin Elastic Plate," presented at the 24th Annual Meeting of the Society of Engineering Science, September 21-23, 1987, Salt Lake City, Utah.

[73] Narasimhan, R., "Mode I, Plane Stress Crack Initiation and Growth in Elastic-Plastic Solids:A Finite Element Analysis," Doctoral Dissertation, California Institute of Technology, Pasadena, California, 1986.

[74] Profder, T., Woodbrey, J.C., Clark, J.H., and Drott, E.E., "Gel Permeation Chromatography Calibration: II Preparative GPC Fractionation and Characterization of Poly-(methyl methacrylate) for Calibration in 2,2,2-Triflluoroehanal," in Polymer Molecular Weights, American Chemical Society, Washingtion, D.C., 1973.

[75] Bree, H.W., Heijboer, J., Struik, L.C.E., and Tak, A.G.M., "The Effects of Densification on the Mechanical Properties of Amorphous Glassy Polymers," Journal of Polymer Science: Polymer Physics Edition, Volume 12, 1974, 1857-1864.

[76] McCrum, Read, Williams,"Anelastic and Dielectric Effects in Polymeric Solids", Chaper 8 : Methacrylate and Related Polymers, John Wiley and Sons , New York, New York, 1967.

[77] Bueche, A.M., and Berry, J.P., "The Mechanisms of Polymer Failure," in Fracture, Averbach et al. (editors), Technology Press of MIT, Boston, Massachusetts, 1959.

[78] Wolock, I., Kies, J.A., and Newman, S.B., " Fracture Phenomena in Polymers," in Fracture, Averbach et al. (editors), Technology Press of MIT, Boston, Massachusetts, 1959.

[79] Kausch, H.H., Petrovska, D., Landel, R.F., and Monnerie, L., "Intermolecular Interaction in Polymer Alloys as Studied by Crack Healing," Polymer Engineering and Science, Volume 27, No. 2, 1987, pp. 149-154.

[80] Lee, O.S., and Knauss, W.G., "An Experimental Study on Crack Healing of Glassy Polymers," Graduate Aeronautical Laboratories, California Institute of Technology SM 84-9, 1984.

[81] Chiang, F.P., and Khetan, R.P., "A New Method to Increase the Sensitivity of Photoelasticity," Experimental Mechanics, 1974, pp. 29-32.

[82] Beebe, W.M., Jessey, M.E., Liu, H.W., Valluri, S.R., and Williams, M.L.,"Development and Application of a High Speed Camera for Metallographic and Crack Propagation Studies," Aerospace Research Laboratories, 64-96, April 1964.

[83] Smith, G.C., Doctoral Dissertation, California Institute of Technology, Pasadena, California, 1975.

[84] McCammond, D., and Motycka, J., "Strain-ratio Measurements by an Interferometric Device," Experimental Mechanics, June 1974, pp. 225-229.

[85] Rossmanith, H.P., and Fourney, W.L., "Determination of Crack-Speed History and Tip-Locations for Cracks Moving with Nonuniform Velocity," Experimental Mechanics, 1982, pp. 111-116.

[86] Greiner, R., and Schwarzl, F.R., "Thermal Contraction and Volume Relaxation of Amorphous Polymers," Rheologica Acta, Volume 23, number 4, 1984, pp. 378-395.

[87] Lam, P.S., and Freund, L.B., "Analysis of Dynamic Crack Growth of Tensile Crack in an Elastic-Plastic Material," Journal of Mechanics and Physics of Solids, Volume 33, 1985, pp 153-167.

[88] Lee,O.S., and Hu, C.,"A Data Base for High-Speed Crack Propagation in PMMA-Data Only," Graduate Aeronautical Laboratories, California Institute of Technology SM 86-39, 1986.

[89] Forrestal, M.J., and Sagartz, M.J., "Transient Vibration Experiments for Determination of Properties for Viscoelastic Structures," Journal of Applied Mechanics, March 1975, pp. 205-208.

[90] Radon, J.C., and Fitspatrick, N.P., "Deformation of PMMA at High Rates of Strain," in Dynamic Crack Propagation, edited by Sih, G.C., Noordhoff, Leyden, 1972.

[91] Weidmann, G.W., and Doll, W., "Some Results of Optical Interference Measurements of Critical Displacements at the Crack Tip," International Journal of Fracture, Volume 14, 1978, pp. R189-R193.

[92] Baker, B.R.,"Dynamic Stresses Created by a Moving Crack," Journal of Applied Mechanics, Volume 29, 1962, pp. 449-458.

[93] Rosakis, A.J.,"Analysis of the Optical Method of Caustics for Dynamic Crack Propagation," Engineering Fracture Mechanics, Volume 13, 1980, pp 331-347.

[94] Theocaris, P.S., and Papadopoulos, G.A.,"Elastodynamic Forms of Caustics for Running Cracks under Constant Velocity," Engineering Fracture Mechanics, Volume 13, 1980, pp. 683-698.

[95] Kies, J.A., Sullivan, A.M., and Irwin, G.R., "Interpretation of Fracture Markings," Journal of Applied Physics, Volume 21, 1950, pp. 716-720.

[96] Doll, W., and Weidmann, G.W., "Transition From Slow to Fast Frack Propagation in PMMA," Journal of Material Science-letters, Volume 11, 1976, pp. 2348-2350,

[97] Johnson, F.A., and Radon, J.C., "Molecular Kinetics and the Fracture of PMMA," Engineering Fracture Mechanics, Volume 4, 1972, pp. 555-576.

[98] Ravi-Chandar, K., and Balzano, M., "On the Mechanics and Mechanism of Crack Growth in Polymeric Materials," Engineering Fracture Mechanics, Volume 30, No. 5, 1988, pp. 713-727.

[99] Cotterell, B., "Velocity Effects in Fracture Propagation," Applied Materials Research, 1965, pp. 227-232.

[100] Fuller, K.N.G., Fox, P.G., and Field, J.E.,"The Temperature Rise at the Tip of Fast-Moving Cracks in Glassy Polymers," Proc. R. Soc. Lond. A. 341, 1975, pp. 537-557.

[101] Weichert, R., and Schonert, K., "On the Temperature Rise at the Tip of Fast Running Crack," J. Mech. Phys. Solids, Volume 22, 1974, pp. 127-133.

[102] Weichert, R., and Schonert, K., "Heat Generation at the Tip of a Moving Crack," Journal of Mechanics and Physics of Solids, Volume 26, 1978, pp. 151-161.

[103] Shukla, A., and Dally, J.W., "Influence of Late Breaking Ligaments on Crack Propagation in Compact Specimens - A Photoelastic Study," Experimental Mechanics, 1983, pp. 298-303.

[104] Rolfe, S.T., and Barsom, J.M, "Fracture and Fatigue Control in Structures, Applications of Fracture Mechanics," Prentice Hall, Englewood Cliffs, New Jersey, 1977, pg. 65.